Annexure II

Reprints of published papers

ChemPubSoc Europe

DOI: 10.1002/ejic.201600513

EurJIC European Journal of Inorganic Chemistry

Full Paper

Mesomorphic Assemblies

Induction of Mesomorphism through Supramolecular Assembly in Metal Coordination Compounds of "salphen"-Type Schiff Bases: Photoluminescence and Solvatochromism

Sutapa Chakraborty,[a] Paritosh Mondal,[a] S. Krishna Prasad,[b] D. S. Shankar Rao,[b] and Chira R. Bhattacharjee*[a]

Abstract: Mesomorphism induced by metal (VO^{2+}, Ni^{2+}, Cu^{2+} and Zn^{2+}) coordination and its influence on the photophysical properties of a new series of symmetric "salphen"-type *N*,*N*-bis(4-*n*-alkoxysalicylidene)-4,5-dichloro-1,2-phenylenediamine ligands (*n* = 12, 14, 16) bearing highly electronegative spacer substituents and alkoxy arms of varied length have been investigated. The mesomorphism has been probed by polarizing optical microscopy (POM), differential scanning calorimetry (DSC), and variable-temperature powder X-ray diffraction (XRD). The Schiff base ligands are non-mesomorphic; however, coordination to Ni^{II} and Zn^{II} ions induces columnar mesomorphism, this being stable down to room temperature in the latter case. Interestingly, the complexes of Cu^{II} and VO^{IV} did not show any mesomorphism. The free ligands and the Zn^{II} complexes are luminescent both in the condensed state and in solution, with emission maxima in the condensed state being significantly red-shifted with respect to those in solution. The energy-optimized structure of a representative Zn^{II} complex was ascertained to be distorted square planar in a DFT study employing the GAUSSIAN 09 program. The Zn^{II} and VO^{IV} complexes exhibited solvatochromic effects, showing interesting aggregation behavior in the former case.

Introduction

Ligands based on the π-conjugated "salphen" framework have attracted enormous attention in recent times, attributable primarily to their interesting photophysical and supramolecular properties and reactivity.[1] The extended conjugation offered by the phenyl spacer in a salphen-ligated metal system offers immense possibilities for the fabrication of photoresponsive materials, supramolecular assemblies, nonlinear optical materials, and liquid crystalline entities.[2–9] The electronic properties and steric bulk of the ligand framework can be easily varied in these systems by careful use of substituents to tune the overall potential of the resulting salphen–metal complexes.[1,10–12] Metal coordination often enhances the efficiency of salphen ligands as effective catalysts in many homogeneous and heterogeneous transformations including asymmetric ring-opening of epoxides,[13] oxidation,[14,15] epoxidation of olefins,[16,17] polymerization reactions,[18,19] carbonylation of aniline,[20] and dealkylation of organophosphates,[21] and also as Lewis acid activators in the synthesis of cyclic carbonates from terminal epoxides and carbon dioxide[22] etc.

Metallomesogens based on salphen ligands are yet another major area of application of these systems, providing access to exotic liquid crystalline materials.[8,9] The rigidity of the extensively conjugated ligand offers the required anisotropy for the construction of supramolecular structures favoring mesomorphism. Modification of components either in the salicylideneimine units or in the aryl bridging group often tunes the mesophases exhibited by these complexes, including disappearance of the mesomorphism.[8,23] Incorporating metal in a square-planar geometry is another challenging aspect because tetrahedral distortions away from planar geometry, in some cases, disrupt the required anisotropy of the core, in turn frustrating mesomorphism.[24] In the past few years, we have explored the mesomorphism of salphen-based metal complexes with different electron-donating or -withdrawing substituents across the phenylene spacer and have studied the effects of the substituents and or the nature of the central metal ion on mesomorphism.[23,25–32]

It is pertinent to mention here that the unusual square-planar geometry around the Zn^{II} center generated by the rigid ligand framework in these complexes leaves a vacant axial coordination site, leading to high Lewis acidity of the Zn^{2+} ion.[33] Bulky substituents at the 3,3′-positions of the salicyldehyde fragments in these ligands are known to lead to the isolation of unique square-planar complexes,[34] precluding chelation to suitable Lewis bases/donor ligands or the formation of aggregates/self-assembled structures.[1,33] The Lewis acidity of the Zn^{II}–salphen complexes also makes them versatile supramolecular building blocks,[5] chromogenic and fluorogenic chemosensors for detection of biologically relevant molecules,[35–37] selective receptors for tertiary amines,[38] and catalysts,[22,39] and has motivated exploration of their unique second-order nonlin-

[a] *Department of Chemistry, Assam University, Silchar 788011, Assam, India*
E-mail: crbhattacharjee@rediffmail.com
www.aus.ac.in
[b] *Centre for Nano and Soft Matter Sciences, Jalahalli, Bangalore 560013, India*

Supporting information for this article is available on the WWW under http://dx.doi.org/10.1002/ejic.201600513.

ear optical properties.[6,7] Further, the square-pyramidal geometry of the vanadyl ion in oxovanadium(IV)–salphen complexes renders the coordination sphere unsaturated. The structure can be related to an octahedron with an axial vacant site, which can be filled quite readily through intermolecular dative interactions or coordination to neutral or anionic donors or Lewis bases.[24,40] Dative interactions are of particular interest in the case of the square-pyramidal vanadyl complexes because they produce linear chain-like structures, (•••V=O•••V=O•••) creating a polar order. This offers possibilities for the generation of new ferroelectric/piezoelectric materials.[41]

Against this backdrop, we report a series of "salphen"-type symmetric *N*,*N*-bis(4-*n*-alkoxysalicylidene)-4,5-dichloro-1,2-phenylenediamine ligands (*n* = 12, 14, 16) and their complexes with VO^{IV}, Ni^{II}, Cu^{II}, and Zn^{II} metal ions. The "dichloro-phenylene spacer" was chosen in this work to allow exploration both of the steric and the electronic effects of the two vicinal electronegative chloro groups on the overall mesomorphic and photophysical properties of the newly synthesized compounds. The effects of metal coordination on mesomorphism and on the photophysical properties of the salphen ligands have been investigated. Except in one instance, in which a long (C-12) alkoxy-substituted spacer has been employed to access some mesomorphic Mn^{III} complexes there appear to be no other examples of metallomesogens based on salphen systems with vicinal disubstituted spacer groups in the literature.[8] The free ligands are non-mesomorphic; however, coordination to Ni^{II} and Zn^{II} ions induces columnar mesomorphism in the resulting complexes, although the VO^{IV} and Cu^{II} complexes are non-mesomorphic. Interestingly, for the Zn^{II} complexes, the mesophase formed is observed to be stable down to room temperature. The free ligands and the Zn^{II} complexes showed photoluminescence both in solution and in the condensed state. In addition, the Zn^{II} and VO^{IV} complexes showed interesting solvatochromism, with the former showing concomitant formation of aggregates depending on the coordinating ability of the solvent.

Results and Discussion

Synthesis and Characterization

Condensation of 4-*n*-alkoxy-substituted salicylaldehydes with 4,5-dichlorobenzene-1,2-diamine afforded the corresponding salphen ligands. Complexes were obtained by treatment of the corresponding Schiff bases with vanadyl sulfate ($VOSO_4 \cdot H_2O$), nickel acetate [$Ni(OAc)_2 \cdot 2\,H_2O$], copper acetate [$Cu(OAc)_2 \cdot 2\,H_2O$], or zinc acetate [$Zn(OAc)_2 \cdot 2\,H_2O$] in 1:1 molar ratio. The strategy implemented for the synthesis of ligands [*N*,*N*-bis(4-*n*-alkoxysalicylidene)-4,5-dichloro-1,2-diaminobenzene], abbreviated as *n*c2pd (number of carbon atoms in alkyl chains *n* = 12, 14, and 16) and the mononuclear complexes (VO-*n*c2pd, Ni-*n*c2pd, Cu-*n*c2pd, or Zn-*n*c2pd) is summarized in Scheme 1. The structure of the ligands and the corresponding complexes were ascertained by elemental analyses and UV/Visible, FTIR, and ^1H NMR (for ligands and Ni^{II} and Zn^{II} complexes only) spectroscopy.

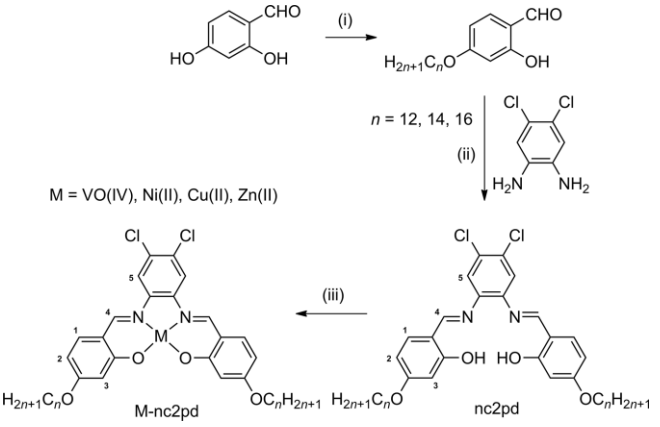

Scheme 1. (i) $C_nH_{2n+1}Br$, $KHCO_3$, KI, dry acetone, Δ, 24 h, (ii) glacial acetic acid, absolute EtOH, Δ, 3 h, (iii) $M(OAc)_2 \cdot 2\,H_2O$ (M = Ni, Cu, Zn)/$VOSO_4 \cdot H_2O$, MeOH, stirring, 3 h.

The IR spectra of the ligands showed bands corresponding to the $\nu_{C=N}$ and ν_{O-H} vibrations at ca. 1614 and 3436 cm^{-1}, respectively. For the corresponding metal complexes the $\nu_{C=N}$ vibrations were observed at lower wavenumbers than for the free ligands along with the absence of ν_{O-H} vibrations, suggesting coordination of the imine nitrogen and phenolate oxygen to the metal center. The VO^{IV} complexes additionally showed $\nu_{V=O}$ stretching at ca. 971 cm^{-1} indicating the absence of any intermolecular (•••V=O•••V=O•••) interaction, consistently with the monomeric nature of the complexes.[25] The V=O stretching frequency is an indicative test for oxygen bridging in five-coordinate square-pyramidal vanadyl(IV) complexes. In general, for polymeric complexes this band appears below 900 cm^{-1}, due to linear chain interactions, whereas for monomeric ones it is located in the 900–1000 cm^{-1} region.[25,42]

The ^1H NMR spectra of the ligands (*n*c2pd) showed characteristic signals at δ = 13.17 ppm, corresponding to the OH protons, and ca. 8.52 ppm, for the symmetric imine protons. The ^1H NMR spectra of the corresponding Ni^{II} and Zn^{II} complexes did not exhibit any signal for the phenolic –OH proton. However, upfield shifts in the peak positions of –N=CH protons with respect to the free ligands were observed for both complexes, confirming azomethine nitrogen coordination.

Liquid Crystalline Properties

The thermal behavior of the ligands and of the corresponding metal complexes was investigated by polarizing optical microscopy (POM), differential scanning calorimetry (DSC), and variable-temperature powder X-ray diffraction (XRD). The ligands are non-mesomorphic, melting directly to isotropic liquids at 80–90 °C. However, coordination of the salphen ligands, particularly to Zn^{II} and Ni^{II} ions, conferred liquid crystalline properties on the resulting complexes. The Cu^{II} complexes decomposed just at the onset of melting at 120 °C. The VO^{IV} analogues, on the contrary, decomposed prior to melting at temperatures higher than 280 °C, precluding any mesomorphic study. This unusual thermal behavior of the VO^{IV} and Cu^{II} complexes can be explained by invoking axial interaction for the stability of the mesophase.

Square-planar copper(II)–salen or –salphen complexes are coordinatively unsaturated and the metal center usually achieves full occupation through interaction with neighboring molecules in the axial direction. This additional interaction favors the formation of a one-dimensional array of the molecules.[24] Tetrahedral distortions away from the square-planar coordination in some cases prevent this axial interaction involving oxygen atoms of neighboring mesogens, preventing mesophase formation.[24,43] In the current salphen-Cu^{II} complexes, the electron-withdrawing dichloro substitution on the phenylene spacer is considered to disturb the axial interaction, hence resulting in decomposition of the complexes. Similar observations were noted earlier in the cases of analogous Cu^{II}–salphen complexes with nitro-substituted phenylene spacers.[23]

The VO^{IV}–salphen complexes, on the other hand, each adopt a square-pyramidal geometry, which is nonplanar and less anisotropic. The axial vanadyl oxygen atom is believed to form a weak dative bond with the vanadium atom of a neighboring mesogen, thus assembling the cores into an one-dimensional array, favoring mesophase formation.[24] Again, too-rigid linear V=O···V=O interactions may lead to polymeric complexes, causing loss of mesomorphism.[42] Therefore, the length of the V=O bond (i.e., the extent of axial interaction) is crucial to the formation of mesophases. The relatively high temperatures of decomposition of the VO^{IV} complexes in this study can thus be accounted for by invoking (i) the presence of the dichloro substituents on the phenyl spacer, which might somewhat obscure the extruding oxo group, or (ii) possible trigonal-bipyramidal distortion in the metal coordination geometry.[24]

The complexes Ni-*n*c2pd and Zn-*n*c2pd exhibited enantiotropic mesomorphism (Table 1). The Ni^{II} complexes displayed a somewhat atypical texture (Figure 1, a) at 150 °C upon slow cooling from the isotropic melt. The Zn^{II} complexes, on the other hand, showed a broken fan-like texture characteristic of columnar phases (Figure 1, b) at 160 °C.[44] The optical texture of the Zn-*n*c2pd complexes remained unaltered down to room temperature.

The DSC thermogram of Ni-16c2pd displayed four endothermic peaks in the first heating cycle, due to two crystal–crystal transitions, one crystal–mesophase transition, and one mesophase–isotropic liquid transition (Figure 2, a). In the cooling cycle, four exothermic peaks were observed, corresponding to

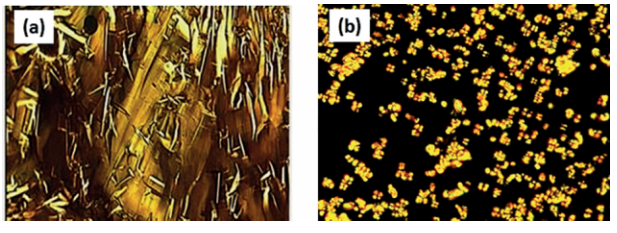

Figure 1. POM photographs of (a) Ni-16c2pd at 150 °C and (b) Zn-16c2pd at 160 °C, on cooling.

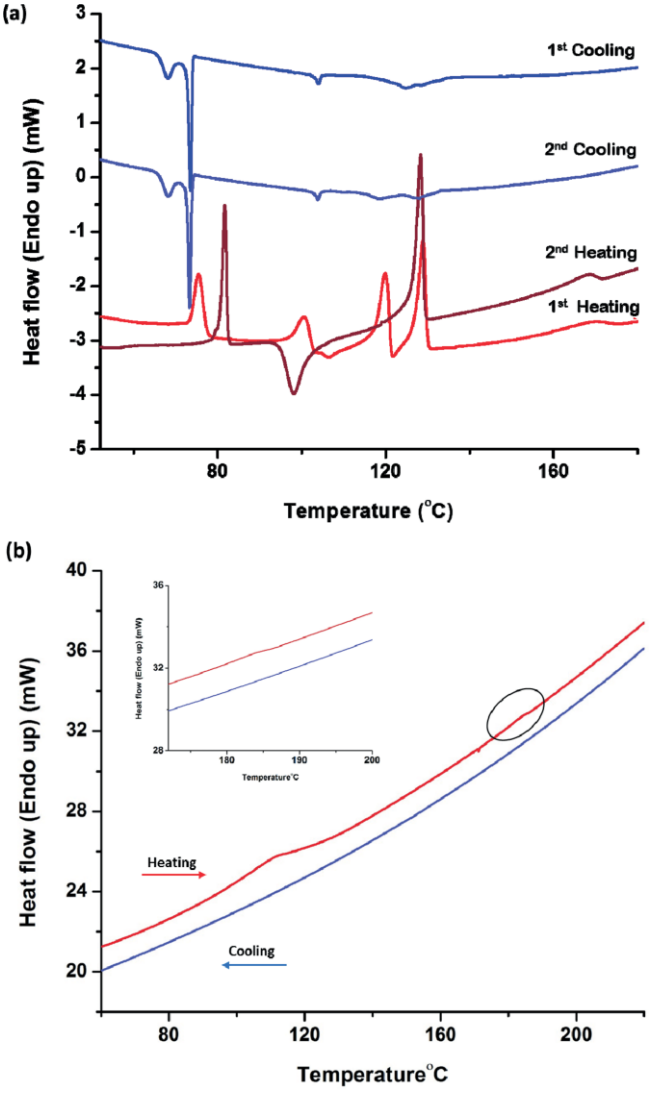

Figure 2. DSC thermogram of (a) Ni-16c2pd during first and second heating and cooling cycles, and (b) Zn-16c2pd during first heating and cooling cycles.

Table 1. Thermodynamic data for the Ni^{II} and Zn^{II} complexes. Transition temperatures are given in °C, and the corresponding enthalpy changes are in parentheses (ΔH, J g^{-1}). Cr, Cr_1, and Cr_2 refer to phases that are crystalline or solid. Col_o: oblique columnar phase. Col_r: rectangular columnar phase.

	Heating cycle[a]	Cooling cycle[a]
Ni-12c2pd	Cr 105(1.3) Col_o 192(21.3) I	I 185(22.9) Col_r 99(1.3) Cr
Ni-14c2pd	Cr 98(59.3) Col_o 184.5(9.9) I	I 172(25.1) Col_o 79(3.5) Cr
Ni-16c2pd[b]	Cr 75.7(20.5) Cr_1 100.6(6.9) Cr_2 128(45.7) Col_o 167(6.8)I	I 127(12.3) Col_o 104(1.3) Cr_2 73(13.3) Cr_1 68(5.5) Cr
Ni-16c2pd[c]	Cr 81.6(20.4) Cr_1 98.3(–3.7) Cr_2 128(29.8) Col_o 169(7.4)I	I 127(11.5) Col_o 103(1.6) Cr_2 73.2(13.1) Cr_1 68(5.3) Cr
Zn-12c2pd	Cr 144(15.4) Col_r 253(1.4) I	I 247.3[d] (–) Col_r
Zn-14c2pd	Cr 122(20.6) Col_r 235(1.7) I	I 225.4[d] (–) Col_r
Zn-16c2pd	Cr 111(23.2) Col_r 183(1.2) I	I 177.2[d] (–) Col_r

[a] DSC peak temperature. [b] First heating. [c] Second heating. [d] Optical microscopy data.

isotropic liquid–mesophase, mesophase–crystal, and two crystal–crystal transitions. The endothermic peak observed at 101 °C in the first heating run appeared as an exothermic peak at 98 °C in the second heating run (Figure 2, a). This is surmised to be originating from a low-energy crystal packing at higher temperatures.[45] The DSC traces for Ni-12c2pd and Ni-14c2pd, however, each consisted of only two peaks both in the heating and in the cooling cycle (Figures S1 and S2 in the Supporting Information and Table 1). The DSC thermogram of Zn-*n*c2pd with ***n*** = 12 (Figure S3 in the Supporting Information), 14 (Figure S4 in the Supporting Information), and 16 (Figure 2, b) each displayed two endothermic peaks in the heating cycle, corresponding to crystal–mesophase and mesophase–isotropic liquid transitions. In the cooling cycle, the isotropic liquid–mesophase transition as observed in the POM could not be identified by DSC. The absence of this peak in the cooling cycle of the DSC thermogram, accompanied by the low enthalpy value for the mesophase–isotropic liquid transition in the heating scan, suggests that the mesophase is highly disordered.[46] A gradual decrease in the clearing temperature was noted on increasing the number of carbon atoms in the alkoxy arms. The isotropic liquid-to-mesophase transition temperature also displayed similar trends with increasing chain length. The reversibility of the thermal behavior was verified by DSC in subsequent heating/cooling cycles.

The XRD pattern of Ni-16c2pd at 126 °C (Figure 3) consisted of a number of Bragg diffraction peaks in the small-angle region. In addition, two diffuse halos were observed in the wide-angle region: a broad one at 4.7 Å for the lateral short-range order of molten alkyl chains and another, less broad halo at 3.7 Å, probably due to the liquid-like correlation between adjacent cores. X-ray diffraction profiles obtained over a wide temperature range (126–80 °C) were very similar (Figures S5 and S6 in the Supporting Information). Profile fitting of the data matched well with those for a two-dimensional oblique columnar phase (Col_o) with a *p*1 space group.[47,48] The lattice parameters *a*, *b*, and γ were found to be 57.39 Å, 99.38 Å, and 69.8°, respectively (Table 2). In a columnar oblique phase, the elementary cell is made up of two columns (Figure 5a, below).[47,48] If a density of 1 g cm^{-3} is assumed for these half-discoid molecules[48] and a periodic stacking value of 3.7 Å of the molecular cores within the column is estimated, we can infer that the columnar cross-section is made up of six molecules (N_{col} = 6). To account for the supramolecular organization in the mesophase, it is assumed that the molecules of the nickel complexes self-assemble into dimers in an antiparallel fashion (Figure 5, c, below).[8,23] Three such dimers stack side by side to cover the surface area of a thin slice of a disk.[8] The lattice constant *a* in this case is considerably greater than the DFT-optimized radius of a fully extended molecule (vide infra), thus further supporting the proposed arrangement.

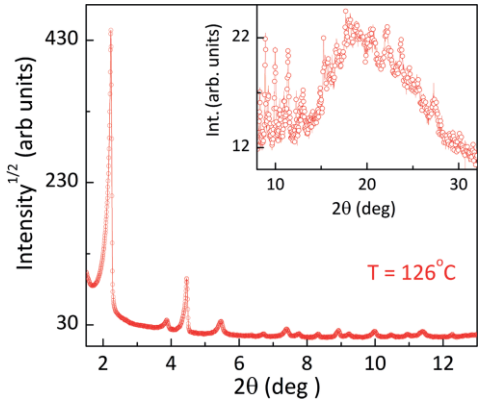

Figure 3. X-ray diffraction pattern of Ni-16c2pd at 126 °C.

Table 2. X-ray diffraction data for Ni-16c2pd and Zn-16c2pd.

	Temp. [°C]	$d_{meas.}$ [Å][a,b]	$d_{calcd.}$ [Å][a]	Miller indices (*hkl*)[c]	Mesophase parameters[d]
Ni-16c2pd	126	39.59^s	39.59	110	Col_o, *p1*
		22.92^s	22.92	130	a_o = 57.32 Å
		19.80^s	19.80	100	b_o = 99.38 Å
		16.21^s	16.21	250	γ = 69.8°
		13.17^s	13.20	330	S_o = 5346.05 Å^2
		11.96^s	12.13	450	V_{cell} = 20052.23 Å^3
		11.41^s	11.44	030	S_{col} = 2673.03 Å^2
		10.63^s	10.72	570	V_{mol} = 1629.86 Å^3
		9.92^s	9.90	200	N_{cell} = 12.3, N_{col} = 6.15
		9.58^s	9.54	380	
		8.87^m	8.73	270	
		8.44^m	8.58	680	
		8.08^m	8.08	430	
		7.77^m	7.77	$\bar{2}$10	
		6.90^m	6.86	050	
		5.80^m	5.77	530	
		4.74^d	4.67	–	
		4.01	4.01	620	
		3.75	–	–	
Zn-16c2pd	140	44.78^s	45.83	100	highly disordered LC
		4.5^d	–	–	
	25	52.12^s	51.35	100	Col_r, *p2mm*
		30.97^s	31.00	010	a_r = 51.35 Å
		24.56^s	25.67	200	b_r = 31.0 Å
		16.47^m	17.12	300	S_r = 1591.85 Å^2
		15.56^m	15.50	020	V_{cell} = 6717.6 Å^3
		4.22^d	–	–	V_{mol} = 1543.20 Å^3
					N_{cell}/N_{col} = 4.35

[a] $d_{meas.}$ and $d_{calcd.}$ are the experimentally measured and calculated diffraction spacings. [b] Intensities of the reflections, s: sharp, m: medium, d: diffuse. The distances are given in Å. [c] [*hkl*] are the Miller indices of the reflections. [d] Phase parameters, Col_o phase: $1/d_{hk} = 1/\sin\gamma\ \sqrt{[(h/a_o)^2 + (k/b_o)^2 - (2hk\cos\gamma/a_ob_o)]}$, γ is columnar tilt angle; lattice area, $S_o = a_ob_o\sin\gamma$; columnar cross-section, $S_{col} = a_ob_o/2$; Col_r phase: $a_r = d_{10}$; $1/d_{hk} = \sqrt{[(h/a_r)^2 + (k/b_r)^2]}$; columnar cross-section in the rectangular cell, $S_r = a_rb_r$. V_{cell}, volume of an elementary cell: Col_o phase, $V_{cell} = a_ob_o\sin\gamma \times h$; Col_r phase, $V_{cell} = a_rb_r \times h$, where *h* is intracolumnar repeating distance. V_{mol} (molecular volume) is determined by considering a density of 1 g cm^{-3} according to the relationship $MW/\lambda\rho N_A$, where *MW* is the molecular weight, N_A is the Avogadro number, and $\lambda(T)$ is a temperature correction coefficient at the temperature of the experiment (*T*), $\lambda(T) = V_{CH_2}(T°)/V_{CH_2}(T)$, where $V_{CH_2}(T) = 26.5616 + 0.02023\ T$ is the volume of a methylene group (in Å^3) at a given temperature (in °C), and $T° = 25$ °C. N_{cell} is the number of molecules per unit cell, and N_{col} is the number of molecules per columnar cross-section.

The X-ray diffractogram of Zn-16c2pd at 140 °C (Figure 4, a) consisted of a single diffraction maximum at low angles that corresponds to Miller index (100). At wide angles, a broad halo was observed at 4.6 Å, corresponding to liquid-like correlation of the molten alkyl chains. The absence of additional characteristic features in the diffraction pattern precluded unambiguous

assignment of the mesophase at higher temperatures. The diffraction pattern at 25 °C (Figure 4, b), however, consisted of five reflections in the small-angle region, at 52.12, 30.97, 24.56, 16.47, and 15.56 Å (Table 2). In fact, spacing for the second reflection, from the lowest-angle side, is far from being a second harmonic of the first peak. Thus, a lamellar structure is ruled out. Accordingly, these were assigned as (100), (010), (200), (300), and (020) reflections of a two-dimensional rectangular lattice. Application of extinction rules to the estimated indexations excluded the possibility of the *c2mm* and *p2gg* plane groups (for *c2mm*, *hk*: $h + k = 2n$, *h*0: $h = 2n$, 0*k*: $k = 2n$; for *p2gg*, *hk*: no conditions, *h*0: $h = 2n$, 0*k*: $k = 2n$) that are commonly observed.[44,49] Also, the absence of reflections with a set of restrictions; hk: no conditions, *h*0: no conditions, 0*k*: $k = 2n$, ruled out the possibility of *p2mg* symmetry.[44,49] In this scenario, because no specific symmetry rules are followed it is presumed that the columns are packed in accordance with an overall *p2mm* symmetry (Figure 5, b).[49] In addition to the small-angle reflections, a broad halo was observed in the wide-angle region at 4.2 Å, corresponding to the liquid-like nature of molten alkyl chains. However, no second diffuse peak such as would be expected for intracolumnar stacking was observed, thus suggesting high disorder along each column, which would also justify small enthalpy values associated with the clearing process.[46] If a stacking periodicity of 4.2 Å for the molecular cores is assumed, it could be deduced that the columnar cross-section is formed by four molecules. In this case, the columnar cross-section is formed by lateral arrangement of two dimers (Figure 5, c). The lattice parameter a_r (51.35 Å) in this case is smaller than that of the Ni^{II} complex, consistently with the proposed organization. Also, the columnar mesophase of the Zn^{II} complex is rather disordered at high temperatures, relative to the Ni^{II} complexes, so indexation of the PXRD pattern was only possible at room temperature, in a frozen state. Size of the metal ion, in addition to the geometry of the core, is therefore an important factor and any significant variation in the ionic radii also affects the thermal stability of the resulting complexes.[50]

A rich mesomorphic diversity has also been found in structurally related salphen systems containing unsubstituted or monosubstituted phenylenediamine spacers, containing either electron-donating methyl or electron-withdrawing chloro or nitro substituents. A critical comparison of the metal complexes of all such ligand systems with regard to mesomorphism is presented in Table 3. In cases of salphen systems with unsubstituted or electron-donating methyl-substituted spacers, although the complexes are all mesomorphic, the thermal stability and/or the nature of the two-dimensional packing of the columns in the lattices are quite different.[23,25,26,29,31,32] For

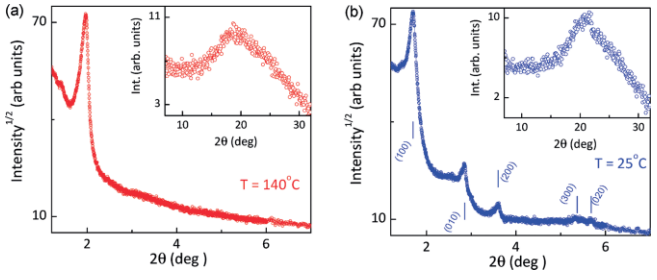

Figure 4. X-ray diffraction pattern of Zn-16c2pd: (a) at 140 °C, and (b) at room temperature (25 °C).

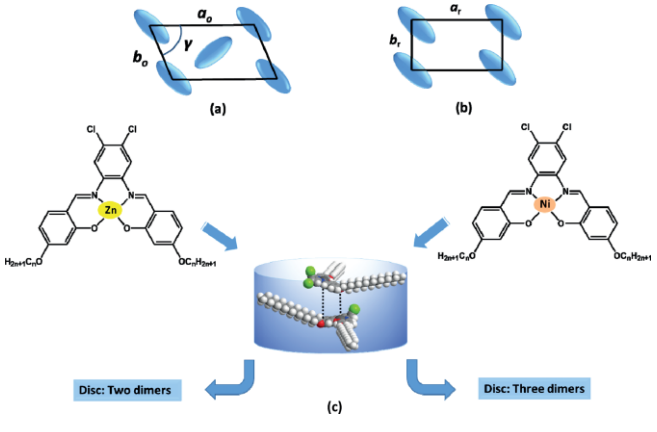

Figure 5. Schematic illustration of (a) unit cell of a two-dimensional columnar oblique lattice (*p1*), (b) unit cell of a two-dimensional rectangular columnar *p2mm* lattice, and (c) model for dimeric association of the molecules and molecular organization in the mesophase.

Table 3. Mesomorphism and photoluminescence of metal complexes with different "salphen" spacer substituents (PL: photoluminescence, +: PL-active.

Spacer	Complex	Mesophase (symmetry)	PL	References
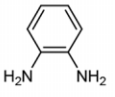	Zn-16opd	Col_r/Col_o (P_{222}/P_{112})	+	[23, 26, 29, 31]
	Ni-16opd	Col_r (*c2mm*)	+	
	VO-16opd	Col_L	–	
	Cu-16opd	Col_{rp}	–	
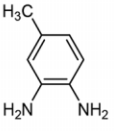	Zn-16mpd	Col_h	+	[23, 25, 26, 32]
	Ni-16mpd	Col_r (*c2mm*)	+	
	VO-16mpd	$Col_{r1} \rightarrow Col_{r2}$ (*c2mm*)	–	
	Cu-16mpd	Col_r (*c2mm*)	–	
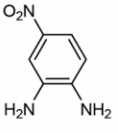	Ni-16npd	Col_r (*c2mm*)	+	[23, 26]
	Cu-16npd	Non-LC	–	
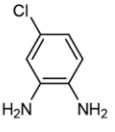	Zn-16cpd	Col_r (*p2gg*)	+	[27]
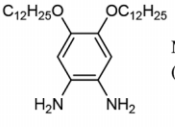	MnXL^4 (X = Cl, Br)	Col_h	–	[8]
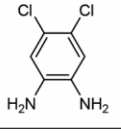	Zn-16c2pd	Col_r (*p2mm*)	+	this work
	Ni-16c2pd	Col_o (*p1*)	–	
	VO-16c2pd	Non-LC	–	
	Cu-16c2pd	Non-LC	–	

nitro-substituted salphen ligands, whereas the Ni^{II} complexes are mesomorphic, the Cu^{II} complexes undergo decomposition.[23,26] Similar behavior has been noted for the Cu^{II} complexes studied here. Cu^{II} complexes of unsubstituted or methyl-substituted ligands were, however, mesomorphic, displaying Col_{rp} or Col_r phase, respectively.[23]

The previously reported Ni^{II} complexes all exhibited rectangular columnar mesophases (*c2 mm*), though the phase transition is monotropic for nitro- and methyl-substituted derivatives and enantiotropic for unsubstituted ones.[26] The Ni^{II} complexes currently under study, however, show enantiotropic oblique columnar phases.

Of the differently substituted Zn^{II} complexes, those without any substituent or with an electron-donating methyl group in the spacer displayed monotropic columnar mesomorphism. Mesophases exhibited by these complexes were either rectangular/oblique columnar (P_{222}/P_{112}) or hexagonal columnar of varied symmetries.[31,32] In contrast, with the electron-withdrawing Cl substituent in the spacer, enantiotropic phase behavior is observed for the chloro-substituted Zn^{II} complexes, which exhibit rectangular columnar phases with *p2gg* symmetry.[27]

In the case of VO^{IV} complexes, whereas the unsubstituted ones exhibited columnar lamellar mesomorphism, a cross-over between two rectangular columnar phases has been observed in the methyl-substituted representatives.[25,29] In each case the mesophase is stable down to room temperature and the nature of the phase transition is enantiotropic. The VO^{IV} complexes under investigation here, however, undergo high-temperature decomposition, frustrating mesomorphism in turn.

Thus, a minor modification of the steric or electronic properties in the spacer can have a major influence on the thermal properties of the salphen systems and the resulting complexes. The role of the metal center is also crucial. A subtle interplay of electronic factors originating from the phenylene spacer and distortions in coordination geometry associated with the nature of metal ions might therefore be responsible for the observed mesomorphic diversity.

Photophysical Properties

The photophysical properties of the salphen ligands *n*c2pd and their corresponding metal complexes – VO-*n*c2pd, Ni-*n*c2pd, Cu-*n*c2pd, and Zn-*n*c2pd – were recorded in dichloromethane solution (conc. 10^{-5} M) and in the solid state at 298 K (Figures 6 and 7). The spectroscopic data for the compounds are listed in Table 4.

The salphen ligands each exhibited two broad absorption bands with maxima at 300 nm and 336 nm and a shoulder at 355 nm corresponding to π–π* transitions of the aromatic rings and the imine unit (Figure 6). After coordination, all the absorption bands were shifted significantly to longer wavelengths, with the longer-wavelength feature acquiring substantial charge-transfer character. For Cu^{II} complexes, an additional peak was observed at 350 nm in each case. For Ni^{II} complexes, the higher-wavelength feature at 475 nm (Figure 6) is believed to be of charge-transfer character. This is ascribed to the excitation of filled d orbital electrons into the empty antibonding π orbitals (d→π*) of the salphen ligand.[51,52] Moreover, the alkyl chain length variation had virtually no effect on the spectral behavior in all cases.

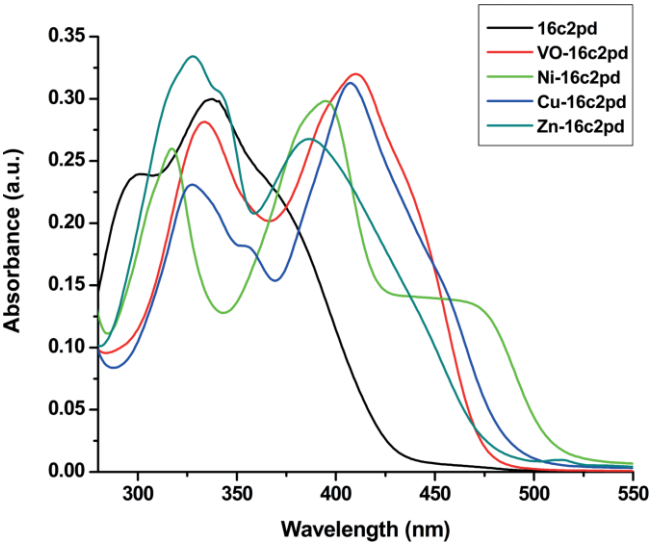

Figure 6. UV/Visible spectra of 16c2pd and its metal complexes in dichloromethane solution (1×10^{-5} M, room temp.).

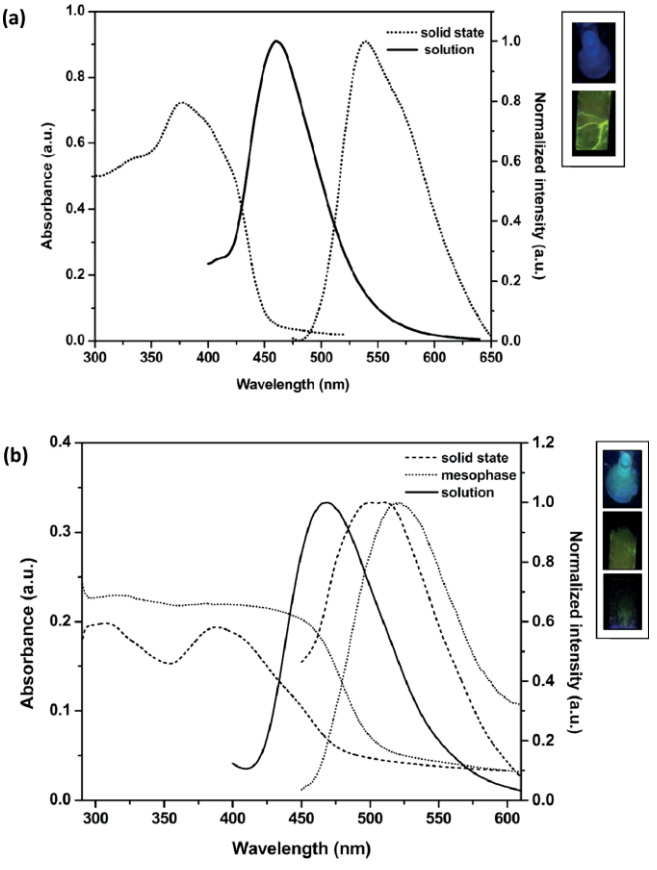

Figure 7. (a) Absorption (left) and normalized fluorescence emission (right) spectra of 16c2pd, and (b) absorption (left) and normalized fluorescence emission (right) spectra of Zn-16c2pd in dichloromethane (1×10^{-5} M, room temp.) solution (–), solid state (----) and mesophase (•••). Side panels show photoluminescence pictures of solution (top), solid state (middle), and mesophase [bottom, (b) only], respectively, as seen after irradiation with 366 nm light.

Table 4. Absorption data for the ligands (n = 12, 14, 16) and their metal complexes in various solvents, molar absorption coefficient (ε) in M^{-1} cm^{-1}, and photoluminescence data for ligands and Zn^{II} complexes in solution and the solid state at 298 K. (-do- stands for a value similar to that of the preceding data in the column.)

	Solvent	$\lambda_{abs}(\varepsilon/10^4)$ nm	[a] λ_{em}^{max} [nm] (solution)	[b] λ_{em}^{max} [nm] (solid)	[c] $\Phi_{F(solution)}$	[d] $\Phi_{F(solid)}$
12c2pd	CH_2Cl_2	300(2.2), 336(2.9), 358(2.5)	460	538	0.09	0.04
14c2pd	-do-	300(2.2), 336(3.1), 358(2.4)	-do-	-do-	0.10	0.03
16c2pd	-do-	300(2.3), 336(3.0), 358(2.5)	-do-	-do-	0.10	0.04
VO-12c2pd	-do-	334(2.8), 410(3.1), 427^{sh} (2.6)	–	–	–	–
VO-14c2pd	-do-	334(2.7), 410(3.1), 427^{sh} (2.5)				
VO-16c2pd	-do-	334(2.8), 410(3.2), 427^{sh} (2.6)				
Ni-12c2pd	-do-	317(2.5), 396(2.9), 475 (1.4)	–	–	–	–
Ni-14c2pd	-do-	317(2.7), 396(3.0), 475 (1.7)				
Ni-16c2pd	-do-	317(2.6), 396(2.9), 475 (1.5)				
Cu-12c2pd	-do-	328(2.2), 350(1.9), 407 (3.2) 433^{sh} (2.4)	–	–	–	–
Cu-14c2pd	-do-	328(2.3), 350(1.8), 407 (3.2) 433^{sh} (2.3)				
Cu-16c2pd	-do-	328(2.3), 350(1.8), 407 (3.1) 433^{sh} (2.3)				
Zn-12c2pd	-do-	327(3.2), 386(2.5), 411^{sh} (2.1)	468	504	0.19	0.07
Zn-14c2pd	-do-	327(3.4), 386(2.6), 411^{sh} (2.3)	-do-	-do-	0.19	0.07
Zn-16c2pd	CH_2Cl_2	327(3.3), 386(2.6), 411^{sh} (2.2)	468	-do-	0.20	0.08
	$CHCl_3$	327(3.5), 386(2.8), 413^{sh} (2.3)	468		0.20	
	toluene	327(3.3), 391(2.9), 415^{sh} (2.4)	468		0.21	
	THF	323(3.5), 403(3.4), 426^{sh} (2.6)	469		0.30	

[a] λ_{ex} = 336 nm (ligand), 320 nm (Zn complex). [b] λ_{ex} = 386 nm (ligand), 320 nm (Zn complex). [c] Estimated error: ± 5 %. [d] Estimated error: ± 10 %.

Photoluminescence study of the compounds was carried out in dichloromethane solution (conc. 10^{-5} M) and in the solid state at room temperature. Emission spectra in the solid state were recorded by placing a uniform powder sheet of the sample between two quartz plates. The ligands and the Zn^{II} complexes are luminescent. As a representative example, Figure 7 shows the photoluminescence spectra of 16c2pd and Zn-16c2pd, respectively. Emission spectra of the ligands in dichloromethane solution each consisted of a broad band with maxima at ca. 460 nm associated with intraligand π–π* electronic transitions. Previously reported unsubstituted or monosubstituted ligands were however, nonluminescent.[26,27,31,32] Further, whereas the corresponding Ni^{II} complexes were both photoluminescent, the Ni^{II} complexes with the dichloro-substituted phenylenediamine spacer currently under investigation are not (Table 4). The emission maxima for the corresponding Zn^{II} complexes were bathochromically shifted (ca. 8 nm) relative to the free ligands. The observed fluorescence emission in the Zn^{II} complexes originates from metal-perturbed π–π* ligand-centered transitions. The emission intensity is increased on complexation because chelation provides additional rigidity to the salphen framework.[27]

The solid-state emission spectra of the ligands and the Zn^{II} complexes indicated a structure similar to that in solution (Figure 7, a and b). However, emission maxima both for the ligands and for the corresponding Zn^{II} complexes were substantially red-shifted with respect to solution, with the associated shifts for the ligands and for the Zn^{II} complexes being 78 nm and 36 nm, respectively. The red shift of the emission maxima in the solid state can be attributed to closer association of aromatic cores with a reduction in the local mobility, which reduces deactivation through non-radiative channels.[27] As for the Zn^{II} complexes, because the mesophase is stable down to room temperature, a photoluminescence study was conducted in this state as well. The mesophase emission maximum is located at 518 nm ($\lambda_{exc.}$ = 320 nm), bathochromically shifted with respect to that observed in solution (468 nm) and in the solid state (504 nm).

In addition, a solvatochromic study of a representative complex from each series – VO-16c2pd, Ni-16c2pd, Cu-16c2pd, and Zn-16c2pd – in dilute solutions in solvents (10^{-5} M) of different polarities was also carried out. For the Cu^{II} and the Ni^{II} complexes, absorption features in coordinating solvent (THF) were similar to those observed in the case of noncoordinating solvents (Figure S8, Figure S9, and Table S1 in the Supporting Information).

Absorption spectra of VO-16c2pd in noncoordinating solvents consisted of two well-defined bands at 334 nm and 410 nm with a shoulder at 427 nm; however, in coordinating solvent (THF) only two bands were observed, with substantial broadening and red shift of the second absorption feature and the shoulder at longer wavelength being overlapped by the second band (Figure S7 and Table S1 in the Supporting Information). This observation can be related to the weak interaction of the solvent molecule *trans* to the vanadyl oxo ligand.[53] The d level ordering in five-coordinate square-pyramidal complexes of vanadyl ion (VO^{2+}) is:[54] $d_{xy} < d_\pi(d_{xz}, d_{yz}) < d_{x^2-y^2} < d_{z^2}$. The lower-wavelength band is ascribed to the $d_{xy} \rightarrow d_{x^2-y^2}$ transition whereas the higher-wavelength band appears to be due to the $d_{xy} \rightarrow d_\pi$ transition of vanadium. The antibonding d_π orbital participates in the $p_\pi \rightarrow d_\pi$ donation from the vanadyl oxygen atom, whereas the antibonding $d_{x^2-y^2}$ orbital depends on the strength of the in-plane ligand field. To minimize the accumulation of charge on V^{IV}, the π donation from the axial oxygen decreases as the in-plane donor strength of the ligand increases.[55] It is speculated that the square-pyramidal structure of the complex is subtly perturbed upon solvent coordination, with the V=O group moving toward the equatorial plane of the ligand, resulting in an enhancement of the ligand–vanadium interaction. Coordination of a solvent molecule in the sixth po-

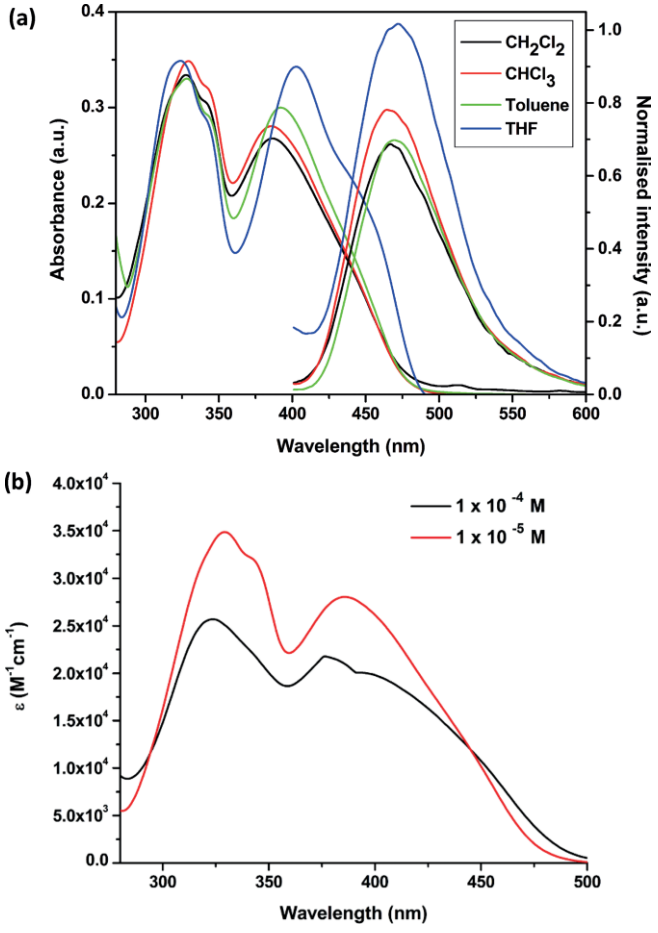

Figure 8. (a) UV/Visible (left) and fluorescence (right) spectra of Zn-16c2pd in noncoordinating and coordinating solvents (1×10^{-5} M). (b) Concentration-dependent UV/Visible absorption spectra of Zn-16c2pd (CH_2Cl_2, room temp.).

sition, *trans* to the axial oxygen, thus decreases the π-donation of the axial oxygen to the metal. As a result the antibonding d_π orbital is stabilized whereas the $d_{x^2-y^2}$ orbital is destabilized. This accounts for the decrease in the molar absorptivity values and the observed shift in THF.

The Zn^{II} complexes, however, exhibited an interesting solvent-induced aggregation phenomenon. The absorption spectra of Zn-16c2pd in noncoordinating solvents (e.g., CH_2Cl_2, $CHCl_3$, toluene) showed two well-defined bands located at ca. 328 nm and 386–391 nm, together with a shoulder at 413 nm (Figure 8, a), indicating the presence of aggregates.[56,57] On switching to a coordinating solvent (e.g., THF), solvent-induced deaggregation caused substantial changes in the optical absorption spectrum. Hyperchromism accompanied by a red shift of the longer-wavelength feature was observed. The results are consistent with the formation of H-type aggregates, similarly to what has been observed in related salphen systems.[56] Concentration variations had no effect on these spectral features up to a concentration of 1×10^{-4} M (Figure 8, b). Photoluminescence spectra of Zn-16c2pd (Figure 8, a) in noncoordinating solvents each consisted of a broad band with a maximum at about 468 nm. This remained virtually unaltered in THF, though an enhancement in fluorescence intensity, indicating the formation of a 1:1 adduct, could be observed. The emission quantum yield (EQY) values in noncoordinating solvents (e.g., CH_2Cl_2, $CHCl_3$, toluene) are close to 20 %; this is enhanced (EQY = 30 %) upon deaggregation in THF. Quenching of fluorescence of face-to-face-stacked H-type dimer aggregates (sandwich-type dimers) relative to monomer in the present case, as well as in previous ones with asymmetrically methyl-substituted Zn^{II}–salen[57] and analogous Zn^{II}–salphen complexes,[56] may be argued to be a consequence of rapid energy relaxation of the lower excited states.[58]

DFT Study

Because diffraction-quality single crystals could not be isolated, density functional theory (DFT) was used to arrive at the energy-optimized electronic structures of the complexes. The representative Zn^{II} complex Zn-16c2pd was chosen for the purpose. All the quantum chemical calculations were performed with the GAUSSIAN 09 program package.[59] The ground-state geometry optimization of the complex in the gas phase was performed by use of the three-parameter fit of the Becke hybrid functional combined with the Lee–Yang–Parr correlation functional termed the B3LYP hybrid,[60,61] as well as generalized gradient approximation (GGA) exchange along with the 6-311+G(d,p), 6-31+G(d,p), 6-31G(d), and 6-31G basis sets[62] for Zn, N and O, C and H, respectively, without imposition of any symmetry constraint. The appropriate structure of the complex was confirmed as an energy minimum by calculation of the vibrational frequency and confirmation of the absence of any

Table 5. Selected interatomic distances [Å] and angles [°] in Zn-16c2pd optimized at the B3LYP level.

Structural parameter	Interatomic distances [Å] and angles [°]
Zn–O1	1.912
Zn–O2	1.912
Zn–N1	2.039
Zn–N2	2.039
O1–Zn–O2	104.2
N1–Zn–N2	81.0
N1–Zn–O1	92.6
N2–Zn–O2	92.6
N1–N2–O2–O2	–33.3
N1–O1–O2–N2	30.9
molecular length	42.6
dipole moment	1.28 D

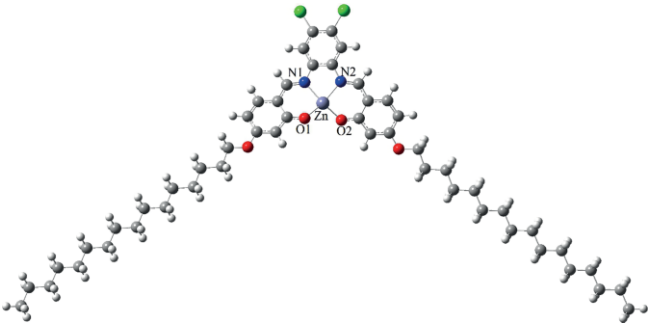

Figure 9. Optimized electronic structure of Zn-16c2pd.

imaginary frequencies. Key geometric parameters of the optimized Zn-16c2pd complex, estimated by DFT at the B3LYP level, are gathered in Table 5. Average bond angles about the metal center suggest a distorted square-planar geometry for the Zn^{II} complex (Figure 9).

Conclusions

In summary, we have presented syntheses of a new series of symmetric "salphen"-type ligands and their 1:1 metal complexes with VO^{2+}, Ni^{2+}, Cu^{2+}, and Zn^{2+} metal ions. Interesting metal-coordination-induced mesomorphic behavior is demonstrated by otherwise non-mesomorphic ligands; the role of the metal ion being crucial. Whereas the Cu^{II} complexes decompose just at the onset of melting, VO^{IV} complexes decompose prior to melting at higher temperatures. The Ni^{II} and Zn^{II} complexes, however, show columnar oblique and columnar rectangular phases, respectively, the latter being stable down to room temperature, thus affording room temperature mesomorphism. The ligands and their Zn^{II} complexes are also luminescent entities both in solution and in the solid state. The photoluminescence properties of the Zn^{II} complexes are preserved in the mesophase as well. Further, the vacant axial coordination sites in the square-planar Zn^{II} and the square-pyramidal VO^{IV} centers in the corresponding complexes facilitate solvatochromism, with the former also exhibiting aggregate or monomer formation in solvents of different coordinating ability. The Cu^{II} and Ni^{II} complexes lack such solvatochromism. The metal-coordination-induced mesomorphism, coupled with solvatochromic effects, in these salphen-ligated systems are of particular relevance to the design of functional entities with both thermo- and chemosensing properties.

Experimental Section

Materials and Physical Measurements: The reagents were procured from Sigma–Aldrich, USA, and TCI Chemicals, Japan. All solvents were purified and dried by standard procedures. Silica (60–120 mesh) from Spectrochem was used for chromatographic separation. Silica gel G (E. Merck, India) was used for TLC. Elemental analyses for carbon, hydrogen, and nitrogen were carried out with an Elementar Vario EL III Carlo–Erba 1108 elemental analyzer. The ^1H NMR spectra were recorded with a Bruker Avance II 400 MHz spectrometer in $CDCl_3$ (chemical shift in δ) solution with TMS as internal standard. Infrared spectra were recorded with a Perkin–Elmer BX series spectrometer on KBr discs in the 400–4000 cm^{-1} range. Absorption spectra of the compounds were recorded with a Perkin–Elmer Lambda 35 spectrophotometer. Photoluminescence spectra were recorded with a Hitachi F-4600 Fluorescence spectrophotometer. The fluorescence emission quantum yields (EQYs) in degassed dichloromethane solutions were determined by the standard optically dilute method with 9,10-diphenylanthracene (EQY = 0.96, in cyclohexane) as standard. Quantum yields in the solid state were measured with a 50 mm integrating sphere, in which the solid sample film was excited by a pulsed Xenon source (400 V, 150 W) coupled with holographic concave grating monochromators for selecting wavelengths. The resulting luminescence was acquired with an intensified charge-coupled detector for subsequent analyses. Optical textures of the different phases of the compounds were recorded with a Nikon ECLIPSE LV100 POL polarizing microscope together with Instec hot and cold stage HCS402, with STC200 temperature controller of 0.1 °C accuracy. The thermal behavior of the compounds was studied with a Pyris-1 system linked to a Perkin–Elmer differential scanning calorimeter (DSC) with a heating or cooling rate of 5 °C min^{-1}. Variable-temperature powder X-ray diffraction (XRD) studies were carried out with samples filled in Lindemann capillaries. The apparatus essentially involved a high-resolution X-ray powder diffractometer (PANalytical X'Pert PRO) with a high-resolution fast detector PIXCEL. Quantum chemical calculation of a representative Zn^{II} complex was performed by density functional theory (DFT) as implemented in the GAUSSIAN 09 package.

Synthesis and Analysis

Synthesis of 4-*n*-Alkoxysalicyldehydes (*n* = 12, 14, 16): These alkoxysalicylaldehydes were prepared as described previously.[27]

Synthesis of Imine Ligands

***N*,*N*-Bis(4-*n*-alkoxysalicylidene)-4,5-dichloro-1,2-phenylenediamines *n*c2pd (*n* = 12, 14 or 16):** A solution of 4,5-dichloro-1,2-phenylenediamine (0.09 g, 0.5 mmol) in ethanol was added to a ethanolic solution of the corresponding 4-*n*-alkoxysalicylaldehyde (1 mmol). The solution mixture was heated under reflux with a few drops of acetic acid as catalyst for 3 h to yield the yellow Schiff base. The product was collected by filtration and recrystallized from absolute ethanol.

***N*,*N*-Bis(4-dodecyloxysalicylidene)-4,5-dichloro-1,2-phenylenediamine (12c2pd):** Yellow solid, yield 0.34 g (85 %). ^1H NMR (400 MHz, $CDCl_3$, Me_4Si at 25 °C): δ = 13.17 (s, 2 H, OH), 8.52 (s, 2 H, H^4), 7.32 (s, 2 H, H^5), 7.27 (d, $^3J_{H,H}$ = 8.0 Hz, 2 H, H^1), 6.54 (d, $^4J_{H,H}$ = 2.0 Hz, 2 H, H^3), 6.51 (dd, $^3J_{H,H}$ = 8.0, $^4J_{H,H}$ = 2.0 Hz, 2 H, H^2), 4.00 (t, $^3J_{H,H}$ = 6.5 Hz, 4 H, OCH_2), 1.82 (m, 4 H, CH_2), 1.25–1.61 (m, 36 H, CH_2), 0.90 (t, $^3J_{H,H}$ = 6.7 Hz, 6 H, CH_3) ppm. IR (KBr): $\tilde{\nu}$ = 3437 (ν_{OH}), 2916 [$\nu_{as(C-H)}$, CH_3], 2850 [$\nu_{s(C-H)}$, CH_3], 1614 ($\nu_{C=N}$), 1298 (ν_{C-O}) cm^{-1}. $C_{44}H_{62}Cl_2N_2O_4$ (753.88): calcd. C 70.10, H 8.29, N 3.72; found C 70.14, H 8.31, N 3.74.

***N*,*N*-Bis(4-tetradecyloxysalicylidene)-4,5-dichloro-1,2-phenylenediamine (14c2pd):** Yellow solid, yield 0.32 g (81 %). ^1H NMR (400 MHz, $CDCl_3$, Me_4Si at 25 °C): δ = 13.18 (s, 2 H, OH), 8.52 (s, 2 H, H^4), 7.31 (s, 2 H, H^5), 7.25 (d, $^3J_{H,H}$ = 8.0 Hz, 2 H, H^1), 6.53 (d, $^4J_{H,H}$ = 2.0 Hz, 2 H, H^3), 6.50 (dd, $^3J_{H,H}$ = 8.0, $^4J_{H,H}$ = 2.0 Hz, 2 H, H^2), 4.00 (t, $^3J_{H,H}$ = 6.6 Hz, 4 H, OCH_2), 1.80 (m, 4 H, CH_2), 1.27–1.57 (m, 44 H, CH_2), 0.89 (t, $^3J_{H,H}$ = 6.8 Hz, 6 H, CH_3) ppm. IR (KBr): $\tilde{\nu}$ = 3435 (ν_{OH}), 2919 [$\nu_{as(C-H)}$, CH_3], 2849 [$\nu_{s(C-H)}$, CH_3], 1614 ($\nu_{C=N}$), 1297 (ν_{C-O}) cm^{-1}. $C_{48}H_{70}Cl_2N_2O_4$ (809.99): calcd. C 71.18, H 8.71, N 3.46; found C 71.21, H 8.74, N 3.50.

***N*,*N*-Bis(4-hexadecyloxysalicylidene)-4,5-dichloro-1,2-phenylenediamine (16c2pd):** Yellow solid, yield 0.38 g (83 %). ^1H NMR (400 MHz, $CDCl_3$, Me_4Si at 25 °C): δ = 13.17 (s, 2 H, OH), 8.52 (s, 2 H, H^4), 7.32 (s, 2 H, H^5), 7.27 (d, $^3J_{H,H}$ = 8.0 Hz, 2 H, H^1), 6.54 (d, $^4J_{H,H}$ = 2.0 Hz, 2 H, H^3), 6.50 (dd, $^3J_{H,H}$ = 8.0, $^4J_{H,H}$ = 2.0 Hz, 2 H, H^2), 4.00 (t, $^3J_{H,H}$ = 6.5 Hz, 4 H, OCH_2), 1.81 (m, 4 H, CH_2), 1.28–1.58 (m, 52 H, CH_2), 0.90 (t, $^3J_{H,H}$ = 6.7 Hz, 6 H, CH_3) ppm. IR (KBr): $\tilde{\nu}$ = 3436 (ν_{OH}), 2916 [$\nu_{as(C-H)}$, CH_3], 2850 [$\nu_{s(C-H)}$, CH_3], 1613 ($\nu_{C=N}$), 1299 (ν_{C-O}). $C_{52}H_{78}Cl_2N_2O_4$ (866.09): calcd. C 72.11, H 9.08, N 3.23; found C 71.12, H 9.11, N 3.25.

Synthesis of Zn^{II} Complexes Zn-*n*c2pd (*n* = 12, 14, 16). General Procedure: A methanolic solution of $Zn(OAc)_2{\cdot}2\,H_2O$ (0.02 g, 0.1 mmol) was added slowly to a solution of imine ligand *n*c2pd (0.1 mmol) in ethanol, and the mixture was stirred for 3 h at room temperature. A bright yellow solid formed and was filtered, washed with diethyl ether, and recrystallized from chloroform/ethanol (1:1).

Zn-12c2pd: Yellow solid, yield 0.06 g (82 %). ^{1}H NMR (400 MHz, $CDCl_3$, Me_4Si at 25 °C): δ = 8.49 (s, 2 H, H^4), 7.29 (s, 2 H, H^5), 7.23 (d, $^3J_{H,H}$ = 8.0 Hz, 2 H, H^1), 6.52 (d, $^4J_{H,H}$ = 2.0 Hz, 2 H, H^3), 6.47 (dd, $^3J_{H,H}$ = 8.0, $^4J_{H,H}$ = 2.0 Hz, 2 H, H^2), 3.97 (t, $^3J_{H,H}$ = 6.5 Hz, 4 H, OCH_2), 1.79 (m, 4 H, CH_2), 1.25–1.60 (m, 36 H, CH_2), 0.88 (t, $^3J_{H,H}$ = 6.7 Hz, 6 H, CH_3) ppm. IR (KBr): $\tilde{\nu}$ = 2919 [$\nu_{as(C-H)}$, CH_3], 2848 [$\nu_{s(C-H)}$, CH_3], 1609 ($\nu_{C=N}$), 1313 (ν_{C-O}) cm^{-1}. $C_{44}H_{60}Cl_2N_2O_4Zn$ (817.25): calcd. C 64.66, H 7.40, N 3.43; found C 64.69, H 7.43, N 3.47.

Zn-14c2pd: Yellow solid, yield 0.07 g (87 %). ^{1}H NMR (400 MHz, $CDCl_3$, Me_4Si at 25 °C): δ = 8.49 (s, 2 H, H^4), 7.29 (s, 2 H, H^5), 7.23 (d, $^3J_{H,H}$ = 8.0 Hz, 2 H, H^1), 6.52 (d, $^4J_{H,H}$ = 2.0 Hz, 2 H, H^3), 6.47 (dd, $^3J_{H,H}$ = 8.0, $^4J_{H,H}$ = 2.0 Hz, 2 H, H^2), 3.97 (t, $^3J_{H,H}$ = 6.5 Hz, 4 H, OCH_2), 1.79 (m, 4 H, CH_2), 1.25–1.60 (m, 44 H, CH_2), 0.88 (t, $^3J_{H,H}$ = 6.7 Hz, 6 H, CH_3) ppm. IR (KBr): $\tilde{\nu}$ = 2918 [$\nu_{as(C-H)}$, CH_3], 2849 [$\nu_{s(C-H)}$, CH_3], 1608 ($\nu_{C=N}$), 1315 (ν_{C-O}) cm^{-1}. $C_{48}H_{68}Cl_2N_2O_4Zn$ (873.36): calcd. C 66.01, H 7.85, N 3.21; found C 66.03, H 7.91, N 3.26.

Zn-16c2pd: Yellow solid, yield 0.08 g (85 %). ^{1}H NMR (400 MHz, $CDCl_3$, Me_4Si at 25 °C): δ = 8.49 (s, 2 H, H^4), 7.30 (s, 2 H, H^5), 7.25 (d, $^3J_{H,H}$ = 8.0 Hz, 2 H, H^1), 6.52 (d, $^4J_{H,H}$ = 2.0 Hz, 2 H, H^3), 6.48 (dd, $^3J_{H,H}$ = 8.0, $^4J_{H,H}$ = 2.0 Hz, 2 H, H^2), 3.98 (t, $^3J_{H,H}$ = 6.5 Hz, 4 H, OCH_2), 1.78 (m, 4 H, CH_2), 1.25–1.58 (m, 52 H, CH_2), 0.88 (t, $^3J_{H,H}$ = 6.7 Hz, 6 H, CH_3) ppm. IR (KBr): $\tilde{\nu}$ = 2917 [$\nu_{as(C-H)}$, CH_3], 2850 [$\nu_{s(C-H)}$, CH_3], 1608 ($\nu_{C=N}$), 1314 (ν_{C-O}) cm^{-1}. $C_{52}H_{76}Cl_2N_2O_4Zn$ (929.47): calcd. C 67.20, H 8.24, N 3.01; found C 67.17, H 8.29, N 3.05.

Synthesis of Ni^{II} Complexes Ni-*n*c2pd (*n* = 12, 14, 16)

General Procedure: The ligand *n*c2pd (0.1 mmol) was dissolved in as small a volume as possible of ethanol. Addition of a methanolic solution of $Ni(OAc)_2$·2 H_2O (0.02 g, 0.1 mmol) resulted in an orange red suspension that turned into a microcrystalline solid on further stirring. The fine, orange, crystalline precipitate was isolated by filtration, washed with diethyl ether, and recrystallized from chloroform/ethanol (1:1).

Ni-12c2pd: Orange solid, yield 0.06 g (80 %). ^{1}H NMR (400 MHz, $CDCl_3$, Me_4Si at 25 °C): δ = 7.92 (s, 2 H, H^4), 7.71 (s, 2 H, H^5), 7.19 (d, $^3J_{H,H}$ = 8.0 Hz, 2 H, H^1), 6.58 (d, $^4J_{H,H}$ = 2.0 Hz, 2 H, H^3), 6.37 (dd, $^3J_{H,H}$ = 8.0, $^4J_{H,H}$ = 2.0 Hz, 2 H, H^2), 3.99 (t, $^3J_{H,H}$ = 6.6 Hz, 4 H, OCH_2), 1.80 (m, 4 H, CH_2), 1.25–1.60 (m, 36 H, CH_2), 0.89 (t, $^3J_{H,H}$ = 6.7 Hz, 6 H, CH_3) ppm. IR (KBr): $\tilde{\nu}$ = 2919 [$\nu_{as(C-H)}$, CH_3], 2851 [$\nu_{s(C-H)}$, CH_3], 1610 ($\nu_{C=N}$), 1314 (ν_{C-O}) cm^{-1}. $C_{44}H_{60}Cl_2N_2NiO_4$ (810.56): calcd. C 65.20, H 7.46, N 3.46; found C 65.23, H 7.43, N 3.47.

Ni-14c2pd: Orange solid, yield 0.06 g (78 %). ^{1}H NMR (400 MHz, $CDCl_3$, Me_4Si at 25 °C): δ = 7.90 (s, 2 H, H^4), 7.72 (s, 2 H, H^5), 7.18 (d, $^3J_{H,H}$ = 8.0 Hz, 2 H, H^1), 6.60 (d, $^4J_{H,H}$ = 2.0 Hz, 2 H, H^3), 6.36 (dd, $^3J_{H,H}$ = 8.0, $^4J_{H,H}$ = 2.0 Hz, 2 H, H^2), 3.98 (t, $^3J_{H,H}$ = 6.7 Hz, 4 H, OCH_2), 1.79 (m, 4 H, CH_2), 1.25–1.59 (m, 44 H, CH_2), 0.90 (t, $^3J_{H,H}$ = 6.8 Hz, 6 H, CH_3) ppm. IR (KBr): $\tilde{\nu}$ = 2918 [$\nu_{as(C-H)}$, CH_3], 2850 [$\nu_{s(C-H)}$, CH_3], 1612 ($\nu_{C=N}$), 1314 (ν_{C-O}) cm^{-1}. $C_{48}H_{68}Cl_2N_2NiO_4$ (866.66): calcd. C 66.52, H 7.91, N 3.23; found C 66.55, H 7.93, N 3.27.

Ni-16c2pd: Orange solid, yield 0.07 g (75 %). ^{1}H NMR (400 MHz, $CDCl_3$, Me_4Si at 25 °C): δ = 7.91 (s, 2 H, H^4), 7.71 (s, 2 H, H^5), 7.19 (d, $^3J_{H,H}$ = 8.0 Hz, 2 H, H^1), 6.60 (d, $^4J_{H,H}$ = 2.0 Hz, 2 H, H^3), 6.35 (dd, $^3J_{H,H}$ = 8.0, $^4J_{H,H}$ = 2.0 Hz, 2 H, H^2), 3.99 (t, $^3J_{H,H}$ = 6.7 Hz, 4 H, OCH_2), 1.80 (m, 4 H, CH_2), 1.28–1.58 (m, 52 H, CH_2), 0.90 (t, $^3J_{H,H}$ = 6.5 Hz, 6 H, CH_3) ppm. IR (KBr): $\tilde{\nu}$ = 2918 [$\nu_{as(C-H)}$, CH_3], 2850 [$\nu_{s(C-H)}$, CH_3], 1611 ($\nu_{C=N}$), 1319 (ν_{C-O}) cm^{-1}. $C_{52}H_{76}Cl_2N_2NiO_4$ (922.77): calcd. C 67.68, H 8.30, N 3.04; found C 67.71, H 8.27, N 3.07.

Synthesis of Cu^{II} Complexes Cu-*n*c2pd (*n* = 12, 14, 16). General Procedure: A methanolic solution of $Cu(OAc)_2$·2 H_2O (0.02 g, 0.1 mmol) was added to a solution of the ligand *n*c2pd (0.1 mmol) in ethanol. This was immediately accompanied by a brown coloration. The mixture was stirred for 3 h at room temperature, and the brown solid was isolated by filtration, washed with diethyl ether, and recrystallized from chloroform/ethanol (1:1).

Cu-12c2pd: Brown solid, yield 0.07 g (86 %). IR (KBr): $\tilde{\nu}$ = 2920 [$\nu_{as(C-H)}$, CH_3], 2849 [$\nu_{s(C-H)}$, CH_3], 1600 ($\nu_{C=N}$), 1314 (ν_{C-O}) cm^{-1}. $C_{44}H_{60}Cl_2CuN_2O_4$ (815.41): calcd. C 64.81, H 7.42, N 3.44; found C 64.84, H 7.46, N 3.47.

Cu-14c2pd: Brown solid, yield 0.07 g (82 %). IR (KBr): $\tilde{\nu}$ = 2920 [$\nu_{as(C-H)}$, CH_3], 2849 [$\nu_{s(C-H)}$, CH_3], 1600 ($\nu_{C=N}$), 1316 (ν_{C-O}) cm^{-1}. $C_{48}H_{68}Cl_2CuN_2O_4$ (871.52): calcd. C 66.15, H 7.86, N 3.21; found C 66.21, H 7.89, N 3.25.

Cu-16c2pd: Brown solid, yield 0.07 g (80 %). IR (KBr): $\tilde{\nu}$ = 2917 [$\nu_{as(C-H)}$, CH_3], 2850 [$\nu_{s(C-H)}$, CH_3], 1599 ($\nu_{C=N}$), 1318 (ν_{C-O}) cm^{-1}. $C_{52}H_{76}Cl_2CuN_2O_4$ (927.62): calcd. C 67.33, H 8.26, N 3.02; found C 67.38, H 8.31, N 3.05.

Synthesis of VO^{IV} Complexes VO-*n*c2pd (*n* = 12, 14, 16). General Procedure: $VOSO_4$·H_2O (0.02 g, 0.1 mmol) in methanol was added with stirring to a solution of the ligand *n*c2pd (0.1 mmol) in ethanol. The solution acquired a green color. Addition of a few drops of triethylamine resulted in a green suspension, affording a microcrystalline solid on further stirring. The light green product was filtered off, washed with diethyl ether, and recrystallized from chloroform/ethanol (1:1).

VO-12c2pd: Light green solid, yield 0.06 g (75 %). IR (KBr): $\tilde{\nu}$ = 2918 [$\nu_{as(C-H)}$, CH_3], 2849 [$\nu_{s(C-H)}$, CH_3], 1608 ($\nu_{C=N}$), 1313 (ν_{C-O}), 971 ($\nu_{V=O}$) cm^{-1}. $C_{44}H_{60}Cl_2N_2O_4OV$ (818.81): calcd. C 64.54, H 7.39, N 3.42; found C 64.57, H 7.43, N 3.45.

VO-14c2pd: Light green solid, yield 0.06 g (77 %). IR (KBr): $\tilde{\nu}$ = 2919 [$\nu_{as(C-H)}$, CH_3], 2848 [$\nu_{s(C-H)}$, CH_3], 1610 ($\nu_{C=N}$), 1314 (ν_{C-O}), 971 ($\nu_{V=O}$) cm^{-1}. $C_{48}H_{68}Cl_2N_2O_4OV$ (874.91): calcd. C 65.89, H 7.83, N 3.20; found C 65.91, H 7.87, N 3.24.

VO-16c2pd: Light green solid, yield 0.06 g (73 %). IR (KBr): $\tilde{\nu}$ = 2919 [$\nu_{as(C-H)}$, CH_3], 2850 [$\nu_{s(C-H)}$, CH_3], 1609 ($\nu_{C=N}$), 1311 (ν_{C-O}), 971 ($\nu_{V=O}$) cm^{-1}. $C_{52}H_{76}Cl_2N_2O_4OV$ (931.02): calcd. C 67.08, H 8.23, N 3.01; found C 67.13, H 8.27, N 3.06.

Acknowledgments

The authors are grateful for financial support from the Department of Science and Technology (DST)-FIST, Ministry of Science and Technology, New Delhi. S. C. acknowledges DST for an (INSPIRE Research Fellowship, code IF110692). P. M. acknowledges DST for financial support. The Sophisticated Analytical Instrumentation Facility (SAIF), North Eastern Hill University, Shillong is acknowledged for help with some spectral analysis. The authors are also thankful to the DBT e-Library Consortium (DeLCON) of the Bio-Informatics Centre, Assam University, India.

Keywords: Metallomesogens · Photoluminescence · Aggregation · Solvent effects · Density functional calculations

[1] C. J. Whiteoak, G. Salassa, A. W. Kleij, *Chem. Soc. Rev.* **2012**, *41*, 622–631.
[2] S. J. Wezenberg, A. W. Kleij, *Angew. Chem. Int. Ed.* **2008**, *47*, 2354–2364; *Angew. Chem.* **2008**, *120*, 2388.
[3] J. Cheng, X. Ma, Y. Zhang, J. Liu, X. Zhou, H. Xiang, *Inorg. Chem.* **2014**, *53*, 3210–3219.
[4] S. J. Wezenberg, E. C. Escudero-Adán, J. Benet-Buchholz, A. W. Kleij, *Org. Lett.* **2008**, *10*, 3311–3314.

[5] A. W. Kleij, *Dalton Trans.* **2009**, 4635–4639.
[6] P. G. Lacroix, *Eur. J. Inorg. Chem.* **2001**, 339–348.
[7] S. Di Bella, *Chem. Soc. Rev.* **2001**, *30*, 355–366.
[8] R. Chico, C. Dominguez, B. Donnio, S. Coco, P. Espinet, *Dalton Trans.* **2011**, *40*, 5977–5983.
[9] K. Binnemans, K. Lodewyckx, B. Donnio, D. Guillon, *Eur. J. Inorg. Chem.* **2005**, 1506–1513.
[10] J. Cheng, K. Wei, X. Ma, X. Zhou, H. Xiang, *J. Phys. Chem. C* **2013**, *117*, 16552–16563.
[11] A. M. Castilla, S. Curreli, M. M. Belmonte, E. C. Escudero-Adán, J. Benet-Buchholz, A. W. Kleij, *Org. Lett.* **2009**, *11*, 5218–5221.
[12] M. Palucki, N. S. Finney, P. J. Pospisil, M. L. Güler, T. Ishida, E. N. Jacobsen, *J. Am. Chem. Soc.* **1998**, *120*, 948–954.
[13] K. Suna, W.-X. Lia, Z. Fenga, C. Li, *Chem. Phys. Lett.* **2009**, *470*, 259–263.
[14] M. Nasr-Esfahani, M. Moghadam, G. Valipour, *Synth. Commun.* **2009**, *39*, 3867–3879.
[15] V. Mirkhani, S. Tangestaninejad, M. Moghadam, I. Mohammadpoor-Baltork, H. Kargar, *J. Mol. Catal. A* **2005**, *242*, 251–255.
[16] S. H. Lee, L. Xu, B. K. Park, Y. V. Mironov, S. H. Kim, Y. J. Song, C. Kim, Y. Kim, S.-J. Kim, *Chem. Eur. J.* **2010**, *16*, 4678–4685.
[17] V. Conte, F. Fabbianesi, B. Floris, P. Galloni, D. Sordi, I. W. C. E. Arends, M. Bonchio, D. Rehder, D. Bogdal, *Pure Appl. Chem.* **2009**, *81*, 1265–1277.
[18] S. I. Vagin, R. Reichardt, S. Klaus, B. Rieger, *J. Am. Chem. Soc.* **2010**, *132*, 14367–14369.
[19] D. J. Darensbourg, P. Ganguly, D. Billodeaux, *J. Polym. Sci., Part A Polym. Chem.* **2005**, *43*, 4172–4186.
[20] L.-J. Chen, J. Bao, F.-M. Mei, G.-X. Li, *Catal. Commun.* **2008**, *9*, 658–663.
[21] A. Mitra, L.-J. DePue, S. Parkin, D. A. Atwood, *J. Am. Chem. Soc.* **2006**, *128*, 1147–1153.
[22] A. Decortes, M. M. Belmonte, J. Benet-Buchholz, A. W. Kleij, *Chem. Commun.* **2010**, *46*, 4580–4582.
[23] C. Datta, R. Chakrabarty, G. Das, C. R. Bhattacharjee, P. Mondal, *Liq. Cryst.* **2014**, *41*, 541–551.
[24] N. Hoshino, *Coord. Chem. Rev.* **1998**, *174*, 77–108.
[25] C. R. Bhattacharjee, C. Datta, G. Das, P. Mondal, *Liq. Cryst.* **2012**, *39*, 819–826.
[26] C. R. Bhattacharjee, C. Datta, G. Das, R. Chakrabarty, P. Mondal, *Polyhedron* **2012**, *33*, 417–424.
[27] C. R. Bhattacharjee, S. Chakraborty, G. Das, P. Mondal, *Liq. Cryst.* **2012**, *39*, 1435–1442.
[28] C. R. Bhattacharjee, C. Datta, G. Das, P. Mondal, *Mater. Sci. Eng. C* **2012**, *32*, 735–741.
[29] C. R. Bhattacharjee, G. Das, P. Mondal, S. K. Prasad, D. S. S. Rao, *Inorg. Chem. Commun.* **2011**, *14*, 606–612.
[30] C. R. Bhattacharjee, G. Das, P. Mondal, *Eur. J. Inorg. Chem.* **2011**, 5390–5399.
[31] C. R. Bhattacharjee, G. Das, P. Mondal, S. K. Prasad, D. S. S. Rao, *Eur. J. Inorg. Chem.* **2011**, 1418–1424.
[32] C. R. Bhattacharjee, G. Das, P. Mondal, N. V. S. Rao, *Polyhedron* **2010**, *29*, 3089–3096.
[33] M. M. Belmonte, S. J. Wezenberg, R. M. Haak, A. Daniele, E. C. Escudero-Adán, J. Benet-Buchholz, A. W. Kleij, *Dalton Trans.* **2010**, *39*, 4541–4550.
[34] E. C. Escudero-Adán, J. Benet-Buchholz, A. W. Kleij, *Chem. Eur. J.* **2009**, *15*, 4233–4239.
[35] I. P. Oliveri, G. Maccarrone, S. Di Bella, *J. Org. Chem.* **2011**, *76*, 8879–8884.
[36] M. Cano, L. Rodríguez, J. C. Lima, F. Pina, A. D. Cort, C. Pasquini, L. Schiaffino, *Inorg. Chem.* **2009**, *48*, 6229–6235.
[37] I. P. Oliveri, S. Di Bella, *J. Phys. Chem. A* **2011**, *115*, 14325–14330.
[38] A. Dalla Cort, L. Mandolini, C. Pasquini, K. Rissanen, L. Russo, L. Schiaffino, *New J. Chem.* **2007**, *31*, 1633–1638.
[39] J. Flapper, J. N. H. Reek, *Angew. Chem. Int. Ed.* **2007**, *46*, 8590–8592; *Angew. Chem.* **2007**, *119*, 8744.
[40] J. D. Lee, *Concise Inorganic Chemistry*, 5th ed., Wiley, India, **2007**, p. 708.
[41] H. Zheng, C. K. Lai, T. M. Swager, *Chem. Mater.* **1995**, *7*, 2067–2077.
[42] A. Serrette, P. J. Carroll, T. M. Swager, *J. Am. Chem. Soc.* **1992**, *114*, 1887–1889.
[43] R. Paschke, D. Balkow, U. Baumeister, H. Hartung, J. R. Chipperfield, A. B. Blake, P. G. Nelson, G. W. Gray, *Mol. Cryst. Liq. Cryst.* **1990**, *188*, 105–118.
[44] S. Laschat, A. Baro, N. Steinke, F. Giesselmann, C. Hägele, G. Scalia, R. Judele, E. Kapatsina, S. Sauer, A. Schreivogel, M. Tosoni, *Angew. Chem. Int. Ed.* **2007**, *46*, 4832–4887; *Angew. Chem.* **2007**, *119*, 4916.
[45] O. N. Kadkin, E. H. Kim, S. Y. Kim, M.-G. Choi, *Polyhedron* **2009**, *28*, 1301–1307.
[46] C. Cuerva, J. A. Campo, P. Ovejero, M. R. Torres, E. Oliveira, S. M. Santos, C. Lodeiro, M. Cano, *J. Mater. Chem. C* **2014**, *2*, 9167–9181.
[47] J.-W. Choi, J.-H. Han, M.-H. Ryu, B.-K. Cho, *Bull. Korean Chem. Soc.* **2011**, *32*, 781–782.
[48] F. Morale, R. W. Date, D. Guillon, D. W. Bruce, R. L. Finn, C. Wilson, A. J. Blake, M. Schröder, B. Donnio, *Chem. Eur. J.* **2003**, *9*, 2484–2501.
[49] N. Godbert, A. Crispini, M. Ghedini, M. Carin, F. Chiaravallotic, A. Ferrise, *J. Appl. Crystallogr.* **2014**, *47*, 668–679.
[50] F. Morale, R. L. Finn, S. R. Collinson, A. J. Blake, C. Wilson, D. W. Bruce, D. Guillon, B. Donnio, M. Schröder, *New J. Chem.* **2008**, *32*, 297–305.
[51] B. Bosnich, *J. Am. Chem. Soc.* **1968**, *90*, 627–631.
[52] A. Akbari, Z. Alinia, *Comput. Res.* **2013**, *1*, 19–26.
[53] S. S. Amin, K. Cryer, B. Zhang, S. K. Dutta, S. S. Eaton, O. P. Anderson, S. M. Miller, B. A. Reul, S. M. Brichard, D. C. Crans, *Inorg. Chem.* **2000**, *39*, 406–416.
[54] L. G. Vanquickenborne, S. P. McGlynn, *Theor. Chim. Acta* **1968**, *9*, 390–400.
[55] L. J. Boucher, T. F. Yen, *Inorg. Chem.* **1968**, *7*, 2665–2667.
[56] G. Consiglio, S. Failla, P. Finocchiaro, I. P. Oliveri, S. Di Bella, *Dalton Trans.* **2012**, *41*, 387–395.
[57] S. Chakraborty, C. R. Bhattacharjee, P. Mondal, S. K. Prasad, D. S. S. Rao, *Dalton Trans.* **2015**, *44*, 7477–7488.
[58] M. Kasha, H. R. Rawls, M. A. El-Bayoumi, *Pure Appl. Chem.* **1965**, *11*, 371–392.
[59] M. J. Frisch, G. W. Trucks, H. B. Schlegel, G. E. Scuseria, M. A. Robb, J. R. Cheeseman, G. Scalmani, V. Barone, B. Mennucci, G. A. Petersson, H. Nakatsuji, M. Caricato, X. Li, H. P. Hratchian, A. F. Izmaylov, J. Bloino, G. Zheng, J. L. Sonnenberg, M. Hada, M. Ehara, K. Toyota, R. Fukuda, J. Hasegawa, M. Ishida, T. Nakajima, Y. Honda, O. Kitao, H. Nakai, T. Vreven, J. A. Montgomery Jr., J. E. Peralta, F. Ogliaro, M. Bearpark, J. J. Heyd, E. Brothers, K. N. Kudin, V. N. Staroverov, R. Kobayashi, J. Normand, K. Raghavachari, A. Rendell, J. C. Burant, S. S. Iyengar, J. Tomasi, M. Cossi, N. Rega, J. M. Millam, M. Klene, J. E. Knox, J. B. Cross, V. Bakken, C. Adamo, J. Jaramillo, R. Gomperts, R. E. Stratmann, O. Yazyev, A. J. Austin, R. Cammi, C. Pomelli, J. W. Ochterski, R. L. Martin, K. Morokuma, V. G. Zakrzewski, G. A. Voth, P. Salvador, J. J. Dannenberg, S. Dapprich, A. D. Daniels, Ö. Farkas, J. B. Foresman, J. V. Ortiz, J. Cioslowski, D. J. Fox, *Gaussian 09*, Gaussian, Inc., Wallingford CT, **2009**.
[60] A. D. Becke, *J. Chem. Phys.* **1993**, *98*, 5648–5652.
[61] C. Lee, W. Yang, R. G. Parr, *Phys. Rev. B* **1988**, *37*, 785–789.
[62] P. C. Hariharan, J. A. Pople, *Theor. Chim. Acta* **1973**, *28*, 213–222.

Received: May 3, 2016
Published Online: August 30, 2016

Polyhedron 105 (2016) 150–158

Contents lists available at ScienceDirect

Polyhedron

journal homepage: www.elsevier.com/locate/poly

Photoluminescent tetrahedral d^{10}-metal Schiff base complexes exhibiting highly ordered mesomorphism

Sutapa Chakraborty [a], Debraj Dhar Purkayastha [a], Gobinda Das [a,1], Chira R. Bhattacharjee [a,*], Paritosh Mondal [a], S. Krishna Prasad [b], D.S. Shankar Rao [b]

[a] Department of Chemistry, Assam University, Silchar 788011, Assam, India
[b] Centre for Nano and Soft Matter Sciences, Jalahalli, Bangalore 560013, India

ARTICLE INFO

Article history:
Received 8 October 2015
Accepted 25 November 2015
Available online 12 December 2015

Keywords:
Schiff base
Mesophase
Luminescence
X-ray diffraction
Density functional theory

ABSTRACT

A series of four-coordinate d^{10}-metal complexes of the type $[ML_2]$ {M = Zn, Cd, Hg; L = 4-nitro-2-((octadecylimino)methyl)phenol}, incorporating a new N-alkylated bidentate [N,O]-donor salicylaldimine Schiff base ligand, has been synthesized and characterized by elemental analyses, FT-IR, UV–Vis, ^{1}H NMR and FAB-mass spectroscopies. The ligand is non-mesomorphic and devoid of any photoluminescence. The zinc(II) and cadmium(II) complexes displayed highly ordered mesophases reminiscent of soft crystals. The phases have been characterized by polarizing optical microscopy (POM), differential scanning calorimetry (DSC) and powder X-ray diffraction (PXRD) studies. The complex of mercury(II) decomposed prior to melting. An orthogonal symmetry with a 'herringbone' array for the zinc complex and a primitive triclinic symmetry (p_1) for the cadmium complex, respectively, has been proposed. The complexes exhibited fluorescence at room temperature, both in the solution and in the solid state, with emission maxima in the blue region. Density functional theory (DFT) calculations carried out using the GAUSSIAN 09 program at the B3LYP level revealed a distorted tetrahedral geometry around the metal center in all the complexes. Natural bond orbital (NBO) analysis suggested appreciable charge transfer from the ligand to the metal center in the complexes.

1. Introduction

Metal-salicylaldimines have been recognized as an important class of coordination compounds with applications in diverse fields ranging from agriculture to optoelectronics [1–3], antimicrobial to therapeutics [4,5], polymers to dyes [6,7] and drugs to catalysts [8–10]. Besides, such compounds currently have also earned a place of interest as liquid-crystalline materials [11]. As for salicylaldimines, the ease of synthesis as well as the flexibility of the coordination environment around the imine moiety renders them a versatile class of ligands in coordination chemistry [9,10].

Materials that are photo-responsive and possess highly ordered fluid-phases are currently enjoying much interest in applications related to OLEDs, information storage, sensors, lasers and enhanced contrast displays, etc. [12,13]. The luminescence properties of metal complexes coupled with the self-organizing ability of liquid crystals (LCs) are of abiding interest, offering a viable option to access multifunctional materials [14,15]. Amongst the metals used, lanthanides have widely been employed in synthesizing luminescent metallomesogens [16,17]. Luminescence of metallomesogens incorporating d-block metals such as palladium(II) [18,19], platinum(II) [20,21], iridium(III) [22,23], nickel(II) [24,25], rhenium(I) [26], gold(I) [27,28], silver(I) [28,29], zinc(II) [30,31] and copper(I) [32] have also attracted a lot of research attention. It is pertinent to mention here that complexes of zinc (II) and its congeners cadmium(II) and mercury(II) display interesting fluorescent properties that originate from a ligand-centered charge transfer or metal-centered luminescent levels, providing access to newer functional materials [33,34].

Salicylaldimine based metallomesogens have been accessed mostly with palladium(II) [35], copper(II) [36,37], oxovanadium (IV) [37,38], nickel(II) [38], iron(III) [39] or manganese(III) [40]. While examples of zinc are scarce [30,31,41], those that incorporate cadmium and mercury ions appear to be virtually non-existent. Apart from a very early account of mesomorphic cadmium alkanoates [42] or with porphyrins as ligands [43], only sporadic mention of cadmium based mesogens has been made in the literature. An unpublished reference to uncharacterized cadmium and

* Corresponding author. Tel.: +91 03842 270848; fax: +91 03842 270342.
E-mail address: crbhattacharjee@rediffmail.com (C.R. Bhattacharjee).
[1] Present address: Polymers and Advanced Materials Laboratory, National Chemical Laboratory, Pune 411008, India.

http://dx.doi.org/10.1016/j.poly.2015.11.053
0277-5387/

mercury complexes of di-thiobenzoate with ill-defined phases was made in 1993 [44]. Aquated cadmium ions, $[Cd(H_2O)_4]^{2+}$, upon complexation with non-ionic oligo(ethylene oxide) surfactants, have been reported to form liquid crystalline phases [45,46]. Further, another interesting variety of complexes, tetrachlorometallates $[MCl_4]^{2-}$ (M = Zn and Cd), with n-alkylpyridinium as a counter-cation were reported to exhibit smectic mesomorphism [47]. Mesomorphic zinc complexes were previously reported to be either square planar or trigonal-bipyramidal [30,48]. The zinc metal ion usually prefers a tetrahedral geometry, which often results in the loss of the mesomorphism [49,50]. Tetrahedral zinc complexes exhibiting mesomorphism have appeared only in the current decade and are limited to only a few examples [40,50–54], and the ones that are both luminescent and liquid crystalline are rare. In fact there appears to be only a couple of instances in the literature of the latter type [41,51–53]. As against tetradentate 'salen' type ligands, which enforce a planar geometry, bidentate ligands with long alkyl arms, giving greater flexibility, allow the metal ion to acquire the thermodynamically stable tetrahedral geometry, ensuring enhanced order in the molecular self-assembly.

Accordingly, we report here the synthesis of a series of luminescent tetrahedral zinc(II), cadmium(II) and mercury(II) complexes of a new flexible one ring N-alkylated [N,O]-donor rod shaped salicylaldimine Schiff base ligand. The ligand is non-mesomorphic and lacks any fluorescence. Except for the mercury(II) complex, which decomposes before melting, the zinc(II) and cadmium(II) complexes exhibit highly ordered mesophases.

2. Experimental section

2.1. Materials

All chemicals used were of the reagent grade quality and used without further purification. The solvents were dried before use following standard procedures.

2.2. Instrumentation and methods

The C, H and N analyses were carried out using a Carlo Erba 1108 elemental analyzer (USA). The ^{1}H NMR spectra of the compounds were recorded on a Bruker Avance II, 300 MHz (for the ligand)/400 MHz (for the complexes) spectrometer (Bruker, India) in $CDCl_3$ (chemical shift in δ) solution with TMS as the internal standard. Mass spectra were recorded on a Jeol SX-102 spectrometer (Jeol, Japan) with fast atom bombardment. UV–Vis absorption spectra of the compounds were recorded in CH_2Cl_2 on a Shimadzu UV-1601PC spectrophotometer (Shimadzu, Asia Pacific, Pte. Ltd., Singapore). Photoluminescence spectra were recorded on a Shimadzu RF-5301PC spectrophotometer (Shimadzu, Asia Pacific, Pte. Ltd., Singapore). The fluorescence emission quantum yields (EQY) in degassed dichloromethane solution were determined by the standard optical dilution method using 9,10-diphenylanthracene (EQY = 0.96, in cyclohexane) as the standard. Infrared spectra were recorded on a Perkin Elmer BX series spectrophotometer (Perkin Elmer, USA) on KBr disks in the 400–4000 cm^{-1} range. The optical textures of the different phase of the compounds were studied using a Nikon optiphot-2-pol polarizing microscope (Nikon Corporation, Tokyo, Japan) attached with Instec hot and cold stage HCS302, with an STC200 temperature controller of 0.1 °C accuracy. The thermal behavior of the compounds were studied using a Pyris-1 system linked to a Perkin Elmer differential scanning calorimeter (DSC; Perkin Elmer, Switzerland) with a heating or cooling rate of 5 °C/min. Variable temperature powder X-ray diffraction (PXRD) experiments were performed in the transmission geometry with the samples in a glass capillary (Capillary Tube Supplies Ltd, UK). The XRD apparatus (X'Pert PRO MP, PANalytical), employing Cu Kα (l = 0.15418 nm) radiation, consisted of a focusing elliptical mirror for beam preparation optics providing a well-focused line beam, a fast high resolution multi-channel solid state detector (PIXCEL) and operated at 45 kV and 30 mA rating. Collimation with 20 mrad Soller slits on the input as well as the diffracted beam side provides very good vertical resolution. Quantum chemical calculations on the zinc(II), cadmium(II) and mercury(II) complexes were carried out using the GAUSSIAN 09 program at the B3LYP level.

2.3. Synthesis and characterization

2.3.1. Synthesis of 4-nitro-2-((octadecylimino)methyl)phenol, HL

A methanolic solution of 5-nitro salicylaldehyde (0.84 g, 5 mmol) was added to a methanolic solution of octadecylamine (1.35 g, 5 mmol). The solution mixture was heated under reflux with a few drop of acetic acid as a catalyst for 3 h to yield the yellow Schiff base. The compound was collected by filtration and re-crystallized from methanol.

Yield: ~1.81 g (82.49%). *Anal.* Calc. for $C_{25}H_{42}N_2O_3$ (418.63): C, 71.66; H, 10.04; N, 6.68. Found: C, 71.66; H, 10.06; N, 6.65%. FAB Mass, m/z: 418.3 $[M]^+$. ^{1}H NMR (300 MHz, $CDCl_3$; Me_4Si at 25 °C, ppm) δ: 15 (s, 1H; H^5), 8.31 (s, 1H; H^1), 8.23 (d, $^4J_{(H,H)}$ = 3.0 Hz, 1H; H^2), 8.19 (dd, $^3J_{(H,H)}$ = 6.0 Hz, $^4J_{(H,H)}$ = 3.0 Hz, 1H; H^3), 6.90 (d, $^3J_{(H,H)}$ = 6.0 Hz, 1H; H^4), 3.66 (t, $^3J_{(H,H)}$ = 6.0 Hz, 2H; =N—CH_2), 0.88 (t, $^3J_{(H,H)}$ = 6.0 Hz, 3H; CH_3), 1.36 (m, —CH_2 of the methylene side chain proton). IR (ν_{max}, cm^{-1}, KBr): 3428 (ν_{OH}), 2917 ($\nu_{as(C-H)}$, CH_3), 2848 ($\nu_{s(C-H)}$, CH_3), 1672 ($\nu_{C=N}$), 1280 (ν_{C-O}).

2.3.2. Synthesis of the zinc(II), cadmium(II) and mercury(II) complexes, $[ML_2]$ (M = Zn, Cd, Hg)

General procedure: To a methanolic solution of the ligand, HL (0.084 g, 0.2 mmol), a methanolic solution of $Zn(OAc)_2{\cdot}2H_2O$ (0.02 g, 0.1 mmol), $Cd(OAc)_2{\cdot}2H_2O$ (0.026 g, 0.1 mmol) or $Hg(OAc)_2$ (0.032 g, 0.1 mmol) was added separately. The mixture was stirred for 2 h at room temperature. A creamy white solid formed in each case which was immediately filtered, washed with diethyl ether and re-crystallized from dichloromethane/methanol (1:1).

$[ZnL_2]$: Yield: ~0.07 g (70%). *Anal.* Calc. for $C_{50}H_{82}N_4O_6Zn$ (900.64): C, 66.62; H, 9.10; N, 6.22. Found: C, 66.63; H, 9.12; N, 6.20%. FAB Mass, m/z: 898.6 $[MH]^+$. ^{1}H NMR (400 MHz, $CDCl_3$; Me_4Si at 25 °C, ppm) δ: 8.30 (s, 1H; H^1), 8.25 (d, $^4J_{(H,H)}$ = 4.0 Hz, 1H; H^2), 8.18 (dd, $^3J_{(H,H)}$ = 8.0 Hz, $^4J_{(H,H)}$ = 4.0 Hz, 1H; H^3), 6.84 (d, $^3J_{(H,H)}$ = 8.0 Hz, 1H; H^4), 3.62 (t, $^3J_{(H,H)}$ = 8.0 Hz, 2H; =N—CH_2), 0.88 (t, $^3J_{(H,H)}$ = 8.0 Hz, 3H; CH_3), 1.55 (m, —CH_2 of the methylene side chain proton). IR (ν_{max}, cm^{-1}, KBr): 2920 ($\nu_{as(C-H)}$, CH_3), 2849 ($\nu_{s(C-H)}$, CH_3), 1656 ($\nu_{C=N}$), 1277 (ν_{C-O}).

$[CdL_2]$: Yield ~0.08 g (74%). *Anal.* Calc. for $C_{50}H_{82}N_4O_6Cd$ (947.67): C, 63.31; H, 8.65; N, 5.91. Found: C, 63.33; H, 8.67; N, 5.87%. FAB Mass, m/z: 948.5 $[MH]^+$. ^{1}H NMR (400 MHz, $CDCl_3$; Me_4Si at 25 °C, ppm) δ: 8.30 (s, 1H; H^1), 8.24 (d, $^4J_{(H,H)}$ = 4.0 Hz, 1H; H^2), 8.19 (dd, $^3J_{(H,H)}$ = 8.0 Hz, $^4J_{(H,H)}$ = 4.0 Hz, 1H; H^3), 6.93 (d, $^3J_{(H,H)}$ = 8.0 Hz, 1H; H^4), 3.66 (t, $^3J_{(H,H)}$ = 8.0 Hz, 2H; =N—CH_2), 0.88 (t, $^3J_{(H,H)}$ = 8.0 Hz, 3H; CH_3), 1.71 (m, —CH_2 of the methylene side chain proton). IR (ν_{max}, cm^{-1}, KBr): 2919 ($\nu_{as(C-H)}$, CH_3), 2850 ($\nu_{s(C-H)}$, CH_3), 1639 ($\nu_{C=N}$), 1275 (ν_{C-O}).

$[HgL_2]$: Yield: ~0.07 g (67%). *Anal.* Calc. for $C_{50}H_{82}N_4O_6Hg$ (1035.85): C, 57.92; H, 7.91; N, 5.40. Found: C, 57.95; H, 7.93; N, 5.54%. FAB Mass, m/z: 1036.6 $[MH]^+$. ^{1}H NMR (400 MHz, $CDCl_3$; Me_4Si at 25 °C, ppm) δ: 8.30 (s, 1H; H^1), 8.24 (d, $^4J_{(H,H)}$ = 4.0 Hz, 1H; H^2), 8.18 (dd, $^3J_{(H,H)}$ = 8.0 Hz, $^4J_{(H,H)}$ = 4.0 Hz, 1H; H^3), 6.89 (d, $^3J_{(H,H)}$ = 8.0 Hz, 1H; H^4), 3.66 (t, $^3J_{(H,H)}$ = 8.0 Hz, 2H; =N—CH_2), 0.88 (t, $^3J_{(H,H)}$ = 8.0 Hz, 3H; CH_3), 1.46 (m, —CH_2 of the methylene

side chain proton). IR (ν_{max}, cm^{-1}, KBr): 2916 ($\nu_{as(C-H)}$, CH_3), 2848 ($\nu_{s(C-H)}$, CH_3), 1642 ($\nu_{C=N}$), 1273 (ν_{C-O}).

3. Results and discussion

3.1. Synthesis and characterization

The ligand was synthesized by the condensation of 5-nitrosalicylaldehyde and octadecylamine. The complexes were prepared by slow addition of a methanolic solution of 1 equivalent of $M(OAc)_2 \cdot nH_2O$ (M = Zn, Cd; n = 2 or Hg; n = 0) to a methanolic solution of the ligand (2 equivalents) (Scheme 1). Structures were ascertained by elemental analysis, ^{1}H NMR, FT-IR, UV–Vis and FAB-mass spectroscopy. The FAB-mass spectral data were in compliance with the calculated formula weights of the compounds. The IR spectrum of the ligand exhibited a broad band at ~3432 cm^{-1} due to the presence of a phenolic-OH group. The C=N stretching vibration of the ligand was located at ~1672 cm^{-1}. In the complexes, the ν_{CN} vibrational stretching frequency was shifted to a lower wave number ($\Delta\nu$ ~30 cm^{-1}) and ν_{OH} mode was absent. This clearly suggests the coordination of the azomethine nitrogen and phenolate oxygen atoms to the metal in the complexes. The ^{1}H NMR spectrum of the ligand consisted of a singlet at δ 15 ppm due to the phenolic-OH proton and another singlet at δ 8.31 ppm due to the imine proton. A relatively small upfield shift (~0.01 ppm) of the —N=CH proton and the absence of a signal for the phenolate proton in the ^{1}H NMR spectra of the metal complexes further suggests coordination through the phenolate oxygen and the azomethine nitrogen atoms of the ligand. DFT studies (*vide infra*) revealed the geometry of the complexes to be distorted tetrahedral. The computed metal-O/N bond lengths and the bond angles (*vide infra*) complied well with related crystallographically characterized non-mesomorphic tetrahedral zinc-Schiff base complexes [55].

3.2. Mesomorphic properties

The phase behavior of the compounds was studied by polarizing optical microscopy (POM), differential scanning calorimetry (DSC) and variable temperature powder-XRD techniques. The phase sequence, transition temperatures and associated enthalpies are summarized in Table 1. The ligand is non-mesomorphic, the greater conformational flexibility of the uncoordinated ligand molecule is believed to be one plausible reason for its non-mesomorphic character. On complexation, this flexibility is reduced, which might be responsible for induction of mesomorphism in the zinc(II) and cadmium(II) complexes. The mercury(II) complex, however, decomposed at 270 °C precluding any mesomorphic study. Upon cooling the sample from isotropic melt, the zinc(II) complex showed a 'platelet texture' (Fig. 1) at 127 °C, typical of the smectic E (or crystal E) phase [56]. The DSC profile (Fig. 2) showed four transitions on heating and two in the cooling cycle. The peaks below the melting point are believed to have arisen from a crystal-to-crystal transition which could not be detected in the POM study. In the case of the cadmium(II) complex, a fibrous texture was observed (Fig. 3) upon cooling at 228 °C. The DSC trace (Fig. 4) revealed two transitions each in the heating and cooling scans. In contrast to the zinc complex, interestingly the mesophase for the cadmium(II) complex was quite stable over a wide temperature range (231–88 °C). The reversibility of the thermal behavior of the zinc(II) and cadmium(II) complexes was established by DSC through repeated heating and cooling runs.

The powder XRD profile of the zinc(II) complex, recorded at 122 °C (Fig. 5a), consisted of one very sharp and three relatively weak reflections in the low angle region with a reciprocal spacing ratio of 1:2:3:4. The spacing could be assigned to (001), (002), (003) and (004) reflections of a lamellar lattice (Table 2) [56,57]. The (001) reflection is attributed to the smectic layer-spacing, d. Additionally, in the wide-angle region multiple harmonics corresponding to spacings of 5.0 Å (111) and 4.9 Å (200) were observed. Also, a broad-scattering halo at ~4.6 Å for the molten alkyl chains was observed. Presence of three strong reflections in the wide angle region indexed to (111), (200) and (112) is a signature of the SmE phase [56,57]. The phase was also validated by the characteristic 'platelet texture' observed in the POM study. The calamitic molecules thus are presumed to be arranged in layers with orthorhombic symmetry and a herringbone array, typical for an SmE phase (Fig. 6) [57]. The aromatic core π–π interactions and hydrophobic interactions of the alkyl chains renders them to act as segregated parts. The lattice parameters of the SmE phase are deduced as a = 9.89 Å, b = 6.05 Å, c = 24.65 Å and V_{cell} = 1461.24 $Å^3$ (Table 2). The calculated interlayer distance of 24.65 Å is about half the length of the fully extended molecule as computed (*vide infra*) by DFT (42.1 Å). The molecular area for the proposed arrangement, A_M (65.38 $Å^2$) is deduced from the relation $A_M = V_M/d$; (molecular volume, V_M = 1608.28 $Å^3$, density, ρ = 1 g/cm^3). Assuming a parallel arrangement of the molecules perpendicular to layer direction, the calculated A_M value would correspond to a cross-sectional area per aliphatic arm, $A_{ch} = A_M/2$ = 32.69 $Å^2$, which is considerably larger than the cross-sectional area of a stretched molten alkyl arm (A_{ch} = 20.915 + 0.01593, T = 22.85 $Å^2$ at 122 °C). The alkyl arms are therefore believed to be considerably interdigitated within the layers [16]. The V_{cell}/V_M ratio (= 0.9) also suggests approximately one molecule per unit cell.

The diffractogram at 80 °C (Fig. 5b) consisted of a number of sharp reflections in both the low as well as wide angles, consistent with the existence of a crystalline phase. Moreover, the diffractogram was devoid of any diffuse band at wide angles, thus pointing to the crystalline nature of the material.

The PXRD profile of the cadmium(II) complex, recorded at 210 °C (Fig. 7), exhibited one very sharp and a number of relatively less intense reflections in the small angle region. The first and fifth peak are indexed to (001) and (002) reflections, respectively, corresponding to a layered structure (Table 2). Other small and mid-angle reflections, however, indicated a three dimensional order of the mesophase. A poorly resolved diffuse halo at 4.6 Å in the wide angle region indicated lateral short-range order of the molten alkyl chains. On the basis of these features, a highly ordered mesophase reminiscent of soft crystals has been suggested, possessing both a layer arrangement and a 3D structure [58–60]. The observed pattern could be indexed to a primitive triclinic lattice (p_1) with lattice parameters a = 9.9 Å, b = 21.7 Å, c = 37.1 Å; α = 47°, β = 68.6°, γ = 57° and V_{cell} = 4870 $Å^3$. The mesophase with a triclinic lattice may thus be designated as M_T [59]. The molecular volume, V_M = 1462.45 $Å^3$ was calculated assuming a density close to 1.2 g/cm^3. Customarily, a density of 1 g/cm^3 is presumed for liquid crystalline mesophases, resulting from organic molecules or metallomesogens incorporating lighter metals. In some instances, higher density values ($\rho \approx$ 1.1–1.2 g/cm^3) were reported for some smectic gold enriched dendrimers [61], discotic gold pyrazolate compounds [62], discotic cyclopalladated metallomesogens [63], some potassium salts of crown ethers [64] and columnar hexaalkyloxytriphenylenes [65]. A higher density has thus been considered for the newly synthesized cadmium(II) complex, considering a heavier metal core. Thus approximately three molecules per unit cell in the triclinic lattice in the soft crystalline phase has been worked out.

Variation in the type of mesophase formed on changing the metal from zinc(II) to cadmium(II) and the lack of mesomorphism or thermal instability of the complex of the other congener, mercury(II), is not discernible at this moment. A noticeable aspect is

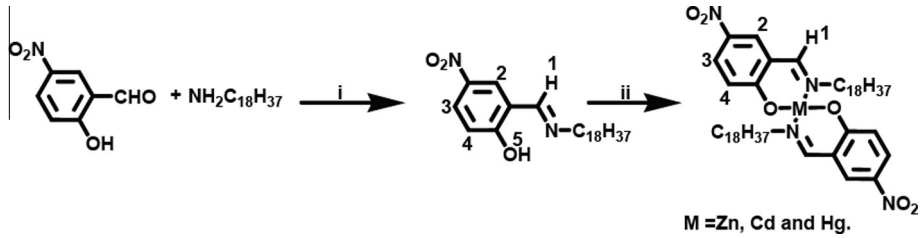

Scheme 1. (i) Glacial acetic acid, methanol, reflux 3 h, (ii) $M(OAc)_2{\cdot}nH_2O$ (M = Zn, Cd; n = 2 or Hg; n = 0), Methanol, stir, 2 h.

Table 1
Phase transition data of $[ZnL_2]$ and $[CdL_2]$.

Compounds	T[a] (°C)	Transition[b]	ΔH (kJ mol^{-1})	$_{\Delta trs}S$ (J K^{-1} mol^{-1})
$[ZnL_2]$	85.7	Cr–Cr_1	16.9	47.1
	104.5	Cr_1–Cr_2	17.9	47.4
	121.1	Cr_2–SmE	36.9	93.6
	133.6	SmE–I	22.8	56.1
	127.1	I–SmE	25.2	62.9
	114.2	SmE–Cr_2	37.2	96.0
$[CdL_2]$	116.0	Cr–M_T	62.6	160.9
	235.8	M_T–I	15.4	30.2
	231.2	I–M_T	14.9	29.5
	88.6	M_T–Cr	47.4	131.0

[a] DSC peak temperature.
[b] Cr: crystal, SmE: smectic E or soft crystal E, M_T = mesophase triclinic.

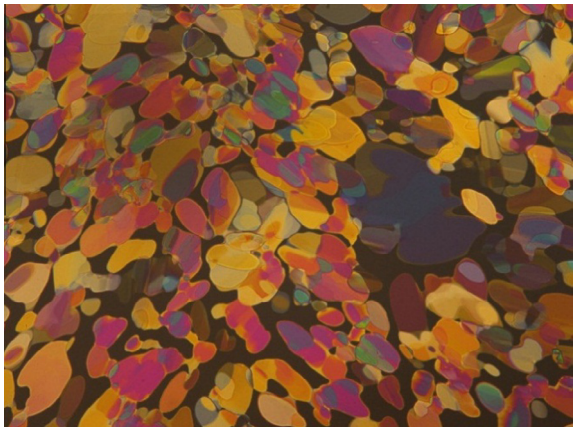

Fig. 1. Platelet texture of $[ZnL_2]$ upon cooling at 127 °C.

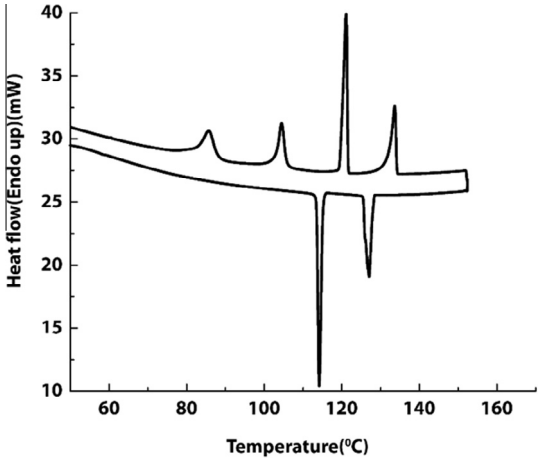

Fig. 2. DSC thermogram of $[ZnL_2]$.

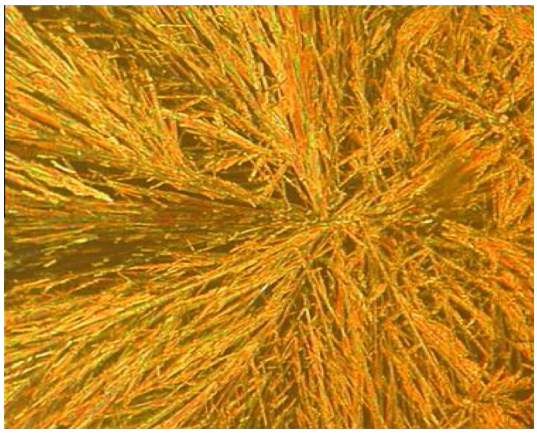

Fig. 3. Fibrous texture of $[CdL_2]$ upon cooling at 228 °C.

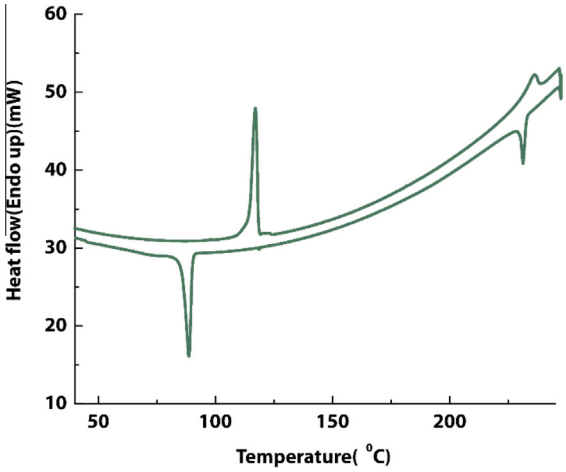

Fig. 4. DSC thermogram of $[CdL_2]$.

the significant variation in the ionic radius of the metal centers (Zn^{2+} = 0.74 Å; Cd^{2+} = 0.95 Å; Hg^{2+} = 1.02 Å) [54,66].

3.3. Photophysical properties

The absorption spectra (Fig. 8) of the compounds were recorded in dichloromethane solution (10^{-5} M) at room temperature. The ligand showed three bands centered at 260, 323 and 403 nm, respectively, attributed to the π–π* transition, localized on the aromatic rings and the C=N fragment (Table 3). Upon complexation, all the π–π* bands were virtually unaltered in the cadmium(II) and mercury(II) complexes. The absorption spectrum of the zinc(II) complex, however, exhibited only two bands at 257 and 343 nm. The low-intensity ligand centered π–π* transition peak at ~400 nm, observed in the spectra of the ligand and the cadmium

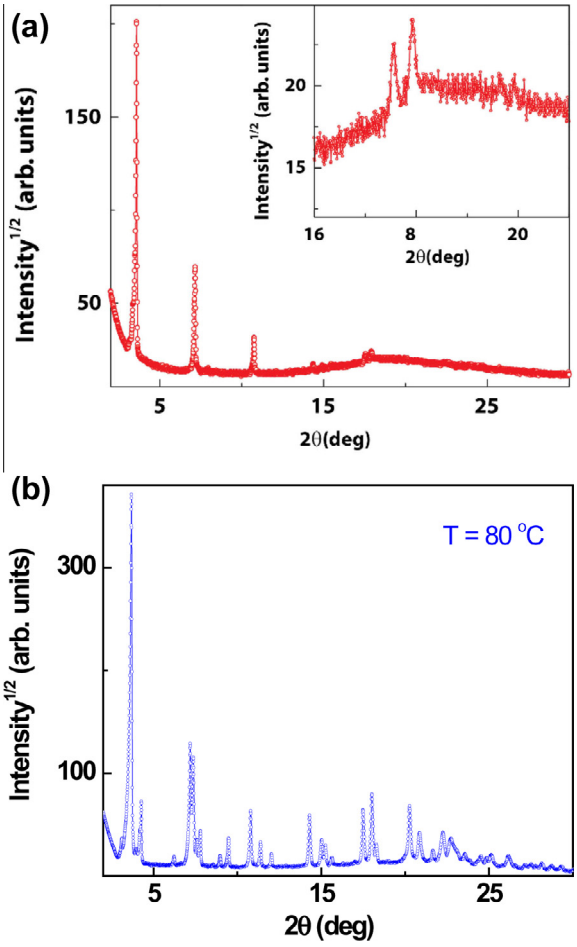

Fig. 5. PXRD pattern of [ZnL_2] recorded at 122 °C (a) and (b) at 80 °C.

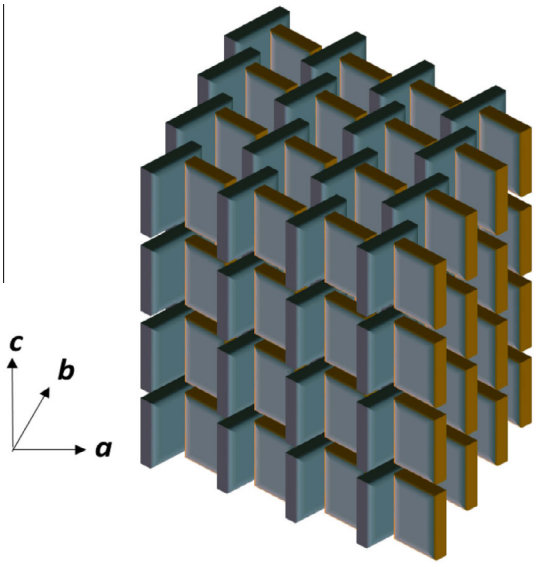

Fig. 6. The 'herringbone' model for the self-assembled rod-like complex molecules in the smectic E phase.

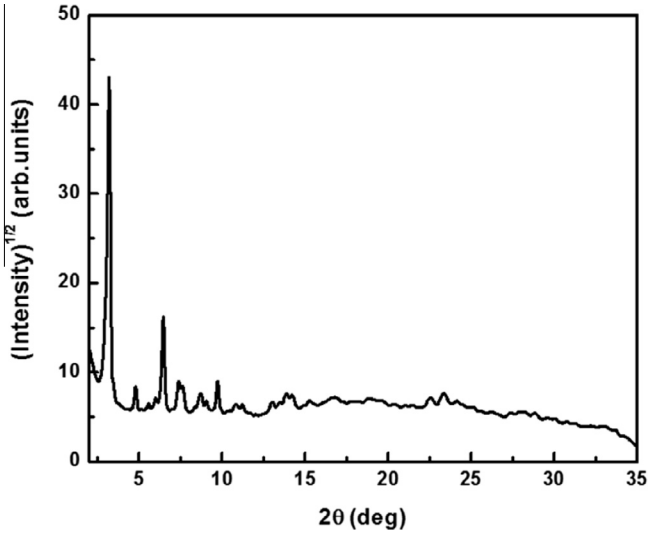

Fig. 7. PXRD profile of [CdL_2] at 210 °C.

Table 2
PXRD data of [ZnL_2] and [CdL_2].

Compound	Mesophase[a] Lattice constants (Å)	d_{obsd} (Å) (d_{calcd} (Å))[b]	Miller indices *hkl*[c]
[ZnL_2]	SmE (at 122 °C)	24.64(24.65)	(001)
	d = 24.65 Å	12.33(12.32)	(002)
	V_M = 1608.28 Å^3	8.22(8.22)	(003)
	A_M = 65.38 Å^2	6.17(6.16)	(004)
	a = 9.89 Å	5.05(5.05)	(111)
	b = 6.05 Å	4.95(4.95)	(200)
	c = 24.65 Å	4.56^{diffuse}	
	V_{cell} = 1461.24 Å^3		
[CdL_2]	M_T (at 210 °C)	27.33(27.14)	(001)
	a = 9.9 Å	18.37(18.05)	(011)
	b = 21.7 Å	15.82(15.91)	(012)
	c = 37.1 Å	14.64(14.28)	(010)
	α = 47°	13.65(13.57)	(002)
	β = 68.6°	11.62(11.51)	(013)
	γ = 57°	10.15(10.29)	(01−1)
	V_{cell} = 4870 Å^3	9.75(9.80)	(111)
	V_M = 1462.45 Å^3	9.08(9.08)	(110)
		8.14(8.14)	(113)
		6.80(6.80)	(025)
		6.38(6.33)	(1−1−1)
		6.22(6.24)	(1−1−2)
		3.95(3.95)	(1−3−3)
		3.80(3.80)	(23−1)
		3.16(3.16)	(2−2−3)
		4.56^{diffuse}	

[a] Molecular volume, V_M is calculated using the formula: $V_M = M/\lambda\rho N_A$, where M is the molecular weight of the compound, N_A is the Avogadro number, ρ is the density (~1 g cm^{-3} for the zinc(II) and 1.2 g cm^{-3} for the cadmium(II) complexes), $\lambda(T)$ is a temperature correction coefficient at the temperature of the experiment (T). $\lambda(T) = V_{CH2}(T°)/V_{CH2}(T)$; where $V_{CH2}(T) = 26.5616 + 0.02023T$ is the volume of a methylene group (in Å^3) at a given temperature (in °C), and T ° = 25 °C [75].
V_{cell}; unit cell volume: in the orthorhombic lattice, $V_{cell} = abc$; in triclinic lattice, $V_{cell} = abc\,(1 - \cos^2\alpha - \cos^2\beta - \cos^2\gamma + 2\cos\alpha\cos\beta\cos\gamma)^{1/2}$.
[b] d_{obsd} and d_{calcd} are the experimentally observed and calculated diffraction spacings, respectively. The distances are given in Å.
[c] *hkl* are the Miller indices of the reflections in SmE and M_T phases.

(II) and mercury(II) complexes, appeared as a weak shoulder in the spectrum of the zinc(II) complex, while the second absorption peak was considerably bathochromically shifted (~33 nm) compared to the free ligand. Photoluminescence studies of the compounds were performed both in dichloromethane solution and in the solid state. The ligand is non-emissive, the probable reason being the greater conformational flexibility. The complexes, however, exhibited fluorescence at room temperature with emission maxima at ~479 nm (Fig. 9 and Table 3). The emission observed at room temperature

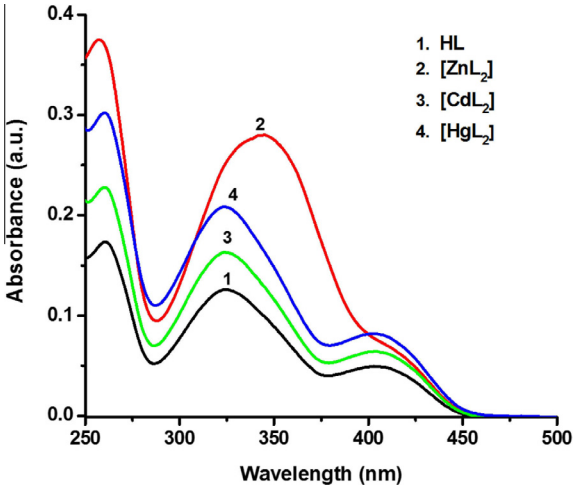

Fig. 8. UV–Vis spectra of the ligand and the complexes (CH_2Cl_2; 10^{-5} M).

Table 3
UV–Vis and photoluminescence data of the ligand and metal complexes.

Compounds	$\pi\rightarrow\pi^*$ (λ, nm; ε, l mol^{-1} cm^{-1})	[a]PL (λ, nm; solution)	[a]PL (λ, nm; solid)
HL	260 (17464) 323 (12689) 403 (5090)	–	–
ZnL_2	257 (37547) 343 (28107) 400^{sh} (7894)	475	470
CdL_2	259 (22961) 324 (16478) 400 (6557)	479	467
HgL_2	259 (30310) 322 (20880) 399 (8397)	470	466

[a] PL: photoluminescence; *sh*: shoulder.

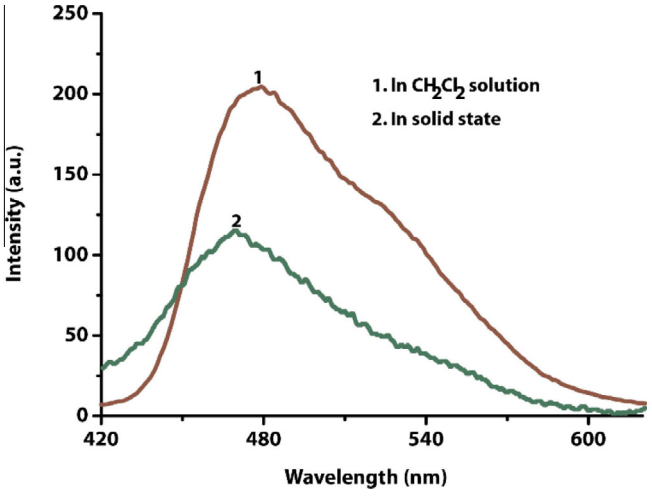

Fig. 9. Photoluminescence spectrum of $[CdL_2]$ (10^{-5} M; $\lambda_{ex.}$ = 325 nm).

in the complexes stems from the intra-ligand π–π^* transition. Chelation provides rigidity to the ligand and reduces energy loss via non-radiative de-activation. The luminescence intensities of the complexes were found to decrease in the order: Zn > Cd > Hg. The emission quantum yields of the complexes have been determined in dichloromethane solution at room temperature and are found to be 0.20, 0.16 and 0.09, respectively for the zinc, cadmium and mercury complexes. The lowest value of the quantum yield for the mercury complex might be due to the 'heavy atom' effect [67]. The solid state emission spectra of the complexes were recorded on a uniform thin film. The emission band of the complexes was quite broad and exhibited an unusual blue shift (~467 nm) compared to the solution spectra, while the emission intensities were largely quenched. In the solid state somewhat larger aggregation causes enhanced intermolecular interactions, which explains the reduced luminescence intensity [68]. Further it has been argued that a tetrahedral geometry or formation of a non-planar molecular shape, as in the present case, prevent interchromophoric contacts leading to a blue shift of the emission maxima with respect to those observed in solution [50].

3.4. DFT study

Density functional theory (DFT) calculations at the B3LYP level of theory on the ligand and its zinc(II), cadmium(II) and mercury (II) complexes were carried out using the GAUSSIAN 09 program [69]. The geometries of all the species were fully optimized at the gradient corrected DFT level using a three parameters fit of Becke's hybrid functional combined with the Lee–Yang–Parr correlation functional, termed as B3LYP [70,71]. For the zinc, cadmium and mercury atoms the Los Alamos effective core potential plus double zeta (LanL2DZ) basis set were employed [72] and the 6-311G(d,p) basis set was employed for all non-metal atoms. The gas phase ground state geometries of the ligand and its zinc, cadmium and mercury complexes were fully optimized using the restricted B3LYP methods without imposing any symmetry constraints. Calculations for vibrational frequencies were performed alongside each geometry optimization to ensure the stability of the ground state, as denoted by the absence of imaginary frequencies. Natural bond orbital (NBO) calculations were performed with the NBO code included in the GAUSSIAN 09 program at the same level of theory [73].

3.5. Geometry optimization

DFT calculations were performed in order to get better insight into the electronic structure of the ligand as well as its complexes with zinc, cadmium and mercury. Optimized geometries of the ligand, zinc, cadmium and mercury complexes (Figs. 10a–d) and computed significant geometric parameters of the complexes were evaluated at B3LYP level (Table 4). All the metal (M = Zn, Cd, Hg) centers are tetra coordinated with two [N,O] donor bidentate ligands through two nitrogen atoms of two C=N groups and two oxygen atoms of two phenolic groups. The average M—O and M—N bond lengths in the complexes are 1.971 and 2.087, 2.159 and 2.290, and 2.266 and 2.357 Å, respectively (Table 4). The average O1—M—O2 bond angles are 128.4°, 135.8° and 139.3° and the average N1—M—N2 bond angles are found to be 125.3°, 129.0° and 137.6°, respectively, around the zinc, cadmium and mercury atoms, which deviate substantially from those expected for a square planar motif, indicating a distorted tetrahedral geometry. The molecular lengths of the zinc(II), cadmium(II) and mercury (II) complexes computed from DFT are found to be 42.1, 42.4 and 42.7 Å, respectively.

3.6. Natural bond orbital (NBO) analysis

DFT with natural bond orbital (NBO) analysis allows deeper insight into the nature of metal–ligand bonding. The natural charges and electronic configuration of the atoms of the complexes and free ligand evaluated by natural bond orbital (NBO) analysis

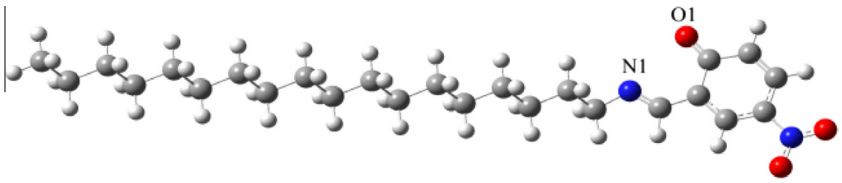

Fig. 10a. Optimized structure of the ligand, HL.

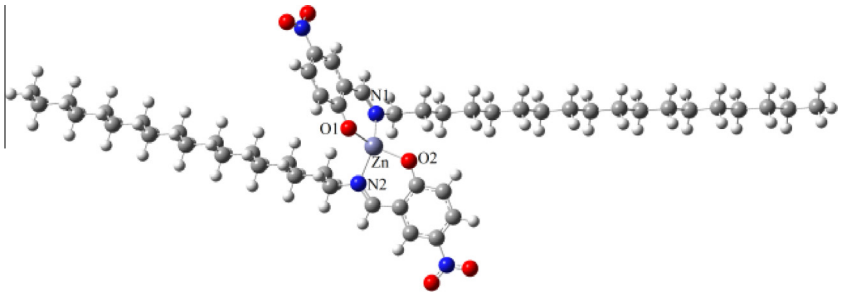

Fig. 10b. Optimized structure of $[ZnL_2]$.

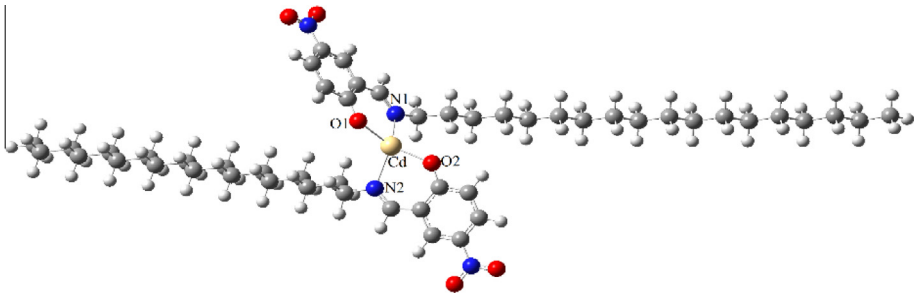

Fig. 10c. Optimized structure of $[CdL_2]$.

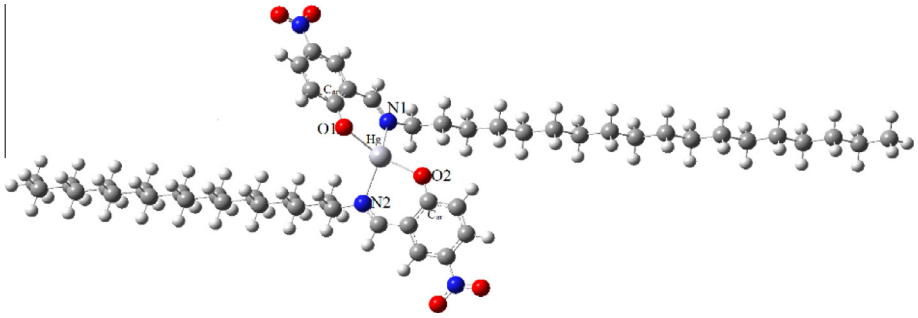

Fig. 10d. Optimized structure of $[HgL_2]$.

Table 4
Selected bond lengths (Å) and bond angles (°) for the zinc(II), cadmium(II) and mercury(II) complexes evaluated at the B3LYP level.

Structural parameters	Zn	Cd	Hg
M—O1	1.971	2.159	2.269
M—O2	1.971	2.158	2.263
M—N1	2.087	2.289	2.354
M—N2	2.088	2.291	2.361
O1—M—O2	128.4	135.8	139.3
N1—M—N2	125.3	129.0	137.6
O1—M—N1	93.0	86.2	83.7
O2—M—N2	92.8	86.0	83.5
O1—M—N2	108.6	111.8	108.7
O2—M—N1	112.1	114.4	113.8

are summarized in Table 5. The calculated natural charges on the metal ions zinc, cadmium and mercury are considerably lower than the formal charge of +2. The electronic populations on the p_x, p_y and p_z orbitals of the zinc, cadmium and mercury atoms in their respective complexes are found to be (0.0990, 0.1133 and 0.1026), (0.0730, 0.0800 and 0.0700) and (0.0529, 0.0695 and 0.0640), respectively. The d_{xy}, d_{zx}, d_{yz}, $d_{x^2-y^2}$ and d_{z^2} orbitals of zinc, cadmium and mercury atoms in their complexes, however, are occupied by more than 1.99 e^-. Comparing the atomic charges in the free ligand and its complexes with zinc, cadmium and mercury, it can be suggested that atomic charge re-distribution occurs on all the atoms. The calculated natural atomic charges on zinc, cadmium and mercury are found to be +1.405, +1.487 and +1.394, respec-

Table 5
Natural atomic charges and natural electron configuration of selected atoms of the ligand and zinc(II), cadmium(II) and mercury(II) complexes evaluated at the B3LYP level.

Atoms	Ligand		Zn^{2+}		Cd^{2+}		Hg^{2+}	
	Charge	Configuration	Charge	Configuration	Charge	Configuration	Charge	Configuration
O1	−0.614	[core]$2S^{1.72}2p^{4.89}$	−0.795	[core]$2S^{1.67}2p^{5.12}3p^{0.01}$	−0.807	[core]$2S^{1.68}2p^{5.12}3p^{0.01}$	−0.785	[core]$2S^{1.69}2p^{5.09}3p^{0.01}$
O2			−0.800	[core]$2S^{1.67}2p^{5.12}3p^{0.01}$	−0.812	[core]$2S^{1.68}2p^{5.12}3p^{0.01}$	−0.779	[core]$2S^{1.69}2p^{5.08}3p^{0.01}$
N1	−0.433	[core]$2S^{1.39}2p^{4.03}3p^{0.01}$	−0.634	[core]$2S^{1.35}2p^{4.26}3p^{0.01}$	−0.637	[core]$2S^{1.36}2p^{4.26}3p^{0.01}$	−0.613	[core]$2S^{1.36}2p^{4.24}3p^{0.01}$
N2			−0.629	[core]$2S^{1.35}2p^{4.26}3p^{0.01}$	−0.633	[core]$2S^{1.36}2p^{4.25}3p^{0.01}$	−0.68	[core]$2S^{1.36}2p^{4.24}3p^{0.01}$
M			1.405	[core]$4S^{0.30}3d^{9.97}4p^{0.31}$	1.487	[core]$5S^{0.30}4d^{9.98}5p^{0.22}$	1.394	[core]$5S^{0.44}5d^{9.97}6p^{0.19}6d^{0.01}$

tively, which reflects ligand-to-metal charge transfer in all the complexes. According to the NBO, the electronic configuration of Zn is: [core] $4s^{0.303}d^{9.974}p^{0.31}$, which corresponds to 18 core electrons, 10.27 valence electrons (on 4s and 3d atomic orbitals) and 0.31 Rydberg electrons (mainly on 4p orbitals), giving 28.58 electrons. This is consistent with the calculated natural atomic charge on the zinc atom (+1.405) in its complex. The electronic configuration of Cd is: [core] $5s^{0.30}4d^{9.985}p^{0.22}$, with 36 core electrons, 10.28 valence electrons (on 5s and 4d atomic orbitals) and 0.22 Rydberg electrons (mainly on 5p orbitals) leading to 46.50 electrons, which matched well with the calculated natural charge on the cadmium atom (+1.487) in the complex. The electronic configuration of the mercury atom in its complex is calculated to be [core] $6s^{0.445}d^{9.976}p^{0.196}d^{0.01}$ that matches well with the calculated natural charge on the mercury atom (+1.394) in the complex. The natural atomic charges on the oxygen atoms of the ligand bound to metal ions change from −0.614 to −0.795 and −0.800 in the zinc complex, to −0.807 and −0.812 in the cadmium complex and to −0.785 and −0.779 in the mercury complex, while the atomic charges on the nitrogen atoms of the ligand change from −0.433 to −0.634 and −0.629, to −0.637 and 0.633, and to −0.618 and −0.613 on complexation with zinc, cadmium and mercury, respectively (Table 5). The optimized geometry also revealed that the distance between the oxygen and aromatic carbon atoms (O—$C_{ar.}$) increases from 1.271 Å in the free ligand to 1.314, 1.318 and 1.286 Å in the zinc, cadmium and mercury complexes, respectively. The O—$C_{ar.}$ bond is weakened upon complex formation, implying coordination through the oxygen atom.

3.7. Frontier molecular orbitals

Frontier molecular orbitals play an important role in determining the electronic properties of molecules [74]. The LUMO and HOMO energies of the free ligand and its complexes with zinc, cadmium and mercury are calculated to be −0.254 and −1.816, −2.349 and −6.520, −2.568 and −6.524, and −2.244 and −6.384 eV, respectively. The corresponding energy differences (ΔE) are 1.562, 4.171, 3.956 and 4.140 eV, respectively. A small HOMO–LUMO gap implies a low kinetic stability and high chemical reactivity, because it is energetically favorable to add electrons to the LUMO or to extract electrons from the HOMO. The calculated HOMO–LUMO gap of the complexes revealed that the zinc complex is relatively more stable than the rest.

4. Conclusion

A new N-alkylated bidentate [N,O]-donor rod shaped salicylaldimine Schiff base has been synthesized and complexation with Group 12 d^{10} metal ions was achieved by the interaction of the Schiff base ligand and Zn^{2+} or Cd^{2+} or Hg^{2+} ions. The ligand is neither fluorescent nor mesomorphic, however the zinc(II) and cadmium(II) complexes in addition to being fluorescent showed highly ordered mesophases. The complexes exhibited luminescence both in the solid and solution state. The mercury(II) complex, though luminescent, decomposed prior to melting. DFT calculations carried out using the GAUSSIAN 09 program at the B3LYP level revealed a distorted tetrahedral geometry for all the complexes. Examples of tetrahedral coordination geometry exhibiting liquid crystallinity are rather uncommon. The application potential of the newly synthesized complexes as multi-functional materials are avenues to be explored in the near future.

Acknowledgements

S.C. gratefully acknowledges the receipt of INSPIRE Research Fellowship (Code: IF110692) from the Department of Science and Technology, India. D.D.P. thanks the University Grants Commission (UGC) for financial support under the Research Fellowship Scheme for Meritorious Students (RFSMS). P.M. thanks the Department of Science and Technology (Ministry of Science & Technology), New Delhi, India for financial support. Sophisticated Analytical Instrumentation Facility, North Eastern Hill University, Shillong and Central Drug Research Institute, Lucknow are acknowledged for some spectral results. The authors also thank DBT e-Library Consortium (DeLCON) of Bio-Informatics Centre, Assam University, India.

References

[1] A. Kajal, S. Bala, S. Kamboj, N. Sharma, V. Saini, J. Catal. 2013 (2013), http://dx.doi.org/10.1155/2013/893512. Article ID 893512.
[2] H. Xu, R. Chen, Q. Sun, W. Lai, Q. Su, W. Huang, X. Liu, Chem. Soc. Rev. 43 (2014) 3259.
[3] A.K. Neeraj, V. Kumar, R. Prajapati, S.K. Asthana, K.K. Upadhyaya, J. Zhao, Dalton Trans. 43 (2014) 5831.
[4] S. Kumar, D.N. Dhar, P.N. Saxena, J. Sci. Ind. Res. 68 (2009) 181.
[5] S. Dave, N. Bansal, Int. J. Curr. Pharm. Res. 5 (2013) 6.
[6] Y. Xin, J. Yuan, Polym. Chem. 3 (2012) 3045.
[7] K.M. Abuamer, A.A. Maihub, M.M. El-Ajaily, A.M. Etorki, M.M. Abou-Krisha, M. A. Almagani, Int. J. Org. Chem. 4 (2014) 7.
[8] I. Kostova, L. Saso, Curr. Med. Chem. 20 (2013) 4609.
[9] K.C. Gupta, A.K. Sutar, Coord. Chem. Rev. 252 (2008) 1420.
[10] P.G. Cozzi, Chem. Soc. Rev. 33 (2004) 410.
[11] N. Hoshino, Coord. Chem. Rev. 174 (1998) 77.
[12] J. Hanna, Opto-Electron. Rev. 13 (2005) 259.
[13] M. O'Neill, S.M. Kelly, Adv. Mater. 15 (2003) 1135.
[14] F. Vera, J.L. Serrano, T. Sierra, Chem. Soc. Rev. 38 (2009) 781.
[15] A. Crispini, M. Ghedini, D. Pucci, Beilstein J. Org. Chem. 5 (2009) 1.
[16] H.A.R. Pramanik, G. Das, C.R. Bhattacharjee, P.C. Paul, P. Mondal, S. Krishna Prasad, D.S. Shankar Rao, Chem. Eur. J. 19 (2013) 13151.
[17] A.A. Knyazev, Y.G. Galyametdinov, B. Goderis, K. Driesen, K. Goossens, C.G. Walrand, K. Binnemans, T. Cardinaels, Eur. J. Inorg. Chem. (2008) 756.
[18] E. Tritto, R. Chico, G. Sanz-Enguita, C.L. Folcia, J. Ortega, S. Coco, P. Espinet, Inorg. Chem. 53 (2014) 3449.
[19] C.R. Wen, Y.J. Wang, H.C. Wang, H.S. Sheu, G.H. Lee, C.K. Lai, Chem. Mater. 17 (2005) 1646.
[20] M. Krikorian, S. Liu, T.M. Swager, J. Am. Chem. Soc. 136 (2014) 2952.
[21] C. Cuerva, J.A. Campo, P. Ovejero, M.R. Torres, E. Oliveira, S.M. Santos, C. Lodeiro, M. Cano, J. Mater. Chem. C 2 (2014) 9167.
[22] A.M. Talarico, M. Ghedini, C.O. Rossi, E.I. Szerb, Soft Matter 8 (2012) 11661.
[23] A. Santoro, A.M. Prokhorov, V.N. Kozhevnikov, A.C. Whitwood, B. Donnio, J.A.G. Williams, D.W. Bruce, J. Am. Chem. Soc. 133 (2011) 5248.
[24] S. Debnath, H.F. Srour, B. Donnio, M. Fourmigué, F. Camerel, RSC Adv. 2 (2012) 4453.
[25] C.R. Bhattacharjee, G. Das, P. Mondal, Eur. J. Inorg. Chem. (2011) 5390.
[26] T. Cardinaels, J. Ramaekers, P. Nockemann, K. Driesen, K. Van Hecke, L. Van Meervelt, S.B. Lei, S. De Feyter, D. Guillon, B. Donnio, K. Binnemans, Chem. Mater. 20 (2008) 1278.

[27] S. Coco, C. Cordovilla, P. Espinet, J. Martin-Alvarez, P. Munoz, Inorg. Chem. 45 (2006) 10180.
[28] M.J. Mayoral, P. Ovejero, J.A. Campo, J.V. Heras, E. Pinilla, M.R. Torres, C. Lodeiro, M. Cano, Dalton Trans. (2008) 6912.
[29] P. Ovejero, E. Asensio, J.V. Heras, J.A. Campo, M. Cano, M.R. Torres, C. Núñez, C. Lodeiro, Dalton Trans. 42 (2013) 2107.
[30] S. Chakraborty, C.R. Bhattacharjee, P. Mondal, S. Krishna Prasad, D.S. Shankar Rao, Dalton Trans. 44 (2015) 7477.
[31] D. Pucci, A. Crispini, M. Ghedini, M. La Deda, P.F. Liguori, C. Pettinari, E.I. Szerb, RSC Adv. 2 (2012) 9071.
[32] A. Kishimura, T. Yamashita, K. Yamaguchi, T. Aida, Nat. Mater. 4 (2005) 546.
[33] A. Barbieri, G. Accorsi, N. Armaroli, Chem. Commun. (2008) 2185.
[34] R.C. Evans, P. Douglas, C. Winscom, J. Coord. Chem. Rev. 250 (2006) 2093.
[35] O.N. Kadkin, J. An, H. Han, Y.G. Galyametdinov, Eur. J. Inorg. Chem. (2008) 1682.
[36] C.R. Bhattacharjee, C. Datta, G. Das, P. Mondal, Liq. Cryst. 39 (2012) 373.
[37] M. Marcos, A. Omenat, J. Barberá, F. Durán, J.L. Serrano, J. Mater. Chem. 14 (2004) 3321.
[38] K. Nejati, Z. Rezvani, New J. Chem. 27 (2003) 1665.
[39] Y. Galyametdinov, V. Ksenofontov, A. Prosvirin, I. Ovchinnikov, G. Ivanova, P. Gütlich, W. Haase, Angew. Chem., Int. Ed. 40 (2001) 4269.
[40] R. Chico, C. Domínguez, B. Donnio, S. Coco, P. Espinet, Dalton Trans. 40 (2011) 5977.
[41] D. Pucci, I. Aiello, A. Bellusci, A. Crispini, M. Ghedini, M. La Deda, Eur. J. Inorg. Chem. (2009) 4274.
[42] P.A. Spegt, A.E. Skoulios, Acta Crystallogr. 16 (1963) 301.
[43] B.A. Gregg, M.A. Fox, A.J. Bard, J. Am. Chem. Soc. 111 (1989) 3024.
[44] S.A. Hudson, P.M. Maitlis, Chem. Rev. 93 (1993) 861.
[45] O. Celik, O. Dag, Angew. Chem., Int. Ed. 40 (2001) 3799.
[46] O. Dag, S. Alayoğlu, İ. Uysal, J. Phys. Chem. B 108 (2004) 8439.
[47] F. Neve, O. Francescangeli, A. Crispini, Inorg. Chim. Acta 338 (2002) 51.
[48] E. Terazzi, J.-M. Benech, J.-P. Rivera, G. Bernardinelli, B. Donnio, D. Guillon, C. Piguet, Dalton Trans. (2003) 769.
[49] A. Pegenau, T. Hegmann, C. Tschierske, S. Diele, Chem. Eur. J. 5 (1999) 1643.
[50] E. Cavero, S. Uriel, P. Romero, J.L. Serrano, R. Giménez, J. Am. Chem. Soc. 129 (2007) 11608.
[51] C. Cuerva, P. Ovejero, J.A. Campo, M. Cano, New J. Chem. 38 (2014) 511.
[52] R. Giménez, A.B. Manrique, S. Uriel, J. Barberá, J.L. Serrano, Chem. Commun. (2004) 2064.
[53] G. Barberio, A. Bellusci, A. Crispini, M. Ghedini, A. Golemme, P. Prus, D. Pucci, Eur. J. Inorg. Chem. (2005) 181.
[54] F. Morale, R.L. Finn, S.R. Collinson, A.J. Blake, C. Wilson, D.W. Bruce, D. Guillon, B. Donnio, M. Schroder, New J. Chem. 32 (2008) 297.
[55] P. Shang, L. Zhang, J. Chem. (2013), http://dx.doi.org/10.1155/2013/206847.
[56] S.M. Schultz, G. Kehr, R. Fröhlich, G. Erker, N. Kapernaum, C. Hägele, F. Giesselmann, S. Laschat, R. Judele, A. Baro, Liq. Cryst. 34 (2007) 919.
[57] S. Diele, S. Tosch, S. Mahnke, D. Dem, Cryst. Res. Technol. 26 (1991) 809.
[58] F. Lincker, B. Heinrich, R. De Bettignies, P. Rannou, J. Pecaut, B. Grevin, A. Pron, B. Donnio, R. Demadrille, J. Mater. Chem. 21 (2011) 5238.
[59] K. Oikawa, H. Monobe, K. Nakayama, T. Kimoto, K. Tsuchiya, B. Heinrich, D. Guillon, Y. Shimizu, M. Yokoyama, Adv. Mater. 19 (2007) 1864.
[60] B.G. Kim, S. Kim, J. Seo, N.-K. Oh, W.-C. Zin, S.Y. Park, Chem. Commun. (2003) 2306.
[61] C. Cordovilla, S. Coco, P. Espinet, B. Donnio, J. Am. Chem. Soc. 132 (2010) 1424.
[62] J. Barberá, A. Elduque, R. Giménez, F.J. Lahoz, J.A. López, L.A. Oro, J.L. Serrano, Inorg. Chem. 37 (1998) 2960.
[63] A. Ionescu, N. Godbert, A. Crispini, R. Termine, A. Golemme, M. Ghedini, J. Mater. Chem. 22 (2012) 23617.
[64] M. Kaller, C. Deck, A. Meister, G. Hause, A. Baro, S. Laschat, Chem.-Eur. J. 16 (2010) 6326.
[65] V.A. Gunyakov, N.P. Shestakov, S.M. Shibli, Liq. Cryst. 30 (2003) 871.
[66] J.D. Lee, Concise Inorganic Chemistry, fifth ed., Wiley, India, 2007. p. 839.
[67] Y.-W. Dong, R.-Q. Fan, P. Wang, L.-G. Wei, X.-M. Wang, H.-J. Zhang, S. Gao, Y.-L. Yang, Y.-L. Wang, Dalton Trans. 44 (2015) 5306.
[68] T. Yu, W. Su, W. Li, Z. Hong, R. Hua, B. Li, Thin Solid Films 515 (2007) 4080.
[69] M.J. Frisch, G.W. Trucks, H.B. Schlegel, G.E. Scuseria, M.A. Robb, J.R. Cheeseman, G. Scalmani, V. Barone, B. Mennucci, G.A. Petersson, H. Nakatsuji, M. Caricato, X. Li, H.P. Hratchian, A.F. Izmaylov, J. Bloino, G. Zheng, J.L. Sonnenberg, M. Hada, M. Ehara, K. Toyota, R. Fukuda, J. Hasegawa, M. Ishida, T. Nakajima, Y. Honda, O. Kitao, H. Nakai, T. Vreven, J.A. Montgomery Jr., J.E. Peralta, F. Ogliaro, M. Bearpark, J.J. Heyd, E. Brothers, K.N. Kudin, V.N. Staroverov, R. Kobayashi, J. Normand, K. Raghavachari, A. Rendell, J.C. Burant, S.S. Iyengar, J. Tomasi, M. Cossi, N. Rega, J.M. Millam, M. Klene, J.E. Knox, J.B. Cross, V. Bakken, C. Adamo, J. Jaramillo, R. Gomperts, R.E. Stratmann, O. Yazyev, A.J. Austin, R. Cammi, C. Pomelli, J.W. Ochterski, R.L. Martin, K. Morokuma, V.G. Zakrzewski, G.A. Voth, P. Salvador, J.J. Dannenberg, S. Dapprich, A.D. Daniels, Ö. Farkas, J.B. Foresman, J.V. Ortiz, J. Cioslowski, D.J. Fox, GAUSSIAN 09, Gaussian Inc, Wallingford CT, 2009.
[70] A.D. Becke, J. Chem. Phys. 98 (1993) 5648.
[71] C. Lee, W. Yang, R.G. Parr, Phys. Rev. B 37 (1988) 785.
[72] P.J. Hay, W.R. Wadt, J. Chem. Phys. 82 (1985) 270.
[73] J.N. Harvey, Annu. Rep. Prog. Chem. Sect. C.: Phys. Chem. 102 (2006) 203.
[74] I. Fleming, Frontier Orbitals and Organic Chemical Reactions, Wiley, London, 1976.
[75] M. Stępień, B. Donnio, J.L. Sessler, Chem. Eur. J. 13 (2007) 6853.

Dalton Transactions

PAPER

View Article Online
View Journal | View Issue

Cite this: *Dalton Trans.*, 2015, **44**, 7477

Synthesis and aggregation behaviour of luminescent mesomorphic zinc(II) complexes with 'salen' type asymmetric Schiff base ligands

Sutapa Chakraborty,[a] Chira R. Bhattacharjee,*[a] Paritosh Mondal,[a] S. Krishna Prasad[b] and D. S. Shankar Rao[b]

Received 24th December 2014,
Accepted 10th March 2015

DOI: 10.1039/c4dt03989k

www.rsc.org/dalton

A new series of photoluminescent Zn(II)-salen type asymmetric Schiff base complexes, [ZnL], H_2L = [*N*,*N*′-bis-(4-*n*-alkoxysalicylidene)-1,2-diaminopropane] (*n* = 12, 14 and 16) have been accessed and their mesomorphic and photophysical properties investigated. Though the ligands are non-mesomorphic, coordination to Zn^{2+} ion induces liquid crystalline behaviour. The complexes exhibited a lamello-columnar phase (Col_l) as characterized by a variable temperature powder X-ray diffraction (XRD) study. Intense blue emissions were observed for the complexes at room temperature in solution, in the solid state and in the mesophase. Aggregation properties of the complexes were explored in different solvents through absorption and photoluminescence studies. While de-aggregation to monomers occurred in coordinating solvents due to axial coordination to Zn(II), aggregates were formed in the solution of non-coordinating solvents. Density functional theory (DFT) computation carried out on a representative complex using a GAUSSIAN 09 program at the B3LYP level suggested a distorted square planar geometry. The results of a time-dependent DFT (TD-DFT) spectral correlative study showed the electronic properties of the complex molecule to be in compliance with the spectral data.

1. Introduction

Transition metal–salen complexes have been a recurrent theme in synthetic co-ordination chemistry, yet interest in this field continues unabated, possibly due to their wide applicability being unfolded in recent times.[1–4] A plethora of salen based complexes are now known to act as efficient catalysts both in homogeneous and heterogeneous reactions for asymmetric ring-opening of epoxides, aziridination, cyclopropanation, oxidation, reduction reaction of ketones, epoxidation of olefins, formation of cyclic and linear polycarbonates, catalytic enantioselective and diastereoselective redox reactions and Diels–Alder reactions.[5–8] Metal salen complexes are also efficient entities to study interactions with DNA, leading to the development of sensitive chemical probes for DNA.[9–12] Besides, such systems are also known to exhibit interesting fluorescence,[13–17] magnetic,[17,18] non-linear optical[19–21] and liquid crystalline properties[22–30] and act as electrochemical sensors.[31–33] Metallomesogens based on Zn(II)-salen complexes are quite intriguing because of the possibility of combining luminescence with liquid crystallinity to generate newer systems with exotic multifunctional properties.[34–37] Spacer group modification can lead to substantial changes in mesophase as well as photophysical behavior in such hemi-disc shaped complexes.[34–37] In the past few years we have reported some novel fluorescent liquid crystalline Zn(II)-salen complexes with different spacer groups showing hexagonal, rectangular and rectangular/oblique columnar mesomorphism.[35–37] By creating a minor modification at the central aromatic ring (spacer), new symmetry as well as newer organization in the mesophase could be achieved.[35–37]

Zn(II)-salen complexes and their derivatives also facilitate various structures which may be utilized in sensory materials for the detection of alkaloids[38] and nitro aromatics,[39,40] in the recognition of biologically relevant anions,[41] in selective receptors for tertiary amines,[42] in self-assembled heteromultimetallics,[43,44] in supramolecular box-shaped assemblies,[45,46] in molecular templates in catalytic studies,[47,48] in dopants for high performance OLEDS[49–51] and in the exploration of their unique second-order nonlinear optical properties.[19,20] The high Lewis acidity of the co-ordinatively unsaturated Zn^{2+} ion is believed to be the key to such behavior. The pentacoordinate nature of the Zn^{2+} ion boosted by the rigid geometry of the salen framework facilitates the axial binding of donor ligands, resulting in substantial variations in the optical absorption

[a]*Department of Chemistry, Assam University, Silchar 788011, Assam, India. E-mail: crbhattacharjee@rediffmail.com; Fax: +91-03842-270342; Tel: +91-03842-270848*
[b]*Centre for Nano and Soft Matter Sciences, Jalahalli, Bangalore 560013, India*

behaviour and enhanced fluorescence emission. In the absence of an axial ligand, coordinative saturation is achieved through intermolecular Zn···O interactions involving the phenolate oxygen atoms of the salen ligand acquiring a square based pyramidal structure.[52,55]

In continuation of our pursuit of designing photoluminescent metallomesogens, we report herein a new series of Zn(II) complexes of asymmetric 'salen' based *N*,*N*′-bis-(4-*n*-alkoxysalicylidene)-1,2-diaminopropane ligands. Induction of mesomorphism and photoluminescence *via* coordination to Zn(II) ion has been demonstrated. All the complexes are blue light emitters both in the solid state as well as in solution. The complexes all exhibited aggregate formation in non-coordinating solvents while only a monomer is favoured in coordinating solvents. Density functional theory (DFT) calculations carried out using the GAUSSIAN 09 program at the B3LYP level revealed a distorted square planar geometry around the metal center in the complexes. A time-dependent DFT spectral correlative study was undertaken to account for the electronic transitions in the complexes.

2. Results and discussion

2.1. Synthesis and structural assessment

Condensation of 4-alkoxy substituted aldehyde with the unsymmetrical amine, 1,2-diamino propane afforded the 'salen' type asymmetric Schiff base ligands. The strategy implemented for the synthesis of Schiff base ligands, [*N*,*N*′-bis-(4-*n*-alkoxysalicylidene)-1,2-diaminopropane], hereafter abbreviated as ***n*dap** (*n* = 12, 14 and 16 is the number of carbon atoms in alkyl chains; dap = 1,2-diaminopropane) and the mononuclear complexes (**Zn-*n*dap**) is summarized in Scheme 1. The structures of the ligands and the corresponding Zn(II) complexes were probed by elemental analyses, UV-visible, FT-IR and ^{1}H NMR spectroscopy. A broad band at ~3370 cm^{-1} attributed to the phenolic –OH group is observed in the FT-IR spectra of the ligands (***n*dap**). The C═N stretching vibration of the ligands are located in the region of 1653–1655 cm^{-1}. Upon complexation, the shift of the $\nu_{C=N}$ mode to a lower wave number, ~1638 cm^{-1} ($\Delta\nu \approx 16$ cm^{-1}) and the absence of a ν_{O-H} mode attest to the deprotonation of the Schiff-base prior to coordination of azomethine nitrogen and phenolate oxygen to the Zn^{2+} ion. The ^{1}H NMR spectra of the ligands showed two characteristic signals, at δ = 11.45 ppm, corresponding to the OH proton, and at ~8.22 and 8.18 ppm due to the resonance of two asymmetric imine protons. The ^{1}H NMR spectra of the corresponding Zn(II) complexes did not exhibit any signal for the phenolic –OH proton. Additionally, an upfield shift (~0.56 ppm) in the peak position of the –N═CH protons further validated azomethine nitrogen coordination.

2.2. Mesomorphic study

The mesophase behaviour of the compounds has been investigated by polarizing optical microscopy (POM), differential scanning calorimetry (DSC) and variable temperature powder XRD techniques. Free ligands (***n*dap**) are non-mesomorphic, presumably owing to greater conformational flexibility. However, upon complexation with a Zn(II) metal ion, mesomorphism is induced due to enhanced rigidity of the Schiff base ligand framework. The phase sequence, transition temperatures and associated enthalpies for the Zn(II) complexes are presented in Table 1. The complexes all exhibited enantiotropic liquid crystalline behavior. On cooling from the isotropic melt, a grainy texture was observed at 125 °C (Fig. 1). The DSC thermogram of the complexes **Zn-14dap** and **Zn-16dap** (Fig. 2) exhibited two transitions, each in the heating and cooling cycle. In the cooling scan, the grainy texture at the mesophase remains unaltered till ambient temperature, slowly freezing into a glassy state. For the **Zn-12dap** complex, two additional peaks observed in the heating cycle were ascribed to crystal–crystal transitions. No isotropic liquid-mesophase transition

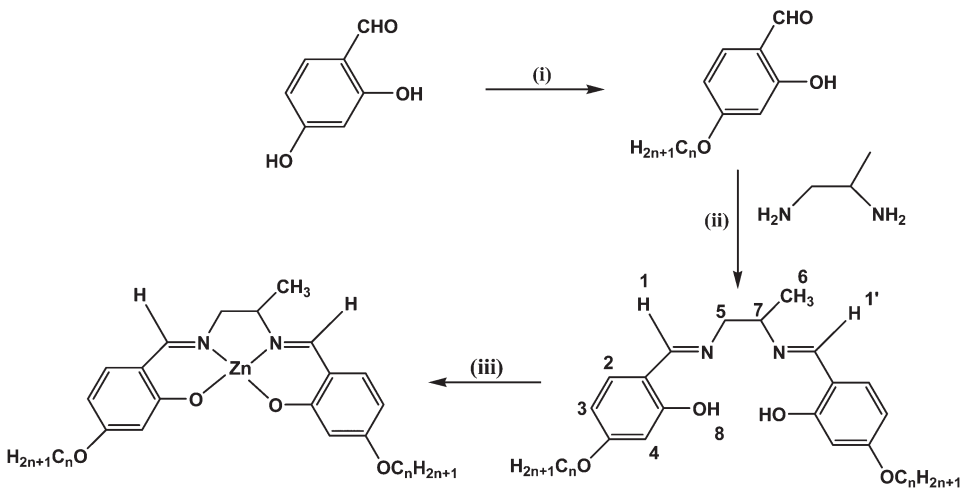

Scheme 1 (i) $C_nH_{2n+1}Br$, $KHCO_3$, KI, dry acetone, Δ, 24 h, (ii) glacial AcOH, absolute EtOH, Δ, 3 h and (iii) $Zn(OAc)_2{\cdot}2H_2O$, MeOH, stir, 3 h.

Table 1 Thermodynamic data for the **Zn-*n*dap** (n = 12, 14, 16) complexes. Transition temperatures are given in °C, and the corresponding enthalpy changes are in parentheses (ΔH; kJ mol^{-1}). Cr, Cr_1, Cr_2 refer to phases that are crystalline or solid; Col_l: lamello-columnar phase

Compounds	Heating[a]	Cooling[a]
Zn-12dap	Cr 94.1 (32.8) Cr_1 103.4 (2.4) Cr_2 134.5 (7.9) Col_l 168.6 (1.5) I	I 83.7 (10.1) Cr
Zn-14dap	Cr 97.6 (7.9) Col_l 167.4 (14.1) I	I 144.9 (12.2) Col_l 92.2 (6.3) Cr
Zn-16dap	Cr 98.5 (7.0) Col_l 162.1 (8.2) I	I 124.2 (6.2) Col_l 90.3 (5.9) Cr

[a] DSC peak temperature.

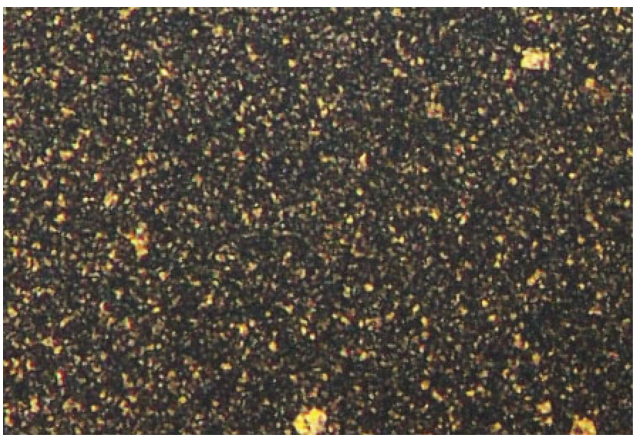

Fig. 1 POM image of **Zn-16dap** upon cooling at 125 °C.

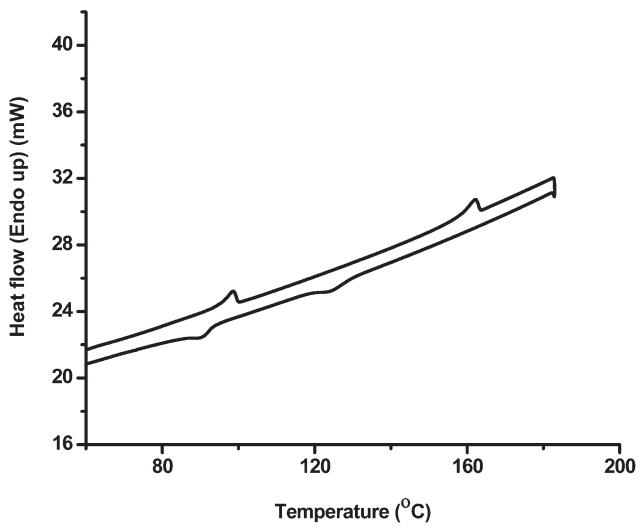

Fig. 2 DSC profile of **Zn-16dap**.

could be detected in the cooling cycle (Table 1). This might be due to the partial vitrification of the mesophase. Viscous nature of the complexes tends to affect the molecular mobility causing a pronounced hysteresis in the phase transition temperature in all the cases. A gradual decrease in the clearing temperature was observed with increasing number of carbon atoms in the pendant alkoxy arm. The isotropic liquid to mesophase transition temperature also displayed similar trends with increasing chain length. Repeated heating and cooling scans confirmed the reversibility of the thermal behaviour.

Variable temperature powder XRD study of a representative complex, **Zn-16dap** was carried out both in the mesophase and at room temperature. The X-ray diffraction pattern recorded at 100 °C (Fig. 3a, Table 2) contained several sharp and intense Bragg reflections in the small-angle region and two broad scattering halos (visualized by profile fitting of the data) in the wide-angle region. The broad maxima centered around 4.7 Å and 4.0 Å correspond, respectively, to the lateral short-range order of the molten chains and the molecular cores, confirm-

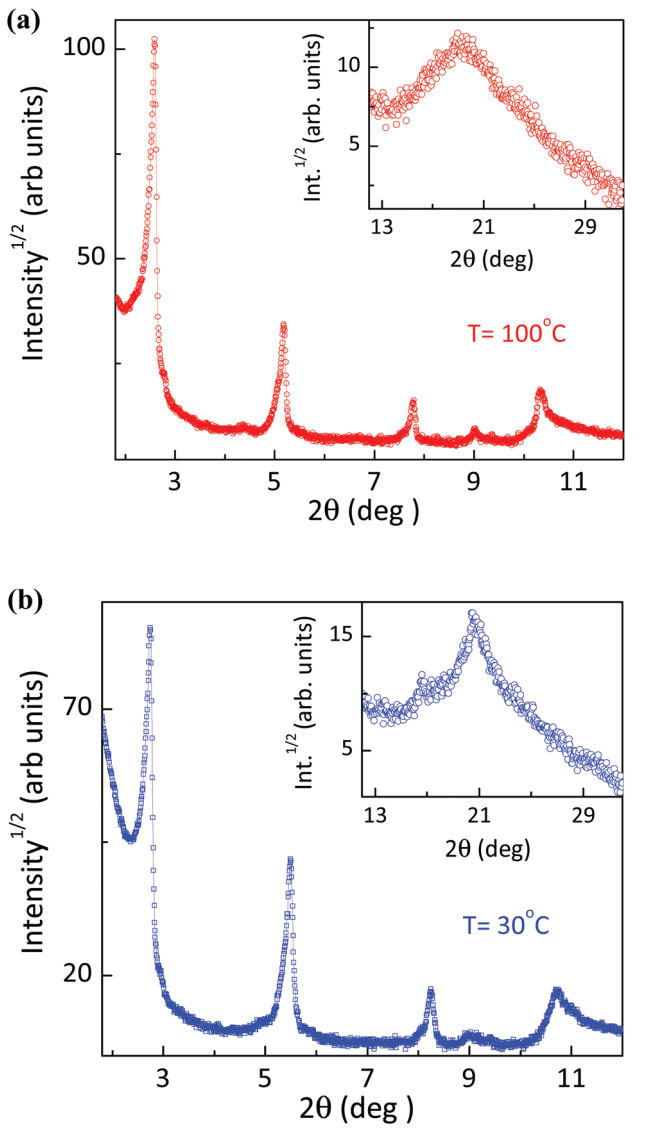

Fig. 3 PXRD pattern of **Zn-16dap** at (a) 100 °C and (b) at room temperature (30 °C).

Table 2 PXRD data of **Zn-16dap**

Temperature (°C)	Parameters	d_{meas} [a,b]/ Å	$d_{calc.}$ [a,b]/ Å	Miller indices (hkl)[c]
At 100 °C	a = 34.06 Å	34.05[s]	34.06	100
	b = 40.46 Å	17.06[s]	17.03	200
	V_{cell} = 5540.5 Å^3	11.37[s]	11.35	300
	d = 34.1 Å	9.81[s]	9.70	140
		8.54[s]	8.70	240
		4.68[d]		
		4.02[d]		
At 30 °C	a = 32.18 Å	32.19[s]	32.18	100
	b = 41.31 Å	16.10[s]	16.09	200
	V_{cell} = 5596.5 Å^3	10.72[s]	10.73	300
	d = 32.18 Å	9.87[s]	9.83	140
		8.24[s]	8.26	050
		7.87[s]	7.90	410
		6.51	6.55	350
		5.72	5.76	450
		5.32	5.32	610
		4.29[d]		
		4.21[d]		

[a] $d_{meas.}$ and $d_{calc.}$ are the experimentally measured and calculated diffraction spacing, respectively. [b] Intensity of the reflections: s; sharp peak, d: diffuse peak. The distances are given in Å. [c] [hkl] are the Miller indices of the reflections. For Col_l phase, $d = (\sum ld_{l00})/N_{l00}$ where N_{l00} is the number of reflections. V_{cell}, is the unit cell volume.

ing the liquid nature of the mesophase. The sharpness of the small-angle reflections indicates long-range correlation of the structure. However, these reflections do not conform to either a purely lamellar or purely columnar structure. The first three reflections (at 34.1, 17.1 and 11.4 Å) being in the reciprocal spacing ratio 1 : 2 : 3, point to a well-defined layered structure. In contrast the remaining two sharp reflections observed at 9.8 Å and 8.5 Å cannot be ascribed to a lamellar form, but can be explained by invoking a columnar ordering. Since these peaks are much less intense than the primary layer peak, they can be considered to be arising due to 2-D columnar modulation of the layers. A mesophase exhibiting structural features which are a combination of the lamellar and columnar features has been referred to as a lamello-columnar (Col_l) phase.[24,26–28,30] Symmetric 4-alkoxy substituted Schiff bases containing ethylene diamine spacer complexed to Pt^{2+}, Cu^{2+}, VO^{2+} and Ni^{2+} have also been shown to exhibit Col_l phases though the 1D ordering is more pronounced in these cases.[24,27,28,30] Though the corresponding Zn(II) complexes have been documented, the mesomorphic properties have not been reported.[52] The low intensity for second wide-angle halo expected due to interaction between the rigid part of one mesomorphic unit and its next nearest neighbour suggests weaker correlation between the cores within the column in the mesophase. The enhanced flexibility associated with the aliphatic spacer group bearing the 'methyl' substituent is believed to induce bending and twisting deformations, with the resulting fluctuations reducing the core–core correlations.[56,57] Similar behaviour has also been noticed for previously reported analogous Zn(II) and Cu(II) complexes with asymmetric methyl substituted aromatic spacer.[22,37]

Spacer group substitution can have marked influence on the mesomorphic properties in the 'salen type' zinc(II) complexes. In our previous reports[35–37] on zinc(II)-salen complexes, the effect of different substituents at the aromatic spacer (X = H, CH_3, Cl *etc.*) were studied and the complexes were shown to exhibit hexagonal, rectangular and oblique columnar mesophases of different symmetries. While complexes without any substituent or with an electron donating methyl group at the aromatic spacer exhibited monotropic phase behaviour, the electron withdrawing substituent (Cl) at the spacer stabilized the mesophase and enantiotropic phase behaviour was observed. Enhanced dipolar interactions due to the electron withdrawing group has been argued in favour of better core–core correlations with an increase in the clearing temperature than analogous compounds with methyl or without any substituent.

The XRD spectrum recorded at 30 °C (Fig. 3b) was quite similar to that recorded at high temperatures. However, the diffractogram consisted of additional reflections which agree with the assignment of the Col_l phase; the presence of diffuse reflections at wide angles and the absence of any mixed-index reflections at low angles rules out the phase being crystalline in nature at this temperature. Further, the core–core peak becomes much stronger. Inserting the full width at half-maximum value of this reflection in the standard Scherer equation yields a correlation length of about 115 Å, associated with the stacking of about 28 molecules along the columns. It may also be mentioned that the calculated inter-layer distance in the mesophase, d = 34.1 Å, is greater than the DFT computed radius (~23.9 Å) of the fully extended half-disc shaped molecule. Though additional information regarding the stacking of the molecular cores in the mesophase is not available, it is presumed that the half-disc shaped molecules might perhaps preferably arrange themselves in an anti-parallel partially interdigitated manner within the layer (Fig. 4).[56,57]

2.3 Photophysical properties

The UV-visible absorption and photoluminescence spectra of the compounds recorded in chloroform, $CHCl_3$ (2×10^{-5} M) at room temperature are shown in Fig. 5a and b and the data are

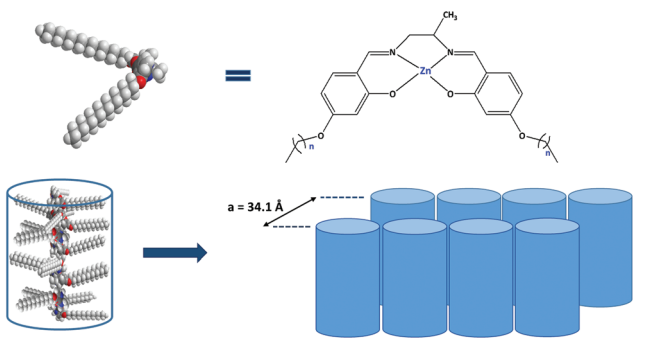

Fig. 4 Anti-parallel interdigitated organization of the molecules in lamello-columnar phase.

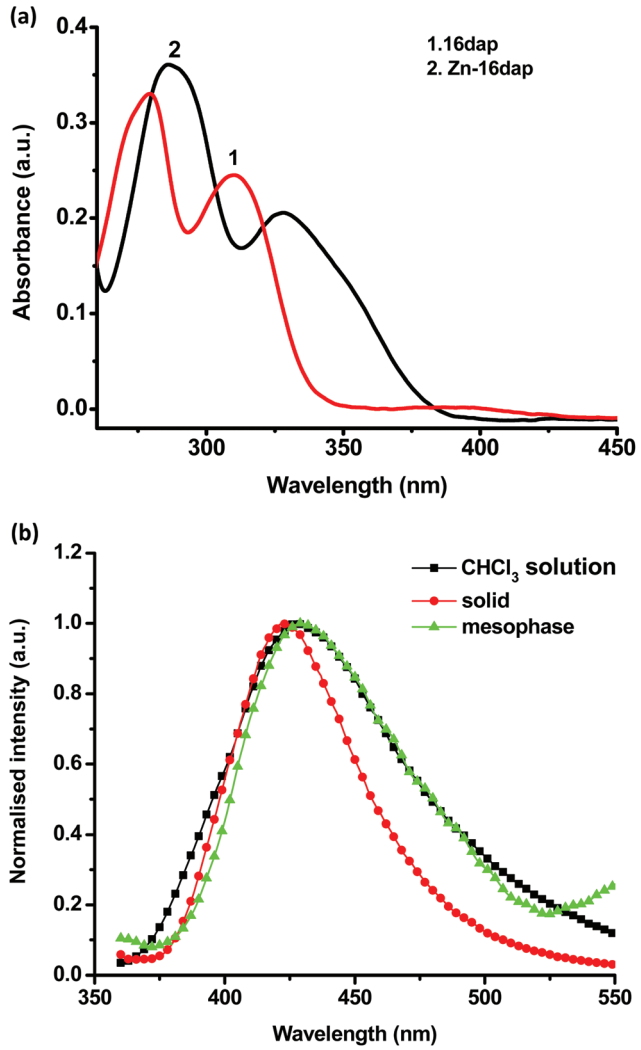

Fig. 5 (a) UV-visible absorption spectra of the ligand (**16dap**) and **Zn-16dap** in chloroform (2×10^{-5} M) and (b) intensity (normalized) *vs.* wavelength photoluminescence profile for the **Zn-16dap** complex in chloroform solution (2×10^{-5} M), solid state and in mesophase ($\lambda_{ex.}$ = 330 nm).

Table 3 UV-visible and photoluminescence spectral data of the ligands (in $CHCl_3$) and **Zn-*n*dap** (*n* = 12, 14, 16) complexes in different solvents

Compounds	Solvents	Absorption λ_{max} (nm)	Absorption ε (l mol^{-1} cm^{-1})	Emission λ_{max} (nm)
12dap	$CHCl_3$	278	16 312	—
		310	12 300	
		386	192	
14dap	$CHCl_3$	278	15 936	—
		310	12 305	
		386	200	
16dap	$CHCl_3$	279	16 530	—
		310	12 296	
		386	174	
Zn-12dap	$CHCl_3$	287	20 359	425
		330	11 240	
		345^{sh}	7875	
	CH_2Cl_2	286	28 967	424
		331	16 543	
		345^{sh}	12 756	
	Toluene	287	16 748	421
		333	10 731	
		346^{sh}	8156	
	THF	288	31 952	432
		345	23 675	
		360^{sh}	18 789	
Zn-14dap	$CHCl_3$	287	19 935	425
		330	10 306	
		347^{sh}	7693	
	CH_2Cl_2	286	28 733	424
		331	16 238	
		347^{sh}	13 085	
	Toluene	287	16 892	422
		333	10 736	
		346^{sh}	9712	
	THF	288	31 132	433
		345	22 925	
		361^{sh}	19 003	
Zn-16dap	$CHCl_3$	287	20 135	425
		329	10 240	
		343^{sh}	7675	
	CH_2Cl_2	286	29 784	424
		331	16 998	
		346^{sh}	12 985	
	Toluene	286	16 998	421
		333	10 706	
		345^{sh}	8215	
	THF	288	32 082	432
		345	23 405	
		359^{sh}	18 715	

sh: shoulder.

summarized in Table 3. The UV-visible absorption spectra of the ligands (***n*dap**; *n* = 12, 14, 16) consisted of two intense absorption bands centered at ~278 and ~310 nm, attributed to the π–π* transition localized on the aromatic rings (Fig. 5a). Another less intense band at ~386 nm may be attributed to n–π* excitation of the C=N fragment. Upon complexation, the former two bands were red-shifted to ~287 and ~329 nm, respectively, with the appearance of an additional shoulder at ~346 nm, while the low intensity band due to the n–π* transition in the ligand disappeared because of the participation of the nitrogen's lone pair in coordination to the Zn^{2+} ion. The photoluminescence spectra of the ligands and Zn(II)–salen complexes were recorded at room temperature in $CHCl_3$ solution (2×10^{-5} M), mesophase and also in the solid state (Fig. 5b). The ligands are non-emissive. The solid state emission spectra of the complexes were recorded by placing a uniform powder sheet between two quartz plates. The complexes showed a blue luminescence with emission maxima centered at ~424 nm and an emission quantum yield of ~23% (solution), and ~5% (solid) under UV irradiation (330 nm). The observed fluorescence emission originates from metal-perturbed π–π* ligand-centered transitions. With respect to solution, the position of the emission maxima is virtually unaltered in the solid state. However, the emission intensity quenches substantially following closer association of molecular cores in the solid state as compared to the solution. In a POM study, the mesophase of the Zn(II) complex that was developed at 125 °C during the cooling cycle freezes into a glassy state persisting till ambient temperature enabling photoluminescence study in the mesophase ($\lambda_{max} \approx 425$ nm) as well.

Similar studies in the frozen glassy state were made earlier for related complexes.[34] The emission energies are virtually unaffected in the solid state, in solution and in the mesophase (Fig. 5b).

Notably, the nature of substituent also has marked influence on the emission behavior of such complexes. When compared to systems with methyl or un-substituted aromatic spacer group, a distinct red shift (~40 nm) of the emission band has been noticed on going from the un-substituted zinc(II) complex to the chloro-substituted one.[35–37] This is believed to arise from the electron withdrawing effect of the chloro group on the π–π* transition of the corresponding complex. The observed photophysical behaviour is consistent with those reported for Zn(II) complexes of Schiff bases substituted with electron donating/withdrawing groups.[58] Emission maxima of complexes with differently substituted (X = H, CH_3, Cl) aromatic spacers studied earlier[35–37] were observed at >500 nm. In the present case of methyl substituted aliphatic bridges, the emissions were significantly blue shifted to ~424 nm consistent with the enhanced flexibility.

UV-visible and photoluminescence spectra of the Zn(II)-salen complexes (Fig. 6a and b) were also recorded in dilute solutions (2×10^{-5} M) of different coordinating and non-coordinating solvents in order to study the de-aggregation/aggregation phenomena. The absorption spectra recorded in non-coordinating solvents (*e.g.* CH_2Cl_2, $CHCl_3$ and toluene) consisted of two well-defined bands located at ~287 nm, 331 nm and a shoulder at 345 nm (Fig. 6a) attesting the formation of aggregates.[53,54] In coordinating solvent (THF), a red shift (~14 nm) of the longer wavelength feature is observed due to the axial coordination of the solvent molecules, suggesting de-aggregation (Fig. 6a).[53,54] The coordinatively unsaturated Zn^{2+} ion behaves as a Lewis acid. This behavior is unlike that observed in the case of the symmetrical molecule containing an ethylene diamine spacer wherein upon de-aggregation a blue shift of longer absorption feature was noticed.[52] A rather unusual optical behavior is attributed to the lack of conjugation between the J-type aggregated salen moieties. The methyl group being electron donating in nature induces a considerable amount of conjugation (+I effect) in the ligand framework in the present complexes. Also the tetrahedral methyl group, due to its steric requirement, tends to restrict the salicylidene groups of each unit in the dimer to H-type aggregate (Fig. 6c). Similar results were obtained in other related systems with conjugated aliphatic and aromatic spacers.[53,54] Concentration variations had virtually no effect on these features up to a concentration of 1×10^{-4} M (Fig. 7). Photoluminescence spectra of the complexes (Fig. 6b) recorded in non-coordinating solvents exhibited a broad band at ~424 nm. In coordinating solvents, the maxima is slightly red shifted (~8 nm) with enhancement in fluorescence intensity suggesting de-aggregation with concomitant formation of 1 : 1 adduct.[53,54] The emission quantum yield values in non-coordinating solvents (*e.g.* CH_2Cl_2, $CHCl_3$ and toluene) are around 22% which were enhanced (EQY = 38%) upon de-aggregation in coordinating solvent. Fluorescence of face-to-face-stacked

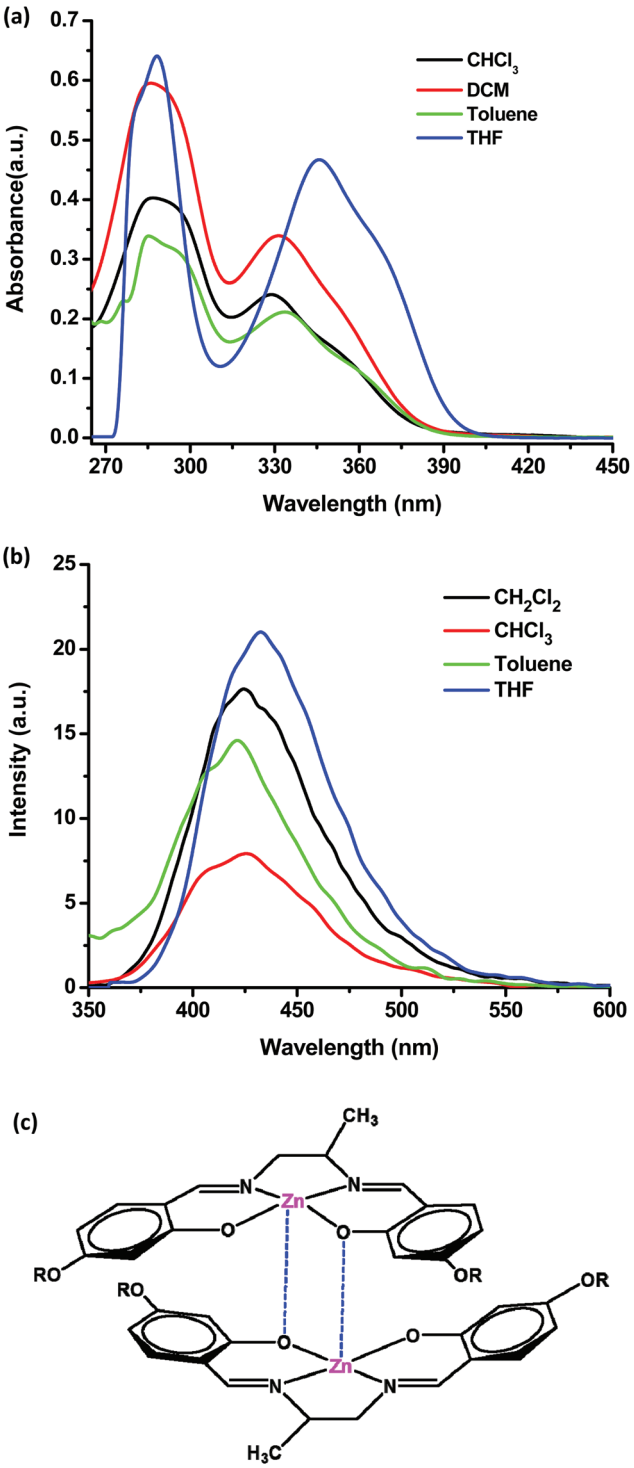

Fig. 6 UV-visible absorption spectra (a), fluorescence spectra (λ = 330 nm; with 10% attenuator) (b) of **Zn-16dap** (2×10^{-5} M) in different non-coordinating and coordinating solvents and (c) the 'H-type' dimer in solution of non-coordinating solvents.

H-type dimer aggregates (sandwich-type dimers) are known to be quenched relative to that of the monomer.[59] A rapid energy relaxation of the lower excited states causes this fluorescence

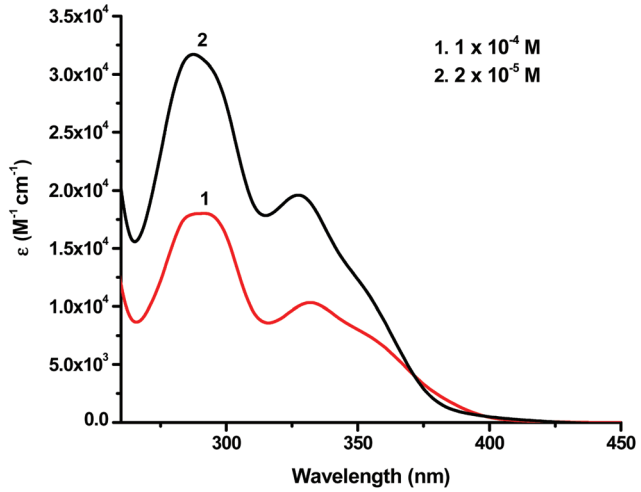

Fig. 7 Concentration dependence of UV-visible absorption spectra of **Zn-16dap** in $CHCl_3$ solutions.

suppression. The absorption or emission characteristics of the complexes are invariant of the alkyl chain lengths (Table 3).

In order to minimize inter-electronic repulsions, Zn(II) ion prefers a tetrahedral geometry to a square planar coordination. However, a short rigid central spacer with steric demands in the present complexes forces the metal center to acquire an unfavourable distorted planar geometry which eventually lead to a dimer, $[ZnL]_2$ [60] instead of more stable helical shape formed by tetrahedral 2 : 2 metal-to-ligand complex, $[Zn_2L_2]$.[61]

2.4. DFT study

In the absence of diffraction quality single crystals, density functional theory (DFT) calculations were carried out on a representative Zn(II) complex (**Zn-16dap**) employing a GAUSSIAN 09 program package[62] to arrive at the optimized electronic structure. The ground state geometry optimization in the gas phase of the zinc complex has been performed using the three-parameter fit of Becke's hybrid functional combined with the Lee–Yang–Parr correlation functional termed a B3LYP hybrid,[63,64] generalized gradient approximation (GGA) exchange along with 6-311+G(d,p), 6-31+G(d,p), 6-31G(d) and 6-31G basis sets[65] for Zn, N and O, C and H, respectively, without imposing any symmetry constraint. The appropriate structure of the complex was confirmed as energy minima by calculating the vibrational frequency and confirming the absence of any imaginary frequencies. Based on the optimized geometry of the zinc complex, TD-DFT calculations on an isolated molecule of the title complex (**Zn-16dap**) have been performed at the B3LYP level to study the spectroscopic and electronic properties. Since the electronic absorption spectra of the compounds were recorded in dichloromethane, the solvent effects were taken into consideration in the theoretical modelling. The GAUSSSUM[66] program was employed to calculate the individual contribution of various groups to each molecular orbital. A solvation method of the polarisable continuum model (PCM)[67] using the integral equation formalism (IEF) variant[68] was considered in the calculations. Important geometric parameters of the optimized Zn(II) complex as evaluated by DFT at the B3LYP level are collected in Table 4. Average Zn–O and Zn–N bond lengths of the Zn(II) complex are calculated to be 1.931 and 2.077 Å, respectively. The O1–Zn–O2 and N1–Zn–N2 bond angles are found to be 108.9° and 80.0°, respectively. The O1–Zn–N1, O2–Zn–N2, O1–Zn–N2 and O2–Zn–N1 bond angles are calculated to be 91.9°, 92.1°, 148.6° and 148.8°, respectively, around the zinc atom indicating a distorted square planar geometry (Fig. 8). The dihedral angle O1–N3–N2–O2 as evaluated from DFT calculation is about 39.7° reflecting a deviation from planarity.

The three-dimensional (3D) iso-surface plots of the lowest unoccupied molecular orbitals (LUMOs) and the highest occupied molecular orbitals (HOMOs) of the zinc complex are presented in Fig. 9. The electron density of the HOMO is localized almost entirely on the aromatic rings, while that of the LUMO is mainly centered on both N=C bonds and aromatic rings. The HOMO and LUMO energies are calculated to be −5.58 eV and −1.41 eV, respectively, the energy difference being ΔE = 4.17 eV. This value is somewhat higher than the HOMO–LUMO energy difference value (ΔE = 3.60 eV) evaluated from the lowest energy UV-Vis band (346 nm). Extensive intermolecular interactions in the solution phase (UV-Vis study) as against a free gaseous molecule (DFT study) could be one plausible reason for such a deviation. While ligand p_π orbitals contribute almost entirely to HOMO−1 (98%), HOMO−2 (99%), HOMO−3 (100%) orbitals, the HOMO−4 orbital receives a negligible contribution from metal d_π orbitals (8%). Electron density on LUMO+1, LUMO+3 and LUMO+4 orbitals is mainly due to ligand p_π* orbitals while that on LUMO+2 is primarily due to metal d_π* orbitals (87%).

TD-DFT calculations have been carried out for the **Zn-16dap** complex to account for the observed bands in the UV-visible region. The key electronic transitions, corresponding oscillator strength (f), orbitals involved in these transitions and their percentage contribution to each transition are summarized in Table 5. The surface of each peak in the spectra is proportional to oscillator strength (f), which also reveals the probability of

Table 4 Selected bond lengths (Å) and bond angles (°) of **Zn-16dap** complex optimized at the B3LYP level

Structural parameter	Bond lengths (Å) and bond angles (°)
Zn–O1	1.932
Zn–O2	1.931
Zn–N1	2.076
Zn–N2	2.078
O1–Zn–O2	108.9
N1–Zn–N2	80.0
O1–Zn–N1	91.9
O2–Zn–N2	92.1
O1–Zn–N2	148.6
O2–Zn–N1	148.8
O1–N1–N2–O2	39.7
Molecular length	47.8

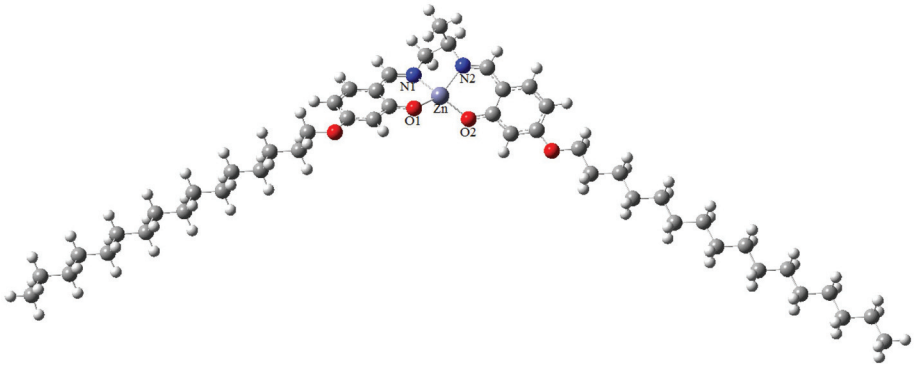

Fig. 8 DFT optimized structure of a representative complex, **Zn-16dap**.

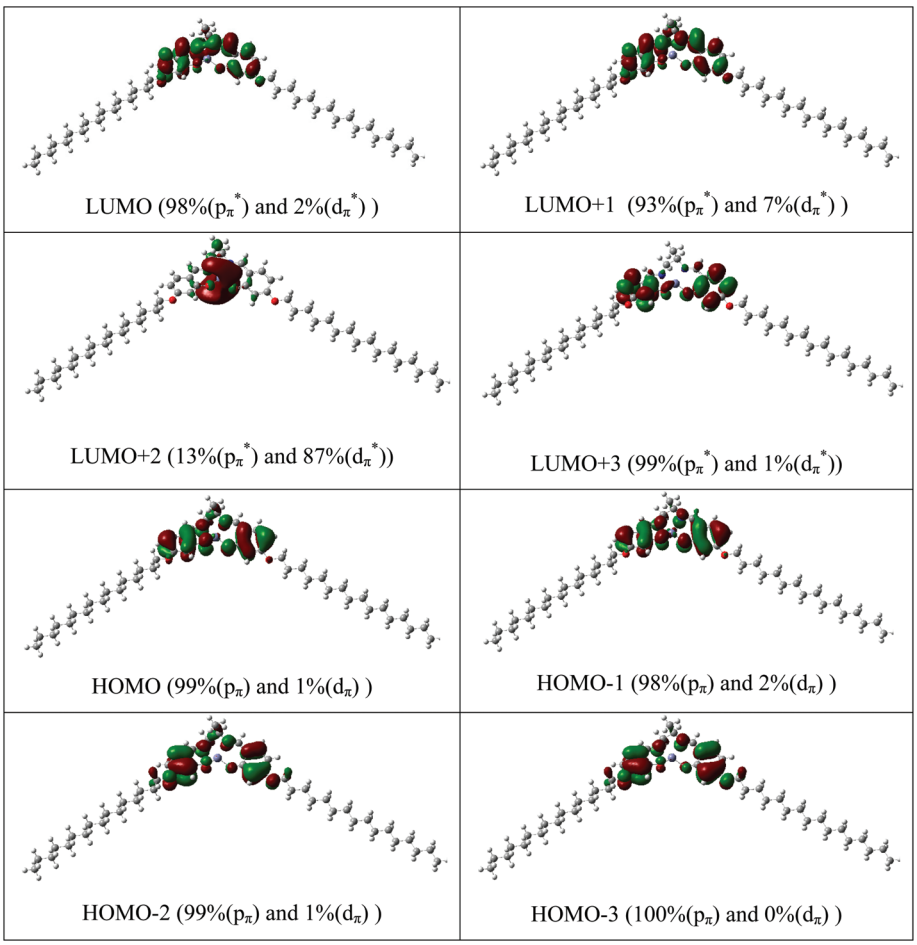

Fig. 9 Frontier molecular orbitals of **Zn-16dap**.

electronic transition. The title complex exhibits three absorption bands at 345, 336 and 295 nm, respectively. The absorption band at 345 nm corresponds to HOMO → LUMO electronic transition owing to the L(π) → L(π*), where HOMO corresponds to π bonding orbitals of aromatic rings of the ligand and LUMO corresponds to π* (anti-bonding) orbitals of the aromatic rings (intra-ligand charge transfer). This transition is consistent with the experimental value of 346 nm. The high energy absorption bands of the complex occur at 336 and 295 nm, which could be assigned to HOMO−1 → LUMO and HOMO−2 → LUMO electronic transitions, predominantly due to intra-ligand (π → π*) charge transfer. These two tran-

Table 5 The experimental absorption bands and the electronic transitions calculated with TD-DFT/B3LYP method of the **Zn-16dap** complex

Key transition	Character	λ (nm)	E (eV)	f (Osc. strength)	Assignments	λ_{exp} (nm) ε (l mol^{-1} cm^{-1})
(90%) HOMO → LUMO	L(π) → L(π^*)	345	3.60	0.124	IL	346 (12 985)
(89%) HOMO−1 → LUMO	L(π) → L(π^*)	336	3.70	0.102	IL	331 (16 998)
(85%) HOMO−2 → LUMO	L(π) → L(π^*)	295	4.21	0.550	IL	286 (29 784)

sitions resemble the experimental value of 331 and 286 nm, respectively.

3. Conclusion

A series of new Zn(II) complexes of 'salen' type asymmetric Schiff base ligands bearing a long pendant alkoxy arm at the 4-position of side aromatic rings and an asymmetric central spacer group have been accessed. Co-ordination of the Zn^{2+} ion to the ligands induces lamello-columnar mesomorphism in otherwise non-mesomorphic ligands. These half-disc shaped molecules assemble in an anti-parallel interdigitated manner within the layer in the mesophase. Metal coordination also brings about interesting fluorescence properties in the solid state, in solution and as well as in the mesophase. In addition, the complexes also exhibit aggregation behaviour in dilute solutions of different non-coordinating and coordinating solvents, suggesting the Lewis acidity of the metal ion in the newly synthesized complexes. Asymmetric methyl substitution at the aliphatic spacer leads to variation in photophysical behaviour and mesophase order in the present complexes as compared to symmetric molecules containing an ethylenediamine spacer. The coordinative unsaturation of Zn(II)-complexes may be utilized for binding with other suitable donor groups to tune the properties.

4. Experimental section

4.1. Physical measurements

The C, H and N analyses were carried out using an Elementar Vario EL III Carlo Erba 1108 elemental analyser. The ^{1}H-NMR spectra were recorded on a Bruker Avance II, 400 MHz spectrometer in $CDCl_3$ (chemical shift in δ) solution with TMS as the internal standard. Ultraviolet-visible absorption spectra of the compounds were recorded on a JASCO V-670 Spectrophotometer. Photoluminescence spectra were recorded on a Perkin Elmer LS 45 Fluorescence Spectrometer. The fluorescence emission quantum yields (EQY) in degassed dichloromethane solutions were determined by the standard optically dilute method[69] using 9,10-diphenylanthracene (EQY = 0.96, in cyclohexane) as the standard.[70] Quantum yield in the solid state was measured by means of an integrating sphere, in which the solid sample film was prepared *via* spin coating and was excited by a 20 kW pulsed xenon source coupled with Monk-Gillieson type monochromators for selecting wavelengths. The resulting luminescence was acquired by an intensified charge-coupled detector for subsequent analyses. Infrared spectra were recorded on a Perkin Elmer BX series spectrometer on KBr disc in the 400–4000 cm^{-1} range. The optical textures of the different phase of the compounds were studied using a Nikon ECLIPSE LV100 POL polarizing microscope attached with Instec hot and cold stage HCS402, with a STC200 temperature controller of 0.1 °C accuracy. The thermal behaviour of the compounds were studied using a Pyris-1 system linked to a Perkin Elmer differential scanning calorimeter (DSC) at a heating or cooling rate of 5 °C min^{-1}. X-ray diffraction (XRD) studies were carried out using samples filled in Lindemann capillaries. The apparatus essentially involved a high-resolution X-ray powder diffractometer (PANalytical X'Pert PRO) equipped with a high-resolution fast detector PIXCEL. Quantum chemical calculation on Zn(II) complex was performed using density functional theory (DFT) as implemented in a GAUSSIAN 09 package.

4.2. Materials

The materials were procured from Tokyo Kasei, Japan and Lancaster Chemicals, USA. All solvents were purified and dried using standard procedures. Silica (60–120 mesh) from Spectrochem was used for chromatographic separation. Silica gel G (E-Merck, India) was used for TLC.

4.3. Synthesis and analysis

4.3.1. Synthesis of *n*-alkoxysalicylaldehyde (*n* = 12, 14, 16). 2,4-Dihydroxybenzaldehyde (10 mmol, 1.38 g), $KHCO_3$ (10 mmol, 1 g), KI (catalytic amount) and 1-bromododecane (10 mmol, 2.4 g) or 1-bromotetradecane (10 mmol, 2.5 g) or 1-bromohexadecane (10 mmol, 2.8 g) were mixed in 250 mL of dry acetone; the mixture was heated under reflux for 24 h, and then filtered, while hot, to remove any insoluble solids. Dilute HCl was added to neutralize the warm solution and then extracted with chloroform (100 mL). The combined chloroform extract was concentrated to give a purple solid. The solid was purified by column chromatography using a mixture of chloroform and hexane (v/v, 1/1) as an eluent. Evaporation of the solvents afforded a white solid product.

4.3.2. Synthesis of *N*,*N*′-bis(4-(4′-*n*-alkoxy)-salicylidene)-1,2-diaminopropane (*n*dap), *n* = 12, 14 or 16

4.3.2.1. General procedure. Schiff bases (***n*dap**) were prepared by adding an ethanolic solution of 2-hydroxy-4-(*n*-alkoxy) salicylaldehyde (1 mmol) to an ethanolic solution of 1,2-diaminopropane (0.5 mmol). The solution mixture was heated under reflux with a few drops of acetic acid as a catalyst for 3 h to yield the light yellow Schiff base, *N*,*N*′-bis(4-(4′-*n*-alkoxy)-

salicylidene)-1,2-diaminopropane. The product was collected by filtration and re-crystallized from absolute ethanol to obtain a pure compound.

4.3.3. *N,N′*-Bis(4-(4′-dodecyloxy)-salicylidene)-1,2-diaminopropane (12dap). Yield = 0.23 g (74%); Anal. Calc. for $C_{41}H_{66}N_2O_4$ (651): C, 75.65; H, 10.22; N, 4.30. Found: C, 75.63; H, 10.21; N, 4.33%. ^{1}H NMR (400 MHz, $CDCl_3$; Me_4Si at 25 °C, ppm): δ = 11.45 (s, 1H, H^7), 8.21 (s, 1H, H^1), 8.17 (s, 1H, $H^{1'}$), 7.01–6.72 (m, 4H, H^2, H^3), 6.21 (s, 2H, H^4), 3.98 (t, $^3J_{H,H}$ = 8 Hz, 4H, O-CH_2), 3.70–3.63 (m, 2H, H^5), 1.68 (m, 3H, H^6), 1.35–1.30 (m, 1H, H^7), 1.22–1.03 (m, –CH_2 of methylene proton in side chain), 0.89 (t, $^3J_{H,H}$ = 8 Hz, 6H, –CH_3). IR (ν_{max}, cm^{-1}, KBr): 3370 (ν_{OH}), 2923 ($\nu_{as(C-H)}$, CH_3), 2857 ($\nu_{s(C-H)}$, CH_3), 1653 ($\nu_{C=N}$), 1227 (ν_{C-O}).

4.3.4. *N,N′*-Bis(4-(4′-tetradecyloxy)-salicylidene)-1,2-diaminopropane (14dap). Yield = 0.29 g (77%); Anal. Calc. for $C_{45}H_{74}N_2O_4$ (707.1): C, 76.44; H, 10.55; N, 3.96. Found: C, 76.47; H, 10.57; N, 3.95%. ^{1}H NMR (400 MHz, $CDCl_3$; Me_4Si at 25 °C, ppm): δ = 11.43 (s, 1H, H^7), 8.23 (s, 1H, H^1), 8.20 (s, 1H, $H^{1'}$), 7.03–6.75 (m, 4H, H^2, H^3), 6.23 (s, 2H, H^4), 3.98 (t, $^3J_{H,H}$ = 8 Hz, 4H, O–CH_2), 3.72–3.65 (m, 2H, H^5), 1.67 (m, 3H, H^6), 1.34–1.27 (m, 1H, H^7), 1.22–1.01 (m, –CH_2 of methylene proton in side chain), 0.89 (t, $^3J_{H,H}$ = 8 Hz, 6H, –CH_3). IR (ν_{max}, cm^{-1}, KBr): 3372 (ν_{OH}), 2922 ($\nu_{as(C-H)}$, CH_3), 2854 ($\nu_{s(C-H)}$, CH_3), 1655 ($\nu_{C=N}$), 1225(ν_{C-O}).

4.3.5. *N,N′*-Bis(4-(4′-hexadecyloxy)-salicylidene)-1,2-diaminopropane (16dap). Yield = 0.31 g (77%); Anal. Calc. for $C_{49}H_{82}N_2O_4$ (763.2): C, 77.11; H, 10.83; N, 3.67. Found: C, 77.13; H, 10.81; N, 3.70%. ^{1}H NMR (400 MHz, $CDCl_3$; Me_4Si at 25 °C, ppm): δ = 11.47 (s, 1H, H^7), 8.22 (s, 1H, H^1), 8.19 (s, 1H, $H^{1'}$), 7.01–6.74 (m, 4H, H^2, H^3), 6.25 (s, 2H, H^4), 3.98 (t, $^3J_{H,H}$ = 8 Hz, 4H, O–CH_2), 3.77–3.58 (m, 2H, H^5), 1.66 (m, 3H, H^6), 1.35–1.28 (m, 1H, H^7), 1.27–1.00 (m, –CH_2 of methylene proton in side chain), 0.88 (t, $^3J_{H,H}$ = 8 Hz, 6H, –CH_3). IR (ν_{max}, cm^{-1}, KBr): 3371(ν_{OH}), 2924 ($\nu_{as(C-H)}$, CH_3), 2856 ($\nu_{s(C-H)}$, CH_3), 1654 ($\nu_{C=N}$), 1225 (ν_{C-O}).

4.3.6. Synthesis of Zinc(II) complexes (Zn-*n*dap, *n* = 12, 14, 16)

4.3.6.1. General procedure. The ligand **12dap** (0.06 g, 0.1 mmol) or **14dap** (0.07 g, 0.1 mmol) or **16dap** (0.08 g, 0.1 mmol) was dissolved in a minimum volume of absolute ethanol. To this, an equimolar amount of zinc acetate $Zn(OAc)_2{\cdot}2H_2O$ (0.02 g, 0.1 mmol) in methanol was then added slowly and stirred for 3 h at room temperature. A white solid formed in each case was filtered, washed with diethyl ether and re-crystallized from chloroform–ethanol (1 : 1).

4.3.7. Zn-12dap. Yield = 0.05 g (75%); Anal. Calc. for $C_{41}H_{64}N_2O_4Zn$ (714.3): C, 68.94; H, 9.03; N, 3.92. Found: C, 68.91; H, 9.07; N, 3.95%. ^{1}H NMR (400 MHz, $CDCl_3$; Me_4Si at 25 °C, ppm): δ = 7.65 (s, 1H, H^1), 7.63 (s, 1H, $H^{1'}$), 6.97–6.70 (m, 4H, H^2, H^3), 6.26 (s, 2H, H^4), 3.99 (t, $^3J_{H,H}$ = 8 Hz, 4H, O–CH_2), 3.73–3.67 (m, 2H, H^5), 1.65 (m, 3H, H^6), 1.36–1.31 (m, 1H, H^7), 1.26–0.99 (m, –CH_2 of methylene proton in side chain), 0.88 (t, $^3J_{H,H}$ = 8 Hz, 6H, –CH_3). IR (ν_{max}, cm^{-1}, KBr): 2919 ($\nu_{as(C-H)}$, CH_3), 2853 ($\nu_{s(C-H)}$, CH_3), 1639 ($\nu_{C=N}$), 1215 (ν_{C-O}).

4.3.8. Zn-14dap. Yield = 0.06 g (78%); Anal. Calc. for $C_{45}H_{72}N_2O_4Zn$ (770.5): C, 70.15; H, 9.42; N, 3.64. Found: C, 70.14; H, 9.45; N, 3.65%. ^{1}H NMR (400 MHz, $CDCl_3$; Me_4Si at 25 °C, ppm): δ = 7.68 (s, 1H, H^1), 7.66 (s, 1H, $H^{1'}$), 6.99–6.71 (m, 4H, H^2, H^3), 6.27 (s, 2H, H^4), 3.99 (t, $^3J_{H,H}$ = 8 Hz, 4H, O–CH_2), 3.76–3.60 (m, 2H, H^5), 1.70 (m, 3H, H^6), 1.37–1.26 (m, 1H, H^7), 1.27–1.07 (m, –CH_2 of methylene proton in side chain), 0.89 (t, $^3J_{H,H}$ = 8 Hz, 6H, –CH_3). IR (ν_{max}, cm^{-1}, KBr): 2921 ($\nu_{as(C-H)}$, CH_3), 2856 ($\nu_{s(C-H)}$, CH_3), 1639 ($\nu_{C=N}$), 1217 (ν_{C-O}).

4.3.9. Zn-16dap. Yield = 0.06 g (77%); Anal. Calc. for $C_{49}H_{80}N_2O_4Zn$ (826.6): C, 71.20; H, 9.76; N, 3.39. Found: C, 71.17; H, 9.78; N, 3.40%. ^{1}H NMR (400 MHz, $CDCl_3$; Me_4Si at 25 °C, ppm): δ = 7.67 (s, 1H, H^1), 7.64 (s, 1H, $H^{1'}$), 7.00–6.73 (m, 4H, H^2, H^3), 6.22 (s, 2H, H^4), 3.99 (t, $^3J_{H,H}$ = 8 Hz, 4H, O–CH_2), 3.74–3.60 (m, 2H, H^5), 1.64 (m, 3H, H^6), 1.34–1.24 (m, 1H, H^7), 1.28–0.98 (m, –CH_2 of methylene proton in side chain), 0.87 (t, $^3J_{H,H}$ = 8 Hz, 6H, –CH_3). IR (ν_{max}, cm^{-1}, KBr): 2917 ($\nu_{as(C-H)}$, CH_3), 2854 ($\nu_{s(C-H)}$, CH_3), 1637 ($\nu_{C=N}$), 1215 (ν_{C-O}).

Acknowledgements

SC and PM acknowledge the Department of Science and Technology (DST), New Delhi, Government of India for the INSPIRE Junior Research Fellowship (Code: IF110692) and financial support (SR/FT/CS-86/2010), respectively. Sophisticated Analytical Instrumentation Facility (SAIF), North Eastern Hill University, Shillong and Central Drug Research Institute (CDRI), Lucknow are acknowledged for some spectral results. The authors are also thankful to DBT e-Library Consortium (DeLCON) of Bio-Informatics Centre, Assam University, India.

References

1 A. W. Kleij, *Eur. J. Inorg. Chem.*, 2009, 193–205.
2 A. W. Kleij, *Chem. – Eur. J.*, 2008, **14**, 10520–10529.
3 S. J. Wezenberg and A. W. Kleij, *Angew. Chem., Int. Ed.*, 2008, **47**, 2354–2364.
4 G. H. Clever and T. Carell, *Angew. Chem., Int. Ed.*, 2007, **46**, 250–253.
5 K. C. Gupta and A. K. Sutar, *Coord. Chem. Rev.*, 2008, **252**, 1420–1450.
6 P. G. Cozzi, *Chem. Soc. Rev.*, 2004, **33**, 410–421.
7 L. Canali and D. C. Sherrington, *Chem. Soc. Rev.*, 1999, **28**, 85–93.
8 E. N. Jacobsen, in *Catalytic Asymmetric Synthesis*, ed. I. Ojima, VCH, New York, 1993, p. 159.
9 G. Barone, N. Gambino, A. Ruggirello, A. Silvestri, A. Terenzi and V. T. Liveri, *J. Inorg. Biochem.*, 2009, **103**, 731–737.
10 Y. Kou, J. Tian, D. Li, W. Gu, X. Liu, S. Yan, D. Liao and P. Cheng, *Dalton Trans.*, 2009, 2374–2382.

11 A. Silvestri, G. Barone, G. Ruisi, D. Anselmo, S. Riela and V. T. Liveri, *J. Inorg. Biochem.*, 2007, **101**, 841–848.
12 C. Liu, M. Wang, T. Zhang and H. Sun, *Coord. Chem. Rev.*, 2004, **248**, 147–168.
13 J. Cheng, K. Wei, X. Ma, X. Zhou and H. Xiang, *J. Phys. Chem. C*, 2013, **117**, 16552–16563.
14 V. Liuzzo, W. Oberhauser and A. Pucci, *Inorg. Chem. Commun.*, 2010, **13**, 686–688.
15 H.-C. Lin, C.-C. Huang, C.-H. Shi, Y.-H. Liao, C.-C. Chen, Y.-C. Lin and Y.-H. Liu, *Dalton Trans.*, 2007, 781–791.
16 E. Hadjoudis and I. M. Mavridis, *Chem. Soc. Rev.*, 2004, **33**, 579–588.
17 M. Andruh, *Chem. Commun.*, 2011, **47**, 3025–3042.
18 H. Miyasaka, A. Saitoh and S. Abe, *Coord. Chem. Rev.*, 2007, **251**, 2622–2664.
19 I. P. Oliveri, S. Failla, A. Columbo, C. Dragonetti, S. Righetto and S. Di Bella, *Dalton Trans.*, 2014, **43**, 2168–2175.
20 S. Di Bella, I. P. Oliveri, A. Colombo, C. Dragonetti, S. Righetto and D. Roberto, *Dalton Trans.*, 2012, **41**, 7013–7016.
21 P. G. Lacroix, *Eur. J. Inorg. Chem.*, 2001, 339–348.
22 C. Datta, R. Chakrabarty, G. Das, C. R. Bhattacharjee and P. Mondal, *Liq. Cryst.*, 2013, **41**, 541–551.
23 C. R. Bhattacharjee, C. Datta, G. Das, R. Chakrabarty and P. Mondal, *Polyhedron*, 2012, **33**, 417–424.
24 Y. Abe, Y. Takagi, M. Nakamura, T. Takeuchi, T. Tanase, M. Yokokawa, H. Mukai, T. Megumi, A. Hachisuga and K. Ohta, *Inorg. Chim. Acta*, 2012, **392**, 254–260.
25 A. Ohta, Y. Yamamoto, H. Kamihata, Y. H. Lee, F. Ichikawa, K. Ohta, Y. Abe, N. Hoshino, M. Kojima and S. Hayami, *Inorg. Chem. Commun.*, 2012, **16**, 89–91.
26 C. R. Bhattacharjee, G. Das, P. Mondal, S. K. Prasad and D. S. S. Rao, *Inorg. Chem. Commun.*, 2011, **14**, 606–612.
27 Y. Abe, N. Nakazima, T. Tanase, S. Katano, H. Mukai and K. Ohta, *Mol. Cryst. Liq. Cryst.*, 2007, **466**, 129–147.
28 Y. Abe, K. Nakabayashi, N. Matsukawa, H. Takashima, M. Iida, T. Tanase, M. Sugibayashi, H. Mukai and K. Ohta, *Inorg. Chim. Acta*, 2006, **359**, 3934–3946.
29 K. Binnemans, K. Lodewyckx, T. Cardinaes, T. N. Parac Vogt, C. Bourgogne, D. Guillon and B. Donnio, *Eur. J. Inorg. Chem.*, 2006, 150–157.
30 Y. Abe, H. Akao, Y. Yoshida, H. Takashima, T. Tanase, H. Mukai and K. Ohta, *Inorg. Chim. Acta*, 2006, **359**, 3147–3155.
31 L. L. Li, H. F. Xiang, X. G. Zhou, M. L. Li and D. Wu, *J. Chem. Educ.*, 2012, **89**, 559–560.
32 V. K. Gupta, R. N. Goyal, A. K. Jain and R. A. Sharma, *Electrochim. Acta*, 2009, **54**, 3218–3224.
33 V. K. Gupta, A. K. Jain and G. Maheshwari, *Talanta*, 2007, **72**, 49–53.
34 D. Pucci, I. Aiello, A. Bellusci, A. Crispini, M. Ghedini and M. La Deda, *Eur. J. Inorg. Chem.*, 2009, 4274–4281.
35 C. R. Bhattacharjee, S. Chakraborty, G. Das and P. Mondal, *Liq. Cryst.*, 2012, **39**, 1435–1442.
36 C. R. Bhattacharjee, G. Das, P. Mondal, S. K. Prasad and D. S. S. Rao, *Eur. J. Inorg. Chem.*, 2011, 1418–1424.
37 C. R. Bhattacharjee, G. Das, P. Mondal and N. V. S. Rao, *Polyhedron*, 2010, **29**, 3089–3096.
38 I. P. Oliveri and S. Di Bella, *Tetrahedron*, 2011, **67**, 9446–9449.
39 M. E. Germain and M. J. Knapp, *J. Am. Chem. Soc.*, 2008, **130**, 5422–5423.
40 M. E. Germain, T. R. Vargo, P. G. Khalifah and M. J. Knapp, *Inorg. Chem.*, 2007, **46**, 4422–4429.
41 M. Cano, L. Rodríguez, J. C. Lima, F. Pina, A. D. Cort, C. Pasquini and L. Schiaffino, *Inorg. Chem.*, 2009, **48**, 6229–6235.
42 A. D. Cort, L. Mandolini, C. Pasquini, K. Rissanen, L. Russo and L. Schiaffino, *New J. Chem.*, 2007, **31**, 1633–1638.
43 S. J. Wezenberg, E. C. Escudero-Adán, J. Benet-Buchholz and A. W. Kleij, *Inorg. Chem.*, 2008, **47**, 2925–2927.
44 A. W. Kleij, M. Kuil, D. M. Tooke, A. L. Spek and J. N. H. Reek, *Inorg. Chem.*, 2007, **46**, 5829–5831.
45 M. Kuil, I. M. Puijk, A. W. Kleij, D. M. Tooke, A. L. Spek and J. N. H. Reek, *Chem. – Asian J.*, 2009, **4**, 50–57.
46 A. W. Kleij, M. Kuil, D. M. Tooke, M. Lutz, A. L. Spek and J. N. H. Reek, *Chem. – Eur. J.*, 2005, **11**, 4743–4750.
47 M. Kuil, P. E. Goudriaan, A. W. Kleij, D. M. Tooke, A. L. Spek, P. W. N. M. van Leeuwen and J. N. H. Reek, *Dalton Trans.*, 2007, 2311–2320.
48 P. G. Cozzi, *Angew. Chem., Int. Ed.*, 2003, **115**, 3001–3004.
49 A. A. Vashchenko, L. S. Lepnev, A. G. Vitukhnovskii, O. V. Kotova, S. V. Eliseeva and N. P. Kuz'mina, *Opt. Spectrosc.*, 2010, **108**, 463–465.
50 O. V. Kotova, S. V. Eliseeva, A. S. Averjushkin, L. S. Lepnev, A. A. Vaschenko, A. Y. Rogachev, A. G. Vitukhnovskii and N. P. Kuzmina, *Russ. Chem. Bull. Int. Ed.*, 2008, **57**, 1880–1889.
51 K. H. Chang, C. C. Huang, Y. H. Liu, Y. H. Hu, P. T. Chou and Y. C. Lin, *Dalton Trans.*, 2004, 1731–1738.
52 G. Consiglio, S. Failla, P. Finocchiaro, I. P. Oliveri and S. Di Bella, *Inorg. Chem.*, 2012, **51**, 8409–8418.
53 G. Consiglio, S. Failla, P. Finocchiaro, I. P. Oliveri and S. Di Bella, *Dalton Trans.*, 2012, **41**, 387–395.
54 G. Consiglio, S. Failla, I. P. Oliveri, R. Purrello and S. Di Bella, *Dalton Trans.*, 2009, 10426–10428.
55 A. W. Kleij, *Dalton Trans.*, 2009, 4635–4639.
56 A. G. Serrette, C. K. Lai and T. M. Swager, *Chem. Mater.*, 1994, **6**, 2252–2268.
57 S. T. Trzaska and T. M. Swager, *Chem. Mater.*, 1998, **10**, 438–443.
58 H.-C. Lin, C.-C. Huang, C.-H. Shi, Y.-H. Liao, C.-C. Chen, Y.-C. Lin and Y.-H. Liu, *Dalton Trans.*, 2007, 781–791.
59 M. Kasha, H. R. Rawls and M. A. El-Bayoumi, *Pure Appl. Chem.*, 1965, **11**, 371–392.
60 G. E. Batley and D. P. Graddon, *Aust. J. Chem.*, 1967, **20**, 885–891.
61 S. Mizukami, H. Houjou, Y. Nagawa and M. Kanesato, *Chem. Commun.*, 2003, 1148–1149.

62 M. J. Frisch, G. W. Trucks, H. B. Schlegel, G. E. Scuseria, M. A. Robb, J. R. Cheeseman, G. Scalmani, V. Barone, B. Mennucci, G. A. Petersson, H. Nakatsuji, M. Caricato, X. Li, H. P. Hratchian, A. F. Izmaylov, J. Bloino, G. Zheng, J. L. Sonnenberg, M. Hada, M. Ehara, K. Toyota, R. Fukuda, J. Hasegawa, M. Ishida, T. Nakajima, Y. Honda, O. Kitao, H. Nakai, T. Vreven, J. A. Montgomery Jr., J. E. Peralta, F. Ogliaro, M. Bearpark, J. J. Heyd, E. Brothers, K. N. Kudin, V. N. Staroverov, R. Kobayashi, J. Normand, K. Raghavachari, A. Rendell, J. C. Burant, S. S. Iyengar, J. Tomasi, M. Cossi, N. Rega, J. M. Millam, M. Klene, J. E. Knox, J. B. Cross, V. Bakken, C. Adamo, J. Jaramillo, R. Gomperts, R. E. Stratmann, O. Yazyev, A. J. Austin, R. Cammi, C. Pomelli, J. W. Ochterski, R. L. Martin, K. Morokuma, V. G. Zakrzewski, G. A. Voth, P. Salvador, J. J. Dannenberg, S. Dapprich, A. D. Daniels, Ö. Farkas, J. B. Foresman, J. V. Ortiz, J. Cioslowski and D. J. Fox, *Gaussian 09*, Gaussian, Inc., Wallingford, CT, 2009.
63 A. D. Becke, *J. Chem. Phys.*, 1993, **98**, 5648–5652.
64 C. Lee, W. Yang and R. G. Parr, *Phys. Rev. B: Condens. Matter*, 1988, **37**, 785–789.
65 P. C. Hariharan and J. A. Pople, *Theor. Chim. Acta*, 1973, **28**, 213–222.
66 N. M. O'Boyle, A. L. Tenderholt and K. M. Langner, *J. Comput. Chem.*, 2008, **29**, 839–845.
67 E. Cance, B. Mennucci and J. Tomasi, *J. Chem. Phys.*, 1997, **107**, 3032–3041.
68 S. Miertus, E. Scrocco and J. Tomasi, *J. Chem. Phys.*, 1981, **55**, 117–129.
69 J. N. Demas and G. A. Crosby, *J. Phys. Chem.*, 1971, **75**, 991–1024.
70 W. R. Ware and W. Rothman, *Chem. Phys. Lett.*, 1976, **39**, 449–453.

Liquid Crystals
Publication details, including instructions for authors and subscription information:
http://www.tandfonline.com/loi/tlct20

Emissive 'zinc(II)-salphen' core: building block for columnar liquid crystals

Chira R. Bhattacharjee [a], Sutapa Chakraborty [a], Gobinda Das [a] & Paritosh Mondal [a]
[a] Department of Chemistry, Assam University, Silchar, India

Version of record first published: 03 Sep 2012.

To cite this article: Chira R. Bhattacharjee, Sutapa Chakraborty, Gobinda Das & Paritosh Mondal (2012): Emissive 'zinc(II)-salphen' core: building block for columnar liquid crystals, Liquid Crystals, 39:12, 1435-1442

To link to this article: http://dx.doi.org/10.1080/02678292.2012.719934

Liquid Crystals,
Vol. 39, No. 12, December 2012, 1435–1442

Taylor & Francis
Taylor & Francis Group

Emissive 'zinc(II)-salphen' core: building block for columnar liquid crystals

Chira R. Bhattacharjee*, Sutapa Chakraborty, Gobinda Das and Paritosh Mondal

Department of Chemistry, Assam University, Silchar, India

(*Received 3 July 2012; final version received 7 August 2012*)

A series of half-discoid [N_2O_2]-donor tetradentate alkoxy substituted salicylaldimine ligands, [N,N′-di-(4-*n*-alkoxysalicylidene)-4-Cl-l,2-diamino-benzene] (L; $n = 12$, 14, 16 and 18) have been prepared. The reaction of the 'salphen'-type Schiff base ligand with $Zn(OAc)_2.4H_2O$ afforded a series of mononuclear zinc(II) complexes. The ligands and the corresponding zinc(II) complexes were characterised by elemental analysis, Fourier transform infrared, proton nuclear magnetic resonance and ultraviolet-visible spectroscopy. Although the ligands are non-mesogenic, columnar mesomorphism is induced upon complexation with the metal. The *p2gg* symmetry of the rectangular columnar phase is confirmed by variable temperature powder X-ray diffraction study. Two 'half-disc'-shaped molecules with four alkoxy legs are presumed to self-assemble via a dimeric interaction filling the space. In contrast to the ligands, the zinc(II) complexes all exhibited moderately intense green emission at room temperature both in solution and in the solid state. Density functional theory calculation, carried out using a DMol3 program, revealed a distorted square planar geometry for the complexes. The mesomorphic and photoluminescence property of the zinc complexes are collated as a function of spacer substituent, as well as alkoxy carbon chain length.

Keywords: zinc; metallomesogen; columnar mesomorphism; fluorescence; density functional theory

1. Introduction

Interest in metallomesogens has steadily grown in the recent past owing to the immense possibility of combining optical, electronic and magnetic characteristics of transition metal complexes with anisotropic fluids [1–5]. Salen-based metallomesogens are considered as one of the major thrust areas of liquid crystals [6–11]. The transition metal-salen complexes have been regarded as promising materials that have been extensively studied owing to their ability to catalyse an extremely broad range of chemical transformations [12–14]. Salen-based zinc(II) complexes, displaying physical properties such as thermal stability, luminescence and charge transporting ability, are very attractive species for applications in the great diversity of tuneable electro-optic devices [15–18]. Many zinc(II) complexes are known to exhibit intense fluorescence at room temperature and there has been substantial research assessing the performances of zinc(II) complexes in fluorescence-based organic light-emitting devices (OLEDs) [19, 20]. Recently, 'zinc(II)-salphen' cores have also been demonstrated to be excellent building blocks for the fabrication of catalytically active supramolecular assemblies [21, 22]. The combination of luminescent molecules and soft materials to generate new multifunctional electronic devices is a rapidly expanding field of research [23–25]. Although early examples of liquid crystals were based on purely organic materials [23], luminescent metallomesogens have captured the attention of researchers in recent years [15, 25, 26–31]. Most luminescent metallomesogens contain lanthanide(III) [26], palladium(II) [27, 32], platinum(II) [28, 29], nickel(II) [33], gold(I) [34] and gallium(III) ions [35]. However, very few examples of luminescent mesomorphic zinc(II) derivatives have been reported to date [36–39]. Pyrazole-based zinc complexes with non-conventional tetrahedral geometry displaying both supramolecular mesomorphic order and luminescence have been reported recently [37]. Pucci et al. [15] reported some blue light-emitting non-linear 4-substituted zinc(II) complexes with a central aliphatic core showing a smectic C (SmC) mesophase. The molecular shape serves as a dominant factor in determining the organisation of molecules into a liquid crystalline phase. Mesogenic, as well as photo-physical, behaviour is dependent on the choice of metal ion and the nature and position of the substituent in the ligand framework. Metal-salen complexes of first row transition metals containing 5-substituted long alkoxy chains have been quite extensively studied [6]. Metallomesogen based on 4-substituted salen-type framework Schiff base ligands have been inadequately addressed [8, 9, 38, 39, 40–43]. Very recently we have reported a series of novel fluorescent liquid crystalline Zn(II)-salphen complexes with different spacer groups showing hexagonal and rectangular/oblique columnar mesomorphism [38, 39]. Quite interestingly, by

*Corresponding author. Email: crbhattacharjee@rediffmail.com

ISSN 0267-8292 print/ISSN 1366-5855 online

http://dx.doi.org/10.1080/02678292.2012.719934
http://www.tandfonline.com

creating only a minor modification (chloro substituted) at the central aromatic ring (spacer), the present complexes were found to exhibit a columnar rectangular mesophase with *p2gg* symmetry different from related analogous systems (un-substituted or methyl substituted) already reported [38, 39]. The effects of fine tuning of the 'salphen' ligand on the mesomorphic and photoluminescence behaviour of the corresponding complexes have been summarised.

2. Results and discussion

The Schiff base ligands were synthesised by condensation of 4-alkoxysubstituted aldehyde with the 4-chloro-1,2-phenylenediamine with slight modification of the literature procedure [38, 39]. The synthetic strategy for the ligands [L = N,N′-bis(4-(4′-n-alkoxy)-salicylidene)-4-Cl-1,2-phenylenediamine], hereafter abbreviated as *n*-cpd, where *n* indicates the number of carbon atoms in alkyl chains, *n* = 12,14,16,18 and cpd = 4-chloro-1,2-phenylenediamine and the mononuclear Zn(II) complexes (Zn-*n*-cpd), are presented in Scheme 1. The ligands *n*-cpd and their corresponding Zn(II) complexes were characterised by elemental analysis, proton nuclear magnetic resonance (^{1}H NMR), Fourier transform infrared (FT-IR) and ultraviolet-visible (UV-Vis) spectroscopy. IR spectra of the ligands (*n*-cpd) exhibited a broad band at ~3432cm^{-1}, attributed to the phenolic -OH group. The C=N stretching vibration of the ligands is located in the region of 1622–1628 cm^{-1}. Upon complexation, the shift of ν_{CN} vibrational stretching frequency to a lower wave number, ca. ~1611–1613 cm^{-1} ($\Delta\nu \sim 15$cm^{-1}) and absence of the ν_{OH} mode clearly suggested the deprotonation of the Schiff base prior to coordination of azomethine nitrogen and phenolate oxygen to the metal. Absence of the phenolic –OH proton and an upfield shift (δ = 8.21–8.24 ppm) in the peak positions of the −N=CH proton in the spectrum of the metal complexes relative to the free ligand further augmented the [N_2O_2] coordination.

The electronic spectra (Figure S1) of the ligands *n*-cpd showed two strong bands at ~294 nm and ~326 nm attributed to the π–π* transitions of the aromatic ring and a low intensity band at ~365 nm, which is due to the π–π* transition of the C=N fragment. Upon complexation, all these bands are red-shifted to ~323, ~403 and ~452 nm. The luminescent spectra (Figure 1) of the complexes were recorded at room temperature, both in solid state and dichloromethane solution, at a concentration of 10^{-4} M (Table 1). The complexes (Zn-*n*-cpd) are all green light emitters, and showed emission maxima at ~532–556 nm with an emission quantum yield of ~10% (solution), and ~5%(solid) under UV irradiation (330 nm, excitation wavelength). The room temperature emission observed is believed to originate from the intra-ligand (π–π*) fluorescence, and the role of the central Zn^{2+} ion is to provide rigidity to the ligand [23, 27, 28, 39]. Interestingly, in solid state, the emission maxima are red shifted, presumably due to the intermolecular aromatic interaction, which is weaker in solution than that in the solid. Moreover, in solid state the free rotation of the flexible bonds is reduced and, hence, deactivation through non-radiative channels diminishes, leading to a shift of emission wavelength to lower energy. It is worth noting that, when compared with related systems [38, 39] with a differently substituted aromatic spacer group, a distinct shift (~40 nm) in the λ_{max} of green emission (Table 2) has been noticed in going from the un-substituted zinc complex to the chloro-substituted one. Expectedly, this is attributed

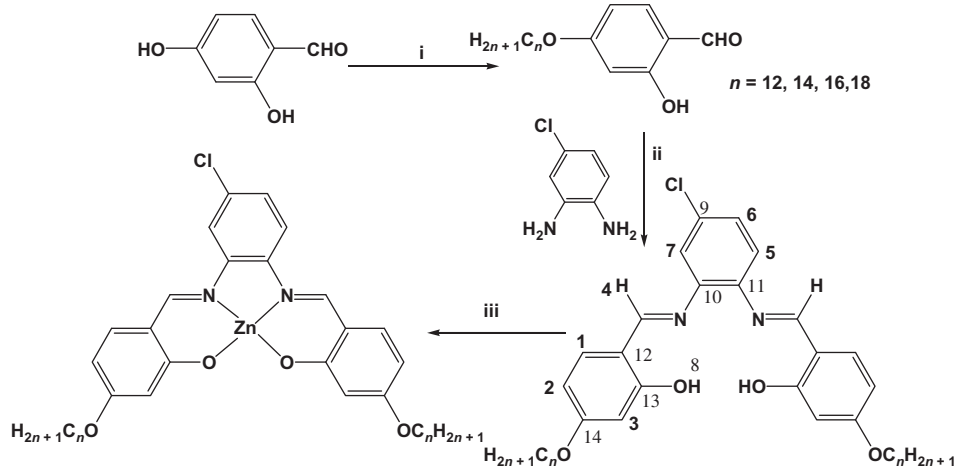

Scheme 1. (i) $C_nH_{2n+1}Br$, $KHCO_3$, KI, dry acetone, Δ, 24 h. (ii) Glacial AcOH, absolute EtOH Δ, 3 h. (iii) $Zn(OAc)_2.2H_2O$, MeOH, Δ, 2 h.

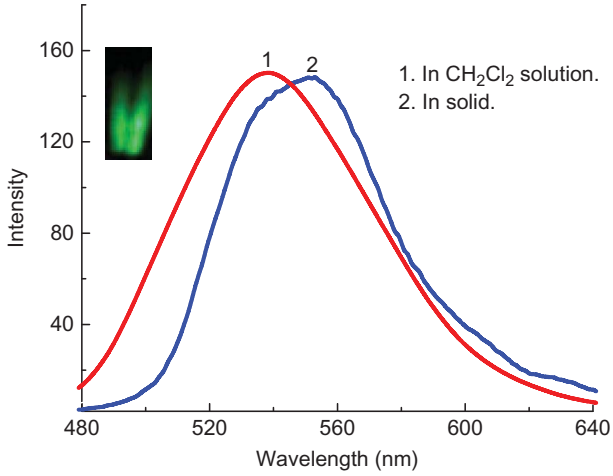

Figure 1. Photoluminescence spectra of Zn-16cpd (excitation wavelength = 330 nm, r.t., 10^{-4} M).

to the electron withdrawing effect on the π–π* transition of the chloro-substituted zinc complex. The quantum yield of the chloro-substituted zinc complex is also substantially diminished. This photophysical behaviour (Table 2) is consistent with those reported for Zn(II) complexes of a Schiff base substituted with electron donating /withdrawing group [28].The UV-Vis and photophysical data remained insensitive to the alkoxy carbon chain length.

Differential Scanning Calorimetry (DSC) and Polarised Optical Microscopy (POM) experiments showed the ligands (HL) *n*-cpd to be non-liquid crystalline, possibly due to greater conformational flexibility of the molecules. However, all the complexes exhibited columnar mesomorphism. Polarised optical microscopy of a representative complex (Zn-16cpd) was carried out. In the POM study, upon cooling the sample from isotropic melt, a typical fan-shaped texture appeared at ~189°C (Figure 2), which was identified to be a rectangular columnar (Col_r) phase on the basis of powder X-ray diffraction (PXRD) study. The optical texture remained unaltered until room temperature was reached. In the DSC study, a mesophase to crystallisation peak could not be detected, presumably due to the slower transition to the more organised phases, and partial or complete vitrification of compounds upon cooling. Zn-16cpd exhibited two transitions (Table 2) in heating and one in cooling cycle (Figure 3). Pertinent here is that analogous zinc complexes with a methyl-substituted phenylenediamine spacer showed a hexagonal columnar (Col_h) phase [38]. In the absence of the methyl/chloro group at the central aromatic spacer, the molecules were earlier found to exhibit columnar primitive rectangular (P_{222}) to monoclinic oblique (P_{112}) lattice phase transformation, the latter being stable down to room temperature [39]. Due to the highly viscous nature of the newly synthesised chloro-substituted complexes and severe restriction in the molecular mobility, a pronounced hysteresis in transition temperature has been noted (a large temperature difference (~24°C) during columnar to isotropisation transition and vice versa). A marginal hike in the isotropisation and mesophase transition temperature as a function of decreasing alkoxy chain length has been noticed. The observed mesomorphic behaviour of the chloro-substituted compounds vis-à-vis the un-substituted/methyl-substituted zinc complexes (Supplementary information, Table S2) reported by us earlier [38, 39] not only provides a point of interest but also clearly demonstrates how slight modification of the 'salphen' ligand framework can influence the mesogenicity of the corresponding complexes.

Table 1. UV-Vis and photoluminescence data of ligands (*n*-cpd) and complexes (Zn-*n*-cpd).

Compounds	π→π* (ε, l mol^{-1} cm^{-1})	π→π* (ε, l mol^{-1} cm^{-1})	PL[b] (Solution)	PL[b] (Solid)
12cpd	292 nm (13,800) 329 nm (17,100)	365 nm (11,600)	-	-
Zn-12cpd	326 nm (13,400) 401 nm (15,500)	451 nm (12,200)	538 nm	551 nm
14cpd	295 nm (13,700) 328 nm (17,200)	365 nm (11,600)	-	-
Zn-14cpd	325 nm (13,400) 398 nm (15,400)	448 nm (12,100)	534 nm	556 nm
16cpd	294 nm (13,500) 326 nm (17,800)	365 nm (11,600)	-	-
Zn-16cpd	323 nm (13,300) 403 nm (15,200)	452 nm (12,700)	532 nm	549 nm
18cpd	296 nm (13,400) 328 nm (17,800)	363 nm (11,200)	-	-
Zn-18cpd	325 nm (13,500)	454 nm (12,300)	536 nm	553 nm

[b] Photoluminescence data.

Table 2. Phase transitions temperatures (T, °C), associated enthalpies (ΔH, kJ mol^{-1}) of *n*-cpd and their complexes.

Compounds	Heating	Cooling
Zn-12cpd	Cr 138.3(4.1) Col_r 222.7(9.2) I	I200.4(9.1)Col_r
Zn-14cpd	Cr 131.2(4.3) Col_r 218.6(8.8) I	I198.2(8.9)Col_r
Zn-16cpd	Cr 129.4(4.7) Col_r 214.4(9.6) I	I189.2(9.9)Col_r
Zn-18cpd	Cr 126.1(4.8) Col_r 210.2(8.9) I	I185.5(8.8)Col_r

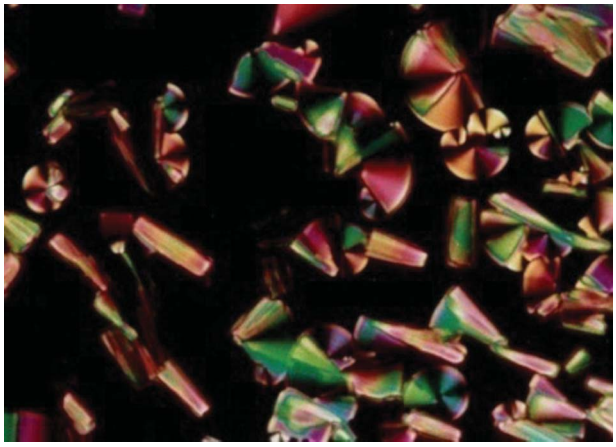

Figure 2. POM texture of Zn-16cpd at 189°C.

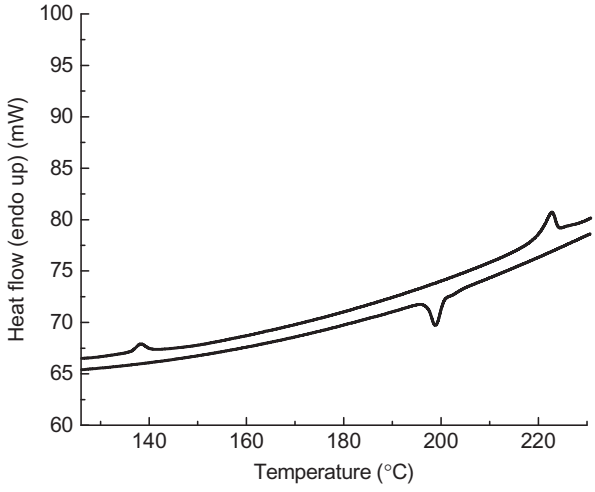

Figure 3. DSC thermogram of Zn-16cpd.

Talbe 3. PXRD data of Zn-16cpd.

Compound	d_{obs}[Å][a]	d_{calc}[Å][b]	hk[c]	Parameters
Zn-16cpd at 194°C	15.13	15.12	11	Col_r- *p2gg*
	13.01	13.03	20	$a = 26.04$ Å
	10.06	10.04	21	$b = 18.63$ Å
	7.8			$S = 484.36$ Å^2
	4.9			$V_m = 1774.13$ Å^3
	3.5			$h = 3.6$
				$S_{col} = 242.18$

[a]d_{obs} and [b]d_{calc} are experimentally and theoretically measured diffraction spacings at 194°C. [hk][c] is the indexation of the reflections. For mesophase parameters, molecular volume V_m is calculated using the formula $V_m = M/\lambda\rho N_A$, where M is the molecular weight of the compound, N_A is the Avogadro number, ρ is the volume mass (≈1 g cm^{-3}) and $\lambda(T)$ is a temperature correction coefficient at the temperature of the experiment (T). $\lambda = V_{CH2}\ (T°)\ /\ V_{CH2}\ (T)$, $T° = 25$°C. $V_{CH2}(T) = 26.5616 + 0.02023$. T, h is the intermolecular repeating distance deduced directly from the measured molecular volume and the lattice area according to $h = V_m\ /\ S$. For the Col_r phase, the lattice parameters a and b are deduced from the mathematical expression $a = 2d_{20}$ and $1/d_{hk} = \sqrt{h^2\ /\ a^2 + k^2\ /\ b^2}$, where a, b are the parameters of the Col_r phase, S is the lattice area and S_{col} is the columnar cross-section ($S = ab$, $S_{col} = S\ /\ 2$).

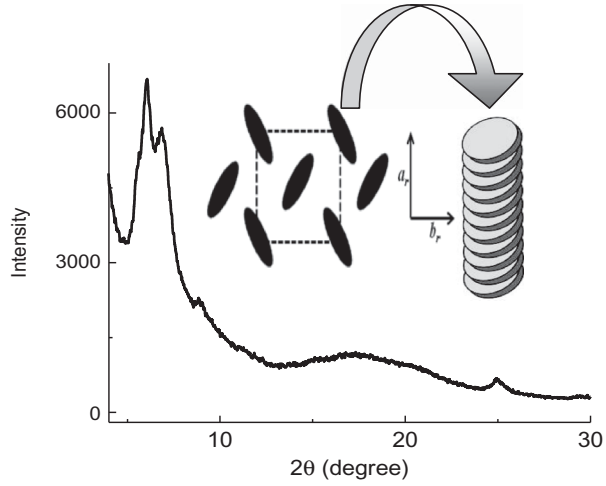

Figure 4. PXRD pattern of Zn-16cpd at 194°C.

To confirm the mesophase textures, temperature-dependent PXRD experiments were carried out for a typical compound Zn-16cpd at 194°C. The X-ray diffraction (XRD) experiment data (Table 3) support the results obtained from optical microscopy and DSC experiment. At 194°C, in the small-angle region, three sharp diffraction peaks at 15.1, 13.01 and 10.06 Å were observed (Figure 4). The first two fundamental reflections can be indexed as the (11) and (20) reflections of a rectangular lattice [30]. Moreover, with the presence of the (21) peak, the symmetry of the lattice can be further assigned to a *p2gg* plane group [30]. In the wide-angle region, a broad diffuse peak (4.9 Å) was observed that confirms the liquid-like order of the molten chains (h_{ch}). The relatively sharper peak at about 3.5 Å, well separated from the broad one, can be attributed to the stacking distance of the discs within the same column (core–core separation). A less intense peak at ca. 7.8 Å possibly indicates a perpendicular stacking of the hemi-disc-shaped molecules, which is necessary to produce a disc-shaped dimer for the formation of the columnar phase. A molecular organisation based on dimeric interaction involving Zn and

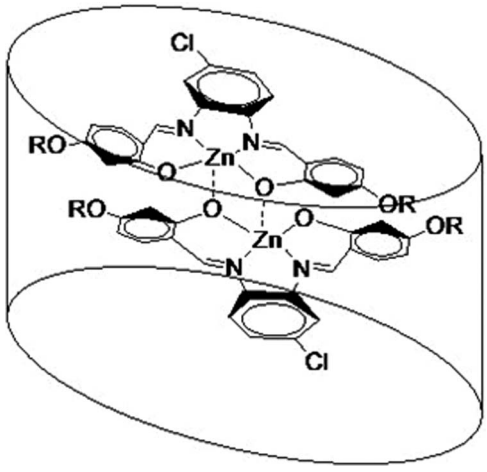

Figure 5. Dimeric interaction of the molecules.

phenolate-O has been invoked to explain the 'disc'-like formation (Figure 5).

As all efforts to obtain single crystals of the ligand or complexes were foiled, the density functional theory (DFT) method (Supplementary information, Table S3) is employed to determine the optimised geometry of a representative compound Zn-16cpd (Figure 6). The ground state geometries in the gas phase of the Zn-16cpd complex were fully optimised using the restricted BLYP (Becke- Lee-Yang-Parr)/DNP (double-numerical atomic orbitals augmented by polarisation functions) methods without imposing any symmetry constrain. Spin restricted calculation has been performed in the framework of the generalised gradient approximation (GGA). At the GGA level, the BLYP functional has been used throughout this study, comprising a hybrid exchange functional as defined by Becke and the non-local Lee–Yang–Parr correlation functional [44]. The basis set chosen in this study is DNP, the double-numerical atomic orbitals augmented by polarisation functions. Convergence in energy, force and displacement was set as 10^{-5} Ha, 0.001 Ha/Å and 0.005 Å, respectively. All

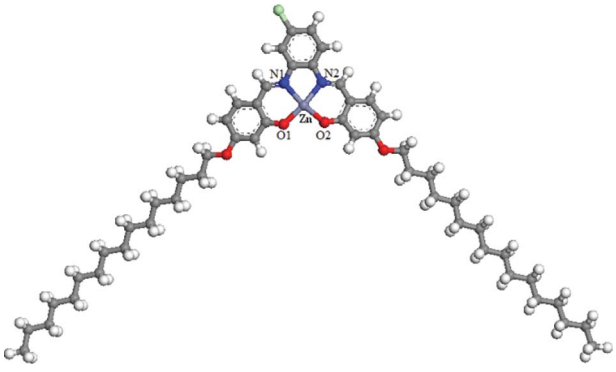

Figure 6. Optimised structure of Zn-16cpd.

calculations were performed with the DMol3 program package [45]. The three-dimensional (3D) iso-surface plots of the lowest unoccupied molecular orbital (LUMO) and the highest occupied molecular orbital (HOMO) of all the zinc complexes are shown (Supplementary information, Figures S2 and S3). The electron density of the HOMO is localised on the aromatic rings, while the LUMO is mainly centred on N–C bonds. The HOMO and LUMO energies of the zinc complex are calculated to be −4.898 and −2.703 eV, respectively, $\Delta E = 2.195$ eV. The HOMO–LUMO energy difference, in fact, is a measure of kinetic stability of the molecule, indicating the reactivity pattern of the molecule [46]. The HOMO–LUMO gap (2.195 eV) in the present case implies high kinetic stability and low chemical reactivity, because it is energetically unfavourable to add electrons to a high-lying LUMO or to extract electrons from a low-lying HOMO [47]. The HOMO–LUMO energy difference evaluated from the lowest energy UV-Vis band (451 nm) is 2.75 eV, which is substantially higher than that obtained from DFT studies ($\Delta E = 2.195$ eV). Extensive intermolecular interactions in the solution phase (UV-Vis study) vis-á-vis free gaseous molecule (DFT study) could be one plausible reason for such a deviation. Based on the spectral and DFT study, four coordinated distorted square planar geometries have been conjectured.

3. Conclusion

A new series of green emissive mesogenic Zn(II)-salphen complexes with a chloro-substituted phenyle nediamine spacer have been successfully synthesised from an interaction of the Schiff base and Zn^{2+}. The ligands are neither fluorescent nor mesogenic. However, the complexes, besides being fluorescent, exhibited columnar rectangular (Col_r) mesophases. Based on spectral and DFT study, four coordinate distorted square planar geometries around the Zn(II) centre have been conjectured. The synthesis strategy adopted herein can be effectively employed to gain entry into the fascinating domain of metallomesogens with tuneable molecular construction motifs possessing multifunctional properties. The effect of substitution in the spacer group on the mesomorphic and photoluminescence behaviour of the complexes has been rationalised.

4. Experimental details

4.1. Physical measurements

The C, H and N analyses were carried out using a CarloErba 1108 elemental analyser (USA). The ^{1}H-NMR spectra were recorded on a Bruker Avance

II, 400 MHz spectrometer (Bruker, India) in $CDCl_3$ (chemical shift in δ) solution with trimethylsilyl (TMS) as the internal standard. UV-Vis absorption spectra of the compounds in CH_2Cl_2 were recorded on a Shimadzu UV-1601PC spectrophotometer (Shimadzu, Asia Pacific, Pte Ltd, Singapore). Photoluminescence spectra were recorded on a Shimadzu RF-5301PC spectrophotometer (Shimadzu, Asia Pacific, Pte Ltd, Singapore). The fluorescence quantum yield in dichloromethane was determined by the dilution method using 9,10-diphenylanthracene as standard. Infrared spectra were recorded on a Perkin Elmer BX series spectrometer (Perkin Elmer, USA) on a KBr disc in the 400–4000 cm^{-1} range. The optical textures of the different phases of the compounds were studied using a Nikon optiphot-2-polpolarising microscope (Nikon Corporation, Tokyo, Japan) with an Instec hot and cold stage HCS302 attached, with an STC200 temperature controller of 0.1°C accuracy. The thermal behaviour of the compounds was studied using a Pyris-1 system linked to a Perkin Elmer differential scanning calorimeter (Perkin Elmer, Switzerland) with a heating or cooling rate of 5°C/min. Variable temperature PXRD of the samples was recorded on a Bruker D8 Discover instrument (Bruker, Germany) using Cu-Ka radiation and an Anton Paar domed hot stage heating attachment; DHS 900 was the heating device. Quantum chemical calculation on a representative complex, Zn-16cpd, was carried out using DFT as implemented in the DMol3 package.

4.2. Materials

The materials were procured from Tokyo Kasei, Japan, and Lancaster Chemicals, USA. All solvents were purified and dried using standard procedures. Silica (60–120 mesh) from Spectrochem was used for chromatographic separation. Silica gel G (E-Merck, India) was used for TLC (Thin Layer Chromatography).

4.3. Synthesis and analysis

4.3.1. Synthesis of n-alkoxysalicyldehyde (n = 12, 14, 16, 18)

2,4-Dihydroxybenzaldehyde (10 mmol, 1.38 g), $KHCO_3$ (10 mmol, 1 g), KI (catalytic amount) and 1-bromododecane (10 mmol, 2.4 g) or 1-bromote tradecane (10 mmol, 2.5 g) or 1-bromohexadecane (10 mmol, 2.8 g) or 1-bromooctadecane (10 mmol, 3 g) were mixed in 250 ml of dry acetone. The mixture was heated under reflux for 24 h, and then filtered, while hot, to remove any insoluble solids. Dilute HCl was added to neutralise the warm solution, which was then extracted with chloroform (100 ml). The combined chloroform extract was concentrated to give a purple solid. The solid was purified by column chromatography using a mixture of chloroform and hexane (v/v, 1/1) as eluent. Evaporation of the solvents afforded a white solid product.

4.3.2. Synthesis of N,N′-bis(4-(4′-dodecyloxy)-salicylidene)-4-Cl-1,2 phenylenediamine (12-cpd)

An ethanolic solution of 2-hydroxy-(4-dodecyloxy)-salicylaldehyde (0.30 g, 1 mmol) was added to an ethanolic solution of 4-Cl-1,2-phenylenediamine (0.07 g, 0.5 mmol).The solution mixture was refluxed with a few drops of acetic acid as a catalyst for 3 h to yield the yellow Schiff base. The compound was collected by filtration and re-crystallised from absolute ethanol to obtain a pure compound.

Yield: 0.27 g (75%); Anal. Calc. for $C_{44}H_{63}ClN_2O_4$ (719.4): C, 73.46; H, 8.83; N, 3.89. Found: C, 73.45; H, 8.82; N, 3.87. %.^{1}H NMR (400 MHz, $CDCl_3$; Me_4Si at 25°C, ppm): δ = 13.06 (s, 1H, H8), 8.57 (s, 1H, H4), 7.72 (d, J = 8.54 Hz, H5), 7.21 (d, 2H, H7), 7.12 (t, J = 8.44 Hz, 2H, H1), 7.11 (dd, J = 2.43 Hz, J = 9.0 Hz, 2H, H6), 6.62 (d, J = 2.42 Hz, 2H, H3), 6.48 (dd, J = 2.43 Hz, J = 8.27 Hz, 2H, H2), 3.96 (t, J = 6.81 Hz, 2H, -OCH_2), 0.96 (t, J = 6.82 Hz, 6H, CH_3), 0.85 (m, -CH_2 of methylene proton in side chain). IR (ν_{max}, cm^{-1}, KBr): 3400 (ν_{OH}), 2924 ($\nu_{as(C\text{-}H),}CH_3$), 2871 ($\nu_{s(C\text{-}H)},CH_3$), 1628 ($\nu_{C=N}$), 1297 ($\nu_{C\text{-}O}$).

4.3.3. N,N′-bis(4-(4′-n-tetradecyloxy)-salicylidene)-4-Cl-1,2 phenylenediamine (14-cpd)

Yield: 0.28 g (70%); Anal. Calc. for $C_{48}H_{71}ClN_2O_4$ (774.5): C, 74.34; H, 9.23; N, 3.61. Found: C, 74.35; H, 9.22; N, 3.65. %. ^{1}H NMR (400 MHz, $CDCl_3$; Me_4Si at 25°C, ppm): δ = 13.01 (s, 1H, H8), 8.67 (s, 1H, H4), 7.76 (d, J = 8.53 Hz, H5), 7.23 (d, 2H, H7), 7.13 (dd, J = 2.41 Hz, J = 9.21 Hz, 2H, H6), 7.13 (t, J = 8.44 Hz, 2H, H1), 6.48 (dd, J = 2.13 Hz, J = 8.29 Hz, 2H, H2), 6.45 (d, J = 2.13 Hz, 2H, H3), 3.91(t, J = 6.84 Hz, 2H, -OCH_2), 0.95(t, J = 6.72Hz, 6H, CH_3), 0.86 (m, -CH_2 of methylene proton in side chain). IR (ν_{max}, cm^{-1}, KBr): 3435 (ν_{OH}), 2915 ($\nu_{as(C\text{-}H)}$, CH_3), 2845 ($\nu_{s(C\text{-}H),}CH_3$), 1626 ($\nu_{C=N}$), 1288 ($\nu_{C\text{-}O}$).

4.3.4. N,N′-bis(4-(4′-n-hexadecyloxy)-salicylidene)-4-Cl-1, 2 phenylenediamine (16-cpd)

Yield: 0.32 g (75%); Anal. Calc. for $C_{52}H_{79}ClN_2O_4$ (831.6): C, 75.10; H, 9.57; N, 3.37. Found: C, 75.12; H, 9.54; N, 3.34. %. ^{1}HNMR (400 MHz, $CDCl_3$; Me_4Si at 25°C, ppm): δ 13.12 (s, 1H, H8), 8.77 (s, 1H, H4), 7.74 (d, J = 8.54 Hz, H5), 7.24 (d, 2H, H7), 7.23 (dd, J = 2.81 Hz, J = 9.0 Hz, 2H, H6), 7.15 (t, J =

8.43 Hz, 2H, H1), 6.66 (d, J = 2.44Hz, 2H, H3), 6.43 (dd, J = 2.44 Hz, J = 8.29 Hz, 2H, H2), 3.97 (t, J = 6.81 Hz, 2H, -OCH_2), 0.99 (t, J = 6.32 Hz, 6H, CH_3), 0.88 (m, -CH_2 of methylene proton in side chain). ^{13}C NMR (75.45 MHz; $CDCl_3$; Me_4Si at 25°C, ppm) δ = 131.5(-C_1), 106.8(-C_2), 102.3(-C_3), 161.6(-C_{14}), 160.2(-C_4), 110.5(-C_{13}), 128.8(-C_6), 161.3(-C_{15}). IR (ν_{max}, cm^{-1}, KBr): 3433(ν_{OH}), 2918($\nu_{as(C\text{-}H)}$, CH_3), 2849($\nu_{s(C\text{-}H)}$, CH_3), 1626($\nu_{C=N}$), 1287($\nu_{C\text{-}O}$).

4.3.5. N,N′-bis(4-(4′-n-octadecyloxy)-salicylidene)-4-Cl-1, 2 phenylenediamine (18-cpd)

Yield: 0.34 g (74%); Anal. Calc. for $C_{56}H_{87}ClN_2O_4$ (887.6): C, 75.76; H, 9.88; N, 3.16. Found: C, 75.74; H, 9.84; N, 3.14. %. ^{1}H NMR (400 MHz, $CDCl_3$; Me_4Si at 25°C, ppm): δ = 13.01 (s, 1H, H8), 8.72 (s, 1H, H4), 7.77 (d, J = 8.54 Hz, H5), 7.24 (d, 2H, H7), 7.15 (dd, J = 2.41 Hz, J = 9.0 Hz, 2H, H6), 7.14 (t, J = 8.43 Hz, 2H, H1), 6.49 (dd, J = 2.14 Hz, J = 8.29 Hz, 2H, H2), 6.45 (d, J = 2.13 Hz, 2H, H3), 3.91 (t, J = 6.81 Hz, 2H, -OCH_2), 0.98 (t, J = 6.85 Hz, 6H, CH_3), 0.82 (m, -CH_2 of methylene proton in side chain). IR (ν_{max}, cm^{-1}, KBr): 3434 (ν_{OH}), 2916 ($\nu_{as(C\text{-}H)}$, CH_3), 2844 ($\nu_{s(C\text{-}H)}$,CH_3), 1622 ($\nu_{C=N}$), 1289 ($\nu_{C\text{-}O}$).

4.3.6. Synthesis of zinc(II) complexes (Zn-n-cpd. n = 12, 14, 16, 18)

The general procedure is as follows.

The ligand 12-cpd (0.071 g, 0.1 mmol) or 14-cpd (0.077 g, 0.1 mmol) or 16-cpd (0.083 g, 0.1 mmol) or 18-cpd (0.088 g, 0.1 mmol) was dissolved in the minimum volume of absolute ethanol. To this, an equimolar amount of zinc acetate $Zn(OAc)_2.2H_2O$(0.02 g, 0.1 mmol) in methanol was added slowly and stirred for 2 h at room temperature. A yellow solid formed immediately, which was filtered, washed with diethyl ether and re-crystallised from chloroform-ethanol (1:1).

4.3.7. Zn-12cpd

Yield: 0.068 g (75%); Anal. Calc. for $C_{44}H_{61}ClN_2O_4Zn$ (782.4): C, 67.51; H, 7.85; N, 3.58. Found: C, 67.52; H, 7.84; N, 3.54. %. ^{1}H NMR (400 MHz, $CDCl_3$; Me_4Si at 25°C, ppm): δ, 8.24 (s, 1H, H4), 7.73 (d, J = 8.53 Hz, H5), 7.22 (d, 2H, H7), 7.15 (t, J = 8.36, 2H, H1), 7.01 (dd, J = 2.36 Hz, J = 8.58, 2H, H6), 6.55 (d, J = 2.45 Hz, 2H, H3), 6.38 (dd, J = 2.36 Hz, J = 8.18 Hz, 2H, H2), 3.98 (t, J = 6.72 Hz, 2H, -OCH_2), 0.89 (t, J = 6.83 Hz, 6H, CH_3), 0.89 (m, -CH_2 of methylene proton in side chain). IR (ν_{max}, cm^{-1}, KBr): 2924($\nu_{as(C\text{-}H)}$, CH_3), 2850($\nu_{s(C\text{-}H)}$, CH_3), 1612($\nu_{C=N}$).

4.3.8. Zn-14cpd

Yield: 0.073 g (76%); Anal. Calc. for $C_{48}H_{69}ClN_2O_4Zn$ (839.4): C, 68.72; H, 8.29; N, 3.34. Found: C, 68.71; H, 8.28; N, 3.35. %. ^{1}H NMR (400 MHz, $CDCl_3$; Me_4Si at 25°C, ppm): δ, 8.21 (s, 1H, H4), 7.76 (d, J = 8.56 Hz, H5), 7.21 (d, 2H, H7), 7.14 (t, J = 8.35 Hz, 2H, H1), 7.01 (dd, J = 2.35 Hz, J = 8.38, 2H, H6), 6.57 (d, J = 2.43 Hz, 2H, H3), 6.39 (dd, J = 2.37 Hz, J = 8.18 Hz, 2H, H2), 3.99 (t, J = 6.54 Hz, 2H, -OCH_2), 0.88 (t, J = 6.82 Hz, 6H, CH_3), 0.92 (m, -CH_2 of methylene proton in side chain). IR (ν_{max}, cm^{-1}, KBr): 2923($\nu_{as(C\text{-}H)}$, CH_3), 2847($\nu_{s(C\text{-}H)}$, CH_3), 1613($\nu_{C=N}$).

4.3.9. Zn-16cpd

Yield: 0.071 g (70%); Anal. Calc. for $C_{52}H_{77}ClN_2O_4Zn$ (895.5): C, 69.78; H, 8.67; N, 3.13. Found: C, 69.76; H, 8.68; N, 3.15. %. ^{1}H NMR (400 MHz, $CDCl_3$; Me_4Si at 25°C, ppm): δ, 8.23 (s, 1H, H4), 7.77 (d, J = 8.54 Hz, H5), 7.26 (d, 2H, H7), 7.18 (t, J = 8.39Hz, 2H, H1), 7.08 (dd, J = 2.34 Hz, J = 8.37, 2H, H6), 6.56 (d, J = 2.45 Hz, 2H, H3), 6.38 (dd, J = 2.37 Hz, J = 8.17 Hz, 2H, H2), 3.95 (t, J = 6.56 Hz, 2H, -OCH_2), 0.89 (t, J = 6.73Hz, 6H, CH_3), 0.96 (m, -$CH_2$of methylene proton in side chain). ^{13}C NMR (75.45 MHz; $CDCl_3$; Me_4Si at 25°C, ppm) δ = 135.6 (-C_1), 109.7(-C_2), 106.9(-C_3), 168.7(-C_{14}), 166.4(-C_4), 114.8(-C_{13}), 133.7(-C_6), 166.2 (-C_{15}). IR (ν_{max}, cm^{-1}, KBr): 2927($\nu_{as(C\text{-}H)}$, CH_3), 2865($\nu_{s(C\text{-}H)}$, CH_3), 1613($\nu_{C=N}$).

4.3.10. Zn-18cpd

Yield: 0.081 g (75%); Anal. Calc. for $C_{56}H_{85}ClN_2O_4Zn$ (949.5): C, 70.72; H, 9.01; N, 2.95. Found: C, 70.72; H, 9.02; N, 2.96. %. ^{1}H NMR (400 MHz, $CDCl_3$; Me_4Si at 25°C, ppm): δ, 8.24 (s, 1H, H4), 7.78 (d, J = 8.55 Hz, H5), 7.29 (d, 2H, H7), 7.17 (t, J = 8.39Hz, 2H, H1), 7.08 (dd, J = 2.35 Hz, J = 8.38Hz, 2H, H6), 6.59 (d, J = 2.48 Hz, 2H, H3), 6.38 (dd, J = 2.37 Hz, J = 8.17 Hz, 2H, H2), 3.95 (t, J = 6.56 Hz, 2H, -OCH_2), 0.91 (t, J = 6.73Hz, 6H, CH_3), 0.97 (m, -CH_2 of methylene proton in side chain). IR (ν_{max}, cm−1, KBr): 2928($\nu_{as(C\text{-}H)}$, CH_3), 2866($\nu_{s(C\text{-}H)}$, CH_3), 1611($\nu_{C=N}$).

Acknowledgements

The authors thank INSPIRE, Department of Science and Technology (Ministry of Science & Technology), New Delhi, for financial support and Prof R.C. Deka (Tezpur University, India) for assistance with the theoretical calculations. Sophisticated Analytical Instrumentation Facility, North Eastern Hill University, Shillong, and CDRI, Lucknow, are acknowledged for some spectral results.

References

[1] Giroud-Godquin, A.M.; Maitlis, P.M. *Angew. Chem. Int. Ed.* **1991**, *30*, 375–402.
[2] Espinet, P.; Esteruelas, M.A.; Oro, L.A.; Serrano, J.L.; Sola, E. *Coord. Chem. Rev.* **1992**, *117*, 215–274.
[3] Serrano, J.L. *Metallomesogens, Synthesis, Properties and Applications*; VCH: Weinheim, 1996.
[4] Hoshino, N. *Coord. Chem. Rev.* **1998**, *174*, 77–108.
[5] Lee, J.-H.; Choi, S.-M.; Pate, B.D.; Chisholm, M.H.; Han, Y.-S. *J. Mater. Chem.* **2006**, *16*, 2785–2791.
[6] Serrette, A.G.; Lai, C.K.; Swager, T.M. *Chem. Mater.* **1994**, *6*, 2252–2268.
[7] Serrette, A.G.; Swager, T.M. *J. Am. Chem. Soc.* **1993**, *115*, 8879–8880.
[8] Abe, Y.; Nakazima, N.; Tanase, T.; Katano, S.; Mukai, H.; Ohta, K. *Mol. Cryst. Liq. Cryst.* **2007**, *466*, 129–147.
[9] Abe, Y.; Nakabayashi, K.; Matsukawa, N.; Takashima, H.; Iida, M.; Tanase, T.; Sugibayashi, M.; Mukai, H.; Ohta, K. *Inorg. Chim. Acta* **2006**, *359*, 3934–3946.
[10] Abe, Y.; Nakabayashi, K.; Matsukawa, N.; Iida, M.; Tanase, T.; Sugibayashia, M.; Ohta, K. *Inorg. Chem. Commun.* **2004**, *7*, 580–583.
[11] Mukaia, H.; Yokokawaa, M.; Hatsusakaa, K.; Ohta, K. *Liq. Cryst.* **2010**, *37*, 13–21.
[12] Cozzi, P.G. *Chem. Soc. Rev.* **2004**, *33*, 410–421.
[13] Gennari, C.; Piarulli, U. *Chem. Rev.* **2003**, *103*, 3071–3100.
[14] Kureshy, R.I.; Ahmad, I.; Khan, N.H.; Abdi, S.H.R.; Pathak, K. *J. Catal.* **2006**, *238*, 134–141.
[15] Pucci, D.; Aiello, I.; Bellusci, A.; Crispini, A.; Ghedini, M.; La Deda, M. *Eur. J. Inorg. Chem.* **2009**, 4274–4281.
[16] Splan, K.E.; Massari, A.M.; Morris, G.A.; Sun, S.-S.; Reina, E.; Nguyen, S.B.T.; Hupp, J.T. *Eur. J. Inorg. Chem.* **2003**, 2348–2351.
[17] Liuzzo, V.; Oberhauser, W.; Pucci, A. *Inorg. Chem. Commun.* **2010**, *13*, 686–688.
[18] Cozzi, P.G.; Dolci, L.S.; Garelli, A.; Montalti, M.; Pordi, L.; Zaccheroni, N. *New J. Chem.* **2003**, *27*, 692–697.
[19] Barbieri, A.; Accorsi, G.; Armaroli, N. *Chem. Commun.* **2008**, 2185–2193.
[20] Lin, H.-C.; Huang, C.-C.; Shi, C.-H.; Liao, Y.-H.; Chen, C.-C.; Lin, Y.-C.; Liu, Y.-H. *Dalton Trans.* **2007**, 781–791.
[21] Kleij, A.W.; Lutz, M.; Spek, A.L.; Leeuwena, P.W.N.M.V.; Reek, J.N.H. *Chem. Commun.* **2005**, 3661–3663.
[22] Kleij, A.W.; Kuil, M D.; Tooke, M.; Lutz, M.; Spek, A.L.; Reek, J.N.H. *Chem. Eur. J.* **2005**, *11*, 4743–4750.
[23] Gime´nez, R.; Pinol, M.; Serrano, J.L. *Chem. Mater.* **2004**, *16*, 1377–1383.
[24] Sagara, Y.; Yamane, S.; Mutai, T.; Araki, K.; Kato, T. *Adv. Funct. Mater.* **2009**, *19*, 1869–1875.
[25] Wang, Y.; Liu, Y.; Qi, H.; Li, X.; Nin, M.; Liu, M.; Shi, D.; Zhu, W.; Cao, Y. *Dalton Trans.* **2011**, *40*, 5046–5051.
[26] Terazzi, E.; Torelli, S.; Bernardinelli, G.; Rivera, J.- P.; Benech, J.- M.; Bourgogne, C.; Donnio, B.; Guillon, D.; Imbert, D.; Bunzli, J.-C.G.; Pinto, A.; Jeannerat, D.; Piguet, C. *J. Am. Chem. Soc.* **2005**, *127*, 888–903.
[27] Ghedini, M.; Pucci, D.; Crispini, A.; Bellusci, A.; La Deda, M.; Aiello, I.; Pugliese, T. *Inorg. Chem. Commun.* **2007**, *10*, 243–246.
[28] Camerel, F.; Ziessel, R.; Donnio, B.; Bourgogne, C.; Guillon, D.; Schmutz, M.; Iacovita, C.; Bucher, J.-P. *Angew. Chem. Int. Ed.* **2007**, *46*, 2659–2562.
[29] Kozhevnikov, V.N.; Donnio, B.; Bruce, D.W. *Angew. Chem. Int. Ed.* **2008**, *47*, 6286–6289.
[30] Pucci, D.; Barberio, G.; Bellusci, A.; Crispini, A.; Deda, M.La; Ghedini, M.; Szerb, E.I. *Eur. J. Inorg. Chem.* **2005**, 2457–2463.
[31] Pucci, D.; Crispini, A.; Ghedini, M.; Sezerb, E.I.; Deda, M.La. *Dalton Trans.* **2011**, *40*, 4614–4622.
[32] Baena, M.; Espinet, J.P.; Folcia, C.L.; Ortega, J.; Etxebarria, J. *Inorg. Chem.* **2010**, *49*, 8904–8913.
[33] Qi, M.H.; Liu, G.F. *J. Mater. Chem.* **2003**, *13*, 2479–2484.
[34] Coco, S.; Cordovilla, C.; Espinet, Martin-Alvarez, P.J.; Munoz, P. *Inorg. Chem.* **2006**, *45*, 10180–10187.
[35] Pucci, D.; Aiello, I.; Bellusci, A.; Crispini, A.; De Franco, I.; Ghedini, M.; La Deda, M. *Chem. Commun.* **2008**, 2254–2256.
[36] Barberio, G.; Bellusci, A.; Crispini, A.; Ghedini, M.; Golemme, A.; Prus, P.; Pucci, D. *Eur. J. Inorg. Chem.* **2005**, 181–188.
[37] Cavero, E.; Uriel, S.; Romero, P.; Serrano, J.L.; Giménez, R. *J. Am. Chem. Soc.* **2007**, *129*, 11608–11618.
[38] Bhattacharjee, C.R.; Das, G.; Mondal, P.; Rao, N.V.S. *Polyhedron* **2010**, *29*, 3089–3096.
[39] Bhattacharjee, C.R.; Das, G.; Mondal, P.; Prasad, S.K.; Rao, D.S.S.; *Eur. J. Inorg. Chem.* **2011**, 1418–1424.
[40] Bhattacharjee, C.R.; Das, G.; Mondal, P. *Eur. J. Inorg. Chem.* **2011**, 5390–5399.
[41] Bhattacharjee, C.R.; Das, G.; Mondal, P.; Prasad, S.K.; Rao, D.S.S. *Inorg. Chem. Commun.* **2011**, *14*, 606–612.
[42] Bhattacharjee, C.R.; Das, G.; Mondal, P. *Liq. Cryst.* **2011**, *38*, 441–449.
[43] Bhattacharjee, C.R.; Das, G.; Mondal, P.; Prasad, S.K.; Rao, D.S.S. *Liq. Cryst.* **2011**, *38*, 615–623.
[44] Lee, C.; Yang, W.; Parr, R.G. *Phys. Rev. B: Condens. Matter Mater. Phys.* **1988**, *37*, 785–789.
[45] Delley, B.J. *Chem. Phys.* **1990**, *92*, 508–517.
[46] Kim, K.H.; Han, Y.K.; Jung, J. *Theor. Chem. Acc.* **2005**, *113*, 233–240.
[47] Aihara, J. *J. Phys. Chem. A* **1999**, *103*, 7487–7495.